

Quantum Computing for High-Energy Physics: State of the Art and Challenges

Alberto Di Meglio^{1,*}, Karl Jansen^{2,3,†}, Ivano Tavernelli^{4,‡}, Constantia Alexandrou⁵,^{3,5}
 Srinivasan Arunachalam,⁶ Christian W. Bauer,⁷ Kerstin Borrás^{8,9}, Stefano Carrazza¹⁰,^{1,10}
 Arianna Crippa¹¹, Vincent Croft¹², Roland de Putter,⁶ Andrea Delgado¹³, Vedran Dunjko¹²,
 Daniel J. Egger⁴, Elias Fernández-Combarro¹⁴, Elina Fuchs^{15,16}, Lena Funcke¹⁷,
 Daniel González-Cuadra^{18,19}, Michele Grossi¹, Jad C. Halimeh^{20,21}, Zoë Holmes,²²
 Stefan Kühn², Denis Lacroix²³, Randy Lewis²⁴, Donatella Lucchesi^{1,25},
 Miriam Lucio Martínez,^{26,27} Federico Meloni⁸, Antonio Mezzacapo,⁶ Simone Montangero¹⁰,^{1,25}
 Lento Nagano²⁸, Vincent R. Pascuzzi⁶, Voica Radescu,²⁹ Enrique Rico Ortega^{30,31,32,33},
 Alessandro Roggero^{34,35}, Julian Schuhmacher⁴, Joao Seixas,^{36,37,38} Pietro Silvi^{1,25},
 Panagiotis Spentzouris³⁹, Francesco Tacchino⁴, Kristan Temme,⁶ Koji Terashi²⁸, Jordi Tura^{12,40},
 Cenk Tüysüz^{2,11}, Sofia Vallecorsa¹, Uwe-Jens Wiese,⁴¹ Shinjae Yoo⁴² and Jinglei Zhang^{43,44}

¹ *European Organization for Nuclear Research (CERN), 1211 Geneva, Switzerland*

² *CQTA, Deutsches Elektronen-Synchrotron DESY, Platanenallee 6, 15738 Zeuthen, Germany*

³ *Computation-based Science and Technology Research Center, The Cyprus Institute, 20 Konstantinou Kavafi Street, CY-2121 Nicosia, Cyprus*

⁴ *IBM Research Europe — Zurich, 8803 Rüschlikon, Switzerland*

⁵ *Department of Physics, University of Cyprus, PO Box 20537, CY-1678 Nicosia, Cyprus*

⁶ *IBM Quantum, IBM T.J. Watson Research Center, Yorktown Heights, NY 10598, USA*

⁷ *Physics Division Lawrence Berkeley National Laboratory, 1 Cyclotron Road, Mailstop 50A5104, Berkeley, California, USA*

⁸ *Deutsches Elektronen-Synchrotron (DESY), Notkestraße 85, 22607 Hamburg, Germany*

⁹ *RWTH Aachen University, Templergraben 55, 52062 Aachen, Germany*

¹⁰ *TIF Lab, Dipartimento di Fisica, Università degli Studi di Milano and INFN Sezione di Milano, Milan, Italy*

¹¹ *Institut für Physik, Humboldt-Universität zu Berlin, Newtonstraße 15, 12489 Berlin, Germany*

¹² *(aQa^L) Applied Quantum Algorithms – Leiden, Leiden, Netherlands*

¹³ *Physics Division, Oak Ridge National Laboratory, Oak Ridge, Tennessee 37831, USA*

¹⁴ *Department of Computer Science, Facultad de Ciencias, University of Oviedo, 33007 Asturias, Spain*

¹⁵ *Institute of Theoretical Physics, Leibniz University Hannover, 30167 Hanover, Germany*

¹⁶ *Physikalisch-Technische Bundesanstalt, 38116 Braunschweig, Germany*

¹⁷ *Transdisciplinary Research Area “Building Blocks of Matter and Fundamental Interactions” (TRA Matter) and Helmholtz Institute for Radiation and Nuclear Physics (HISKP), University of Bonn, Nußallee 14–16, 53115 Bonn, Germany*

¹⁸ *Institute for Theoretical Physics, University of Innsbruck, 6020 Innsbruck, Austria*

¹⁹ *Institute for Quantum Optics and Quantum Information of the Austrian Academy of Sciences, 6020 Innsbruck, Austria*

²⁰ *Department of Physics and Arnold Sommerfeld Center for Theoretical Physics, Ludwig-Maximilians-Universität München, Munich, Germany*

²¹ *Munich Center for Quantum Science and Technology, Munich, Germany*

²² *Institute of Physics, Ecole Polytechnique Fédérale de Lausanne, 1015 Lausanne, Switzerland*

²³ *CNRS/IN2P3, IJCLab, Paris-Saclay University, 91405 Orsay, France*

²⁴ *Department of Physics and Astronomy, York University, Toronto, Ontario M3J 1P3, Canada*

²⁵ *INFN—Sezione di Padova, Via Marzolo 8, 35131 Padua, Italy*


²⁶ *Nikhef—National Institute for Subatomic Physics, Science Park 105, 1098 XG Amsterdam, Netherlands*

* Contact author: alberto.di.meglio@cern.ch

† Contact author: karl.jansen@desy.de

‡ Contact author: ita@zurich.ibm.com

- ²⁷ *Department of Gravitational Waves and Fundamental Physics, Maastricht University, 6200 MD Maastricht, Netherlands*
- ²⁸ *International Center for Elementary Particle Physics, The University of Tokyo, 7-3-1 Hongo, Bunkyo-ku, Tokyo, 113-0033, Japan*
- ²⁹ *IBM Quantum, IBM Deutschland Research & Development GmbH, Schoenaicher Straße 220, 71032 Böblingen Germany*
- ³⁰ *Department of Physical Chemistry, University of the Basque Country UPV/EHU, Box 644, 48080 Bilbao, Spain*
- ³¹ *Donostia International Physics Center, 20018 Donostia–San Sebastián, Spain*
- ³² *EHU Quantum Center, University of the Basque Country UPV/EHU, P.O. Box 644, 48080 Bilbao, Spain*
- ³³ *Basque Foundation for Science, IKERBASQUE, Plaza Euskadi 5, 48009 Bilbao, Spain*
- ³⁴ *Department of Physics, University of Trento, Via Sommarive 14, 38123 Povo, Trento, Italy*
- ³⁵ *INFN-TIFPA Trento Institute of Fundamental Physics and Applications, Via Sommarive 14, 38123 Povo, Trento, Italy*
- ³⁶ *Department Física, Instituto Superior Técnico, Lisbon, Portugal*
- ³⁷ *Center of Physics and Engineering of Advanced Materials (CeFEMA), Instituto Superior Técnico, Lisbon, Portugal*
- ³⁸ *Laboratory of Physics for Materials and Emergent Technologies (LaPMET), Lisbon, Portugal*
- ³⁹ *Fermi National Accelerator Laboratory, Kirk and, Pine Street, Batavia, Illinois 60510, USA*
- ⁴⁰ *Instituut-Lorentz, Universiteit Leiden, P.O. Box 9506, 2300 RA Leiden, Netherlands*
- ⁴¹ *Albert Einstein Center for Fundamental Physics, Institute for Theoretical Physics, University of Bern, Sidlerstrasse 5, 3012 Bern, Switzerland*
- ⁴² *Brookhaven National Laboratory, 98 Rochester Sreet, Upton, New York 11973, USA*
- ⁴³ *Institute for Quantum Computing, University of Waterloo, Waterloo, Ontario N2L 3G1, Canada*
- ⁴⁴ *Department of Physics and Astronomy, University of Waterloo, Waterloo, Ontario N2L 3G1, Canada*

 (Received 25 August 2023; revised 29 March 2024; accepted 25 June 2024; published 5 August 2024)

Quantum computers offer an intriguing path for a paradigmatic change of computing in the natural sciences and beyond, with the potential for achieving a so-called quantum advantage—namely, a significant (in some cases exponential) speedup of numerical simulations. The rapid development of hardware devices with various realizations of qubits enables the execution of small-scale but representative applications on quantum computers. In particular, the high-energy physics community plays a pivotal role in accessing the power of quantum computing, since the field is a driving source for challenging computational problems. This concerns, on the theoretical side, the exploration of models that are very hard or even impossible to address with classical techniques and, on the experimental side, the enormous data challenge of newly emerging experiments, such as the upgrade of the Large Hadron Collider. In this Roadmap paper, led by CERN, DESY, and IBM, we provide the status of high-energy physics quantum computations and give examples of theoretical and experimental target benchmark applications, which can be addressed in the near future. Having in mind hardware with about 100 qubits capable of executing several thousand two-qubit gates, where possible, we also provide resource estimates for the examples given using error-mitigated quantum computing. The ultimate declared goal of this task force is therefore to trigger further research in the high-energy physics community to develop interesting use cases for demonstrations on near-term quantum computers.

DOI: [10.1103/PRXQuantum.5.037001](https://doi.org/10.1103/PRXQuantum.5.037001)

I. INTRODUCTION

This article reports on scientific discussions and conclusions elaborated at a workshop on high-energy physics (HEP) held in November 2022 at CERN in Geneva. This first event of the Quantum Computing for HEP (QC4HEP) Working Group gathered experts on HEP from different academic and research institutions and countries from four

continents, who besides being world experts in theoretical and experimental aspects of HEP also share a common interest in quantum computing (QC) and its potential as a game changer in the field. The main goal of the workshop, and of this article, is to set a common Roadmap for selected topics of interest to this community, in which we believe that QC can have a significant impact in the near future.

To this end, we have investigated classes of problems and corresponding quantum algorithms that can lead to potential quantum advantage with near-term, noisy, quantum devices. We aim to provide a set of physically relevant use cases that could be interesting to execute on utility-scale quantum hardware, i.e., hardware with about 100 qubits capable of reliably executing several thousand two-qubit gates with error mitigation [1]. By “utility-scale quantum calculations” [2] we mean hardware experiments that can deliver meaningful (albeit noisy) results for quantum circuits and related problems for which no exact classical solution is available, but only approximate ones are available. Therefore, while quantum advantage remains the main target for quantum computing, this study focuses on intermediate “utility-scale” experiments of relevance for the HEP community. The most characteristic feature of our work is thus the identification of realistic problems of interest addressable with near-term quantum algorithms, running on state-of-the-art noisy quantum devices, rather than extensions into the fault-tolerant regime.

Crucially, all developments proposed in the Roadmap are fully platform agnostic. This means that any quantum computing platform can take inspiration from our work and participate in designing near-term experiments, which can then be confronted—in a constructive manner—with the results from other classical and quantum platforms. We believe that by following this path, we will succeed in exploring thoroughly the most promising problems in HEP that may lead to the demonstration of quantum utility in the short term and quantum advantage in the medium term (i.e., before the advent of fault-tolerant quantum computing). Importantly, most algorithmic developments for near-term quantum computers are transferable to the fault-tolerant regime, as, for instance, algorithms for quantum state preparation and time propagation.

The problems proposed in this study were selected on the basis of two main aspects: (1) their physical significance as models of relevant phenomena [e.g., low-dimensional lattice gauge theory (LGT)] or as promising alternative solution strategies for data analysis (e.g., anomaly detection in collider experiments), and (2) the level of “hardness” of the corresponding classical solutions due to particular unfavorable scaling or resource and accuracy limitations. The authors were careful in selecting the physically relevant systems, which can already benefit from near-term (before fault-tolerant) quantum computing because of their particular “hardness” for classical calculations. The scientific value of this work lies mostly in the characterization of problems compatible with utility-scale experiments, proposing the algorithms and error mitigation schemes required for their hardware execution.

For practical purposes, we have organized this article into two main domain areas: theoretical methods and algorithms for modeling HEP problems, and numerical methods for the interpretation and analysis of experimental

results as well as detector simulation and event generation. We strongly believe that there are important connections between the two research domains, where many of the quantum algorithms designed for the solution of problems in one field can be transferred to the other.

We therefore start with a short summary of the main HEP domains in theoretical modeling and experimental physics, for which we believe there is the potential for quantum computing to play a significant role in the near term.

A. Quantum computing for theoretical modeling in HEP

Despite the great success of classical lattice field theory [e.g., for quantum electrodynamics (QED) and quantum chromodynamics (QCD) simulations [3,4]], out-of-equilibrium and real-time dynamics (e.g., of particle collisions, thermalization phenomena, or dynamics after a quench) remain out of reach for Euclidean path-integral Monte Carlo simulations. Furthermore, properties of nuclear matter at high fermionic densities, as arise in neutron stars or in the very early universe, for example, cannot be accessed through these classical simulation techniques [5]. The same holds true for theories with topological terms, which are relevant, for example, in QCD for understanding the amount of CP violation or, in the electroweak sector, the sphaleron rate in the early universe. These severe limitations are rooted in the notorious *sign problem*: the highly oscillatory behavior of the path integrals arising in real-time phenomena, in systems with a high fermionic particle density, or in the presence of topological terms implies an exponentially growing sampling runtime complexity with an increasing number of lattice sites [6].

An alternative approach to circumvent the sign problem might be to describe lattice field theories in the equivalent Hamiltonian formalism, instead of the path-integral description based on the Lagrangian formalism [7,8]. In the Hamiltonian approach, however, the total many-particle wave function that describes a general particle state on the whole lattice must be stored throughout the simulation. But since the total discretized Hilbert space \mathcal{H} containing such general states corresponds to a tensor product of Hilbert spaces \mathcal{H}_j on a single lattice site, the required memory to store a full wave function on the lattice scales exponentially with the number of lattice sites.

In recent years, novel tensor network (TN)-based methods have been introduced to alleviate these limitations by allowing a more compact representation of general quantum states on the lattice [9–13]. The underlying mechanism that allows Hamiltonian simulations to be performed is that only a small subspace of the complete Hilbert space describes the low-energy physics of quantum field theories, and TN methods identify and focus exactly on these

physically relevant subspaces. Hence, with tensor network techniques, various phenomena, such as string breaking and real-time dynamics [14–19], or phase diagrams of both Abelian and non-Abelian gauge theories at finite fermionic densities [20–23] have been studied on a few hundred lattice sites at least in one space dimensional model.

A very promising alternative to TNs is simulations on quantum computers that can represent large Hilbert spaces using qubits, its basic unit of information, where the number of required qubits merely grows linearly with the number of lattice sites. Moreover, quantum algorithms have been proposed that implement real-time dynamics with polynomial time complexity for scalar quantum field theories and QED [24–26]. In addition, by sharing with tensor networks the Hamiltonian formulation, quantum computations completely avoid the sign problem. Thus, quantum computers offer a potential framework to fully overcome the limitations outlined above for the simulation of lattice gauge theories and especially their real-time dynamics [27].

Indeed, various proposals for the implementation of general Abelian and non-Abelian LGT on different types of quantum hardware have accumulated in the past few years, and simulations of small LGT systems on real quantum devices have been demonstrated [11, 12, 28–31]. Examples include proposals for implementing lattice gauge theories using optical lattices [32–34] and atomic and ultracold quantum matter [35–46], further proof-of-principle implementations on a real superconducting architecture [28–30, 47, 48], and, ultimately, (1+1)-dimensional ([1+1]D) real-time and variational simulations of quantum electrodynamics on a trapped-ion system [49, 50]. A broad overview of recently proposed quantum simulators and implementation techniques for LGT can be found in Refs. [10–12]. It is noteworthy that lattice gauge theories can be approached by many different physical systems and methods, each featuring its own advantages and disadvantages.

The understanding of the static and dynamical properties of (3+1)-dimensional ([3+1]D) LGT, including QED and QCD, is not the only target of today’s theoretical particle physics. One has to consider an exciting but also demanding Roadmap to reach eventually the goal of performing quantum simulations of (3+1)D systems as relevant for HEP. This Roadmap starts with (1+1)D systems, which are under active research nowadays, moving to (2+1)-dimensional ([2+1]D) systems, which are under consideration now by various groups, and reaching (3+1)D systems in the future.

Lower-dimensional systems in $1 + 1$ and $2 + 1$ dimensions are already very interesting. They share important and challenging problems with their higher-dimensional counterparts. One important example is the study of (2+1)D QED, which shows the phenomena of asymptotic freedom and confinement. Asymptotic freedom is a feature of QCD, i.e., the quantum field theory of the

strong interaction between quarks and gluons. In the limit of high energies (small distances when natural units are used) the quarks become weakly interacting, making perturbation theory well suited for theoretical predictions. In contrast, at low energies the interaction becomes strong, leading to particle confinement. Interestingly, there are also low-dimensional LGTs for which the phenomena of confinement is known, which can help shed new light on the theoretically harder QCD confining mechanism (because of the large dimensionality and the high number of degrees of freedom). As said above, one such model is (2+1)D QED, which is a compact U(1) LGT. As outlined in Sec. II A 2, we therefore propose this model in a lower dimension as a benchmark for exploring the potential of quantum computing in the near-term, noisy, regime.

B. Quantum computing in HEP experiments

HEP experiments are characterized by the ability to probe the intricacies of particle physics in the Standard Model and beyond it, through performing measurements and analyses at the frontier between quantum theory and precision experimentation. The statistical precision of experiments performed at the Large Hadron Collider (LHC) is evaluated on three classes of algorithms:

- (1) Detector operation algorithms allow detectors to efficiently obtain data that cleanly represent the fundamental interactions of matter. These detectors might feature very large amounts of very-high-dimensional data such as those found inside hadron colliders. These detectors require algorithms to sort significant signals from noise. Detector-based algorithms are also used to aid in inferring enhanced features of a given measurement of very rare processes such as neutrino or expected new physics interactions.
- (2) Identification and reconstruction algorithms are an essential part of mapping the vast collection of pixel intensities, timings, and event counts to a coherent underlying physics structure in the data. These algorithms allow the segmentation of datasets into those that feature particular processes or states that are relevant to a given physics goal and therefore must be robust, efficient, and unbiased.
- (3) Robust simulation and inference tools allow particle physics experiments to compare large amounts of complex, highly structured data with parameterized theoretical predictions. These algorithms include the creation of simulated datasets that are used as templates in parametric statistical models, classification tools to increase the sensitivity of a given measurement to some process, or the identification of statistically anomalous signals that might hint at sources of new physics.

QC encompasses several defining characteristics that are of particular interest to experimental HEP: the potential for quantum speedup in processing time, sensitivity to sources of correlations in data, and increased expressivity of quantum systems. Each of the three classes of algorithms mentioned above benefits from all three of these characteristics. Experiments running on high-luminosity accelerators need faster algorithms; identification and reconstruction algorithms need to capture correlations in signals; simulation and inference tools need to express and calculate functions that are classically intractable.

Within the existing data reconstruction and analysis paradigm, access to algorithms that exhibit quantum speedups would revolutionize the simulation of large-scale quantum systems and the processing of data from complex experimental setups. This would enable a new generation of precision measurements to probe deeper into the nature of the universe. Existing measurements may contain the signatures of underlying quantum correlations or other sources of new physics that are inaccessible to classical analysis techniques. Quantum algorithms that leverage these properties could potentially extract more information from a given dataset than classical algorithms. Finally, algorithms that can capture more complex aspects of HEP theory and simulation could provide estimators that are more natively aligned with the quantum mechanical nature of the Standard Model or indeed potentially uncover new physics beyond what can be explained by classical models.

Quantum computing for HEP is of particular interest due to the prospect of algorithms that can leverage the unique properties of quantum systems to achieve computational advantages. Most quantum algorithms with a promise of a superpolynomial advantage exploit the capacity of quantum computers to efficiently simulate quantum many-body systems. The search for potential quantum utility and/or advantage would be accelerated by the identification of computational problems with the right kind of underlying structure that can be leveraged by quantum algorithms. Applications in the HEP domain can clearly offer a controlled experimental benchmark for such test cases. Through the analysis of the data from HEP experiments using quantum algorithms, researchers may be able to gain insights into the behavior of quantum systems and potentially identify new avenues for quantum advantage.

HEP experimental data are typically organized as collections of associated detector signals that can be reconstructed into measured particles. The distributions of these particle measurements are calculable under specific parameterization of the underlying theory such that the distribution of experimental data can be directly compared with theoretical predictions through the use of simulated data. These parameterizations are such that a characterization of any given process as defined in quantum field

theory is maximally described by the data. This method of parameterization allows the accuracy of the estimator to scale consistently and efficiently with repeated measurements. Therefore, although the data recorded in high-energy physics experiments provide information about the behavior of fundamental particles and their interactions, which in turn are described by quantum fields and their dynamics governed by the principles of quantum mechanics, it is important to note that typically the data and their descriptions are classical in nature and therefore may not trivially exhibit the quantum mechanical properties necessary for quantum utility experiments and, later, quantum advantage. In summary, by analyzing experimental data using tools and techniques from both quantum information theory and particle physics, we can gain insights into the fundamental nature of the universe and potentially discover new phenomena that are not described by current theoretical models.

It is worth mentioning that another collective article on quantum simulations for HEP appeared recently in the literature [51]. Despite the broadly similar target, our work differs in several essential aspects: First, our focus is on the identification and detailed characterization of projects that—while approachable with near-term, noisy quantum devices (about 100 qubits and a few thousand two-qubit gates)—can already address problems of interest in the HEP community. Second, our investigation comprises both theoretical models and computational aspects related to particle collision experiments.

This article is organized as follows. In Sec. II, we describe the challenges in the field and goals that one hopes to achieve with quantum hardware. Section III contains a description of various algorithms that we consider as key candidates for achieving the goals outlined in Sec. II. Finally, we present conclusions in Sec. IV. In Appendix A, we outline IBM’s Roadmap for future quantum devices and explain why digital quantum computers are suitable for addressing open challenges in HEP. In Appendix B, we give a short summary of how a problem is executed on a digital quantum computer. In Appendix C, we explicitly show how the Schwinger model is executed on a quantum computer. In Appendix D, we provide a detailed estimation of the required resources for encoding lattice gauge theories in a digital, qubit-based quantum computer, while Appendix E contains information on selected quantum and classical algorithms.

II. CHALLENGES AND GOALS

The list of identified topics is, of course, not exhaustive. The choice is mainly motivated by the research interests of the authors of this paper. However, we hope that the solutions proposed for this selection of problems, and the corresponding algorithms, can be of inspiration in other domains not contemplated here.

A. Selected applications in the theory domain

In this section, we introduce a series of interesting theoretical challenges in different theoretical domains, including many-particle physics, different flavors of lattice gauge theories, and neutrino physics. The applications deal with relatively low-dimensional systems, which, however, preserve some of the key aspects and criticality, that characterize the systems at the full scale. An overview of the proposed applications in the theory domain together with the associated quantum algorithms is given in the upper panel in Fig. 1.

We further stress that the selection of the problems and their sizes was made to ensure both their physical relevance and a level of hardness that would prevent exact solutions with classical computers, in the spirit of the quantum utility concept. Again, here we do not claim any quantum advantage yet (which would imply the impossibility to determine a classical solution because of scaling issues), but claim the possibility to provide a quantum computing solution to a problem that has no exact classical solution or—as in the case of quantum dynamics—that displays an exponential entanglement growth with time, causing most classical approaches (e.g., TN approaches) to fail in the long run.

Since most applications will deal with the dynamical aspects of the different model Hamiltonians, we start this section with an introduction to methods for real-time simulations.

1. Simulations of real-time phenomena

Experimental results from high-energy physics laboratories, such as the Large Hadron Collider, come in the form of data on collision products. It is through scattering processes that we experimentally acquire a deep understanding of the fundamental physics, typically by reconstructing which composite quasiparticles are assembled during intermediate stages of the scattering event, and comparing their properties with the theoretical predictions from the Standard Model (and beyond).

It is clear, however, that this type of prediction has several limitations. First of all, it is indirect, in the sense that the observed composite quasiparticle properties are compared, and not the scattering event distribution per se. Moreover, the analytic calculations of such quasiparticles are limited to those accessible via perturbation theory, in the form of Feynman diagrams, and thus no accurate predictions are expected for the QCD sector, which is far from perturbative. A substantial obstacle towards accurate model predictions of scattering phenomena is that Monte Carlo methods, which excel at capturing equilibrium properties, are hindered when tackling out-of-equilibrium real-time dynamics, again due to the sign problem and complex actions to numerically integrate.

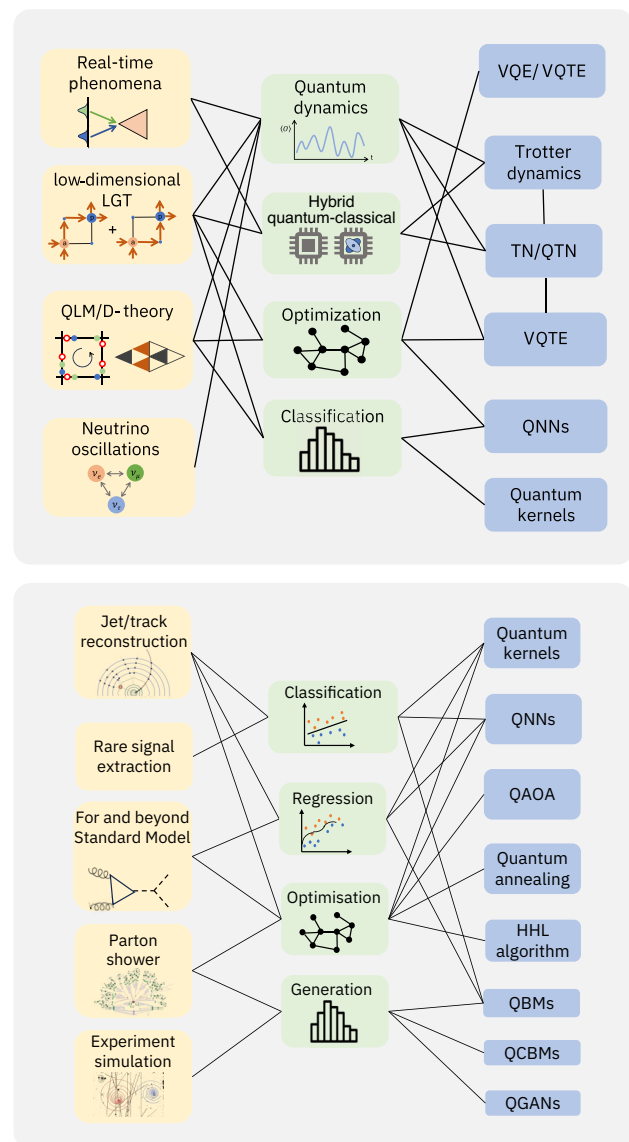


FIG. 1. Upper panel: Proposed theoretical physical model systems (orange) with corresponding approaches (green) and quantum algorithms (blue). For more information on the identified areas of interest, see Sec. II A. Lower panel: Proposed experimental challenges (orange) with corresponding approaches (green) and quantum algorithms (blue). For more information on the identified areas of interest, see Sec. II B. See Appendix E for an overview of a selection of the methods. HHL, Harrow-Hassidim-Lloyd; QBM, quantum Boltzman machine; QCBM, quantum circuit Born machine; QNN, quantum neural network; QTN, quantum tensor network; VQITE, variational imaginary time evolution; VQTE, variational quantum time evolution.

From this perspective, gaining access to direct data from nonperturbative many-body real-time simulations of gauge theories would enable a complete paradigm shift. The simulation could immediately provide the statistics of products so that we could immediately compare them with the observed statistics of collected events from high-energy

laboratories. Lattice gauge theories in the Hamiltonian formulation are perfectly suited for this task: while space dimensions are discretized (typically into a cubic lattice), time is kept as a continuous variable, and thus the many-body real-time evolution operator is formally well defined for any arbitrary time interval. In this framework, the continuum limit can be systematically approached by one taking into account proper nonperturbative renormalization, when necessary. Numerically computing such an evolution operator, and its action onto an arbitrary input state (e.g., converging quasiparticle wave packets), is, however, an exponentially hard problem in the lattice system size and requires the aid of quantum simulators or quantum-inspired numerical algorithms to be done to a good approximation.

Analog and digital quantum simulator strategies can both be used to progress towards this goal. In either case, the real-time evolution operator is applied to a set of qubits (or, more generally, *qudits*) that encode the many-body quantum field state. An analog quantum simulator approximates the target model Hamiltonian by implementing an instantaneous controllable Hamiltonian that is equivalent to the target at a chosen energy scale, and then lets the system evolve with time-independent controls [41]. This approach is inherently scalable, but it is limited by what types of interaction can be engineered. Conversely, digital quantum simulators aim at decomposing the action of the time evolution into a circuit of programmable quantum operations (e.g., gates) [49]. This approach is more general, especially if the quantum resources form a universal set of gates, but it can be demanding in terms of scalability and coherence. Indeed, the number of qubits and the circuit depth required to perform such simulations are largely beyond the capabilities of current near-term, noisy quantum devices [25,52].

Alongside methods based on quantum hardware, we highlight the potential of tensor networks as a numerical strategy working on the same lattice Hamiltonian framework (discrete space, continuous time) as quantum simulators [53–56]. TNs excel in describing lattice quantum states at equilibrium, even in multiple spatial dimensions, and even at finite densities [10,13,22,57]. Moreover, they can accurately capture out-of-equilibrium dynamics as long as the entanglement production is low (i.e., the area laws of entanglement are not violated). While seemingly a strict requirement, it is actually a ubiquitous occurrence, from many-body localization, to slow quenches across phase transitions (Kibble-Zurek mechanism), to short-timescale transient phenomena under Lieb-Robinson bounds. Thus, there are many physical systems whose dynamics are accurately captured by TNs (especially in one dimension). Indeed, the first proof-of-principle demonstration of a scattering event in a lattice gauge theory in one dimension was shown in Ref. [16], where two-wave-packet collisions and subsequent time evolution

of the created entanglement were studied. A more refined study of the process was presented in Ref. [19].

When one is specifically addressing scattering problems with either classical or quantum simulations, there is an additional conceptual complexity that gets added to the already-serious problem of executing the many-body dynamics: namely, preparing the input state. Initial quantum states in particle collider experiments typically involve localized wave packets of composite quasiparticles (e.g., hadrons). Written in the elementary quantum fields, these wave packets have a well-defined center-of-mass momentum and overall number density (usually one quasiparticle), but their internal wave function can be very complex. Clearly, the scattering simulation must include strategies to build these states (and control their momentum) by carefully manipulating the elementary quantum fields encoded as qudits, starting from the (entangled) dressed vacuum. Proposals to achieve such input-state preparation have been put forward, for instance, by tailoring variational tensor networks directly onto the experimental platform, also known as quantum tensor networks [58–60], but the optimal general strategy has yet to be identified, and requires further investigation. Notice that this problem will remain when it becomes possible to study scattering processes in future quantum processors. Thus, any partial or final solution developed for TNs will be highly valuable also for future quantum computations and the simulation of scattering processes. We mention in passing that other real-time phenomena, such as quenching—see, for example, Refs. [18,61]—have also been studied with quantum tensor network techniques.

2. (2 + 1)D QED

As mentioned in Sec. I, (2+1)D QED is one of the simplest quantum field theories that nevertheless retain interesting physics: for example, it shares with QCD important properties such as asymptotic freedom and confinement, and it is an excellent starting point for future analysis of more intricate theories. We therefore propose (2+1)D QED as a very suitable benchmark and test-bed model to explore the potential of quantum computing and, in particular, to compare it with TN calculations.

The most used classical method to study lattice gauge theories numerically nowadays is the Markov chain Monte Carlo (MCMC) approach; see the recent FLAG review [62]. While the MCMC approach can reach lattice sizes on the order of $100^3 \times 200$, which are currently unthinkable for QC and TN techniques, the Hamiltonian formulation used for the latter methods has several advantages. For example, the MCMC approach suffers from very long autocorrelation times towards the continuum limit [63]. In the regime of small to very small lattice spacing, we can take advantage of quantum computing or tensor network approaches, which do not have this drawback.

Furthermore, the Euclidean path integral used in the MCMC approach is afflicted by the infamous sign problem [6], which limits studies to small values of fermion densities, rendering many physically interesting scenarios inaccessible. More specifically for lattice QCD, this prevents the exploration and characterization of regions of the phase diagram at nonzero baryon density, which are relevant to understand the early universe, neutron stars, or the transition to a quark-gluon plasma. Another important aspect is the limitation for classical MCMC techniques in the presence of a topological θ term that, in stark contrast, can be treated straightforwardly in the Hamiltonian formulation, i.e., with QC or TN. In particular, since direct MCMC methods are extremely difficult in the presence of the θ term, this term is considered in the valence sector as part of the observable, for example, through an expansion in the θ parameter [64] or with use of the gradient flow [65]. Finally, a Hamiltonian approach will enable the study of real-time phenomena such as scattering processes, thermalization, or the dynamics of physical systems after quenching; see the discussion in Sec. I and below.

Although we are fully aware of the advancements of TNs [11], in the spirit of this paper, we focus on the quantum computing approach to study quantum field theories and, in particular, on the example of (2+1)D QED.

Another pillar of quantum information science and technology is analog quantum simulators [38,66,67], which allow direct experimental access to various quantum many-body phenomena. Given recent advancements in quantum-simulator technology, such as single-atom resolution through gas microscopes [68–70] and overall high levels of precision and control [71], quantum simulators have become an attractive means by which to probe high-energy phenomena [10,42,72–74], affording the precious advantage of accessible temporal snapshots at any stage of the system dynamics. The *modus operandi* of quantum simulators is to map a *target model* described by a Hamiltonian \hat{H}_0 onto another quantum model amenable for realization in an experimental platform; see Appendix C for a simple example. This mapping is almost never exact but will lead to an effective model where \hat{H}_0 occurs up to leading order in perturbation theory, along with (undesired) subleading terms $\lambda\hat{H}_1$, with strength $\lambda < 1$. In the context of gauge theories, the model \hat{H}_0 hosts a gauge symmetry generated by local operators \hat{G}_j , while \hat{H}_1 explicitly breaks it.

Initially, quantum simulators of gauge theories with both matter and gauge degrees of freedom were restricted to cold-atom realizations of building blocks for the \mathbb{Z}_2 [75] and U(1) [76] gauge groups. The experiment reported in Ref. [75] used two species of bosonic cold atoms in a double-well potential. Periodic driving resonant at the on-site interaction strength and with the appropriate fine-tuning of the modulation parameters resulted in an

effective Floquet Hamiltonian with the desired \mathbb{Z}_2 gauge symmetry. On the other hand, the experiment reported in Ref. [76] used interspecies spin-changing collisions to model the gauge-invariant coupling between matter and gauge fields. Although groundbreaking in their own right, these experiments were restricted to building blocks and suffered from uncontrolled subleading gauge-noninvariant processes that limited useful coherent times [77].

To probe gauge-theory physics relevant to high-energy phenomena, it became essential to devise experimentally feasible methods that could enable large-scale implementations on quantum simulators involving both matter and gauge degrees of freedom. A first step was achieved in this direction by the mapping of a spin-1/2 U(1) quantum link model (QLM), with both matter and gauge degrees of freedom, onto a 71-site tilted Bose-Hubbard optical superlattice quantum simulator [78]. Stabilized gauge invariance was certified by adiabatic sweeping through Coleman’s phase transition and observation of a gauge violation of less than 10% throughout the entire dynamics. This setup was then used to study thermalization in the U(1) quantum link model [79,80], and was further extended to probe rich quantum many-body scattering regimes in this gauge theory [81]. Extensions of this large-scale platform with linear gauge protection have been proposed for higher spatial dimensions [82] and for larger spin representations of the gauge field [83].

It is also worth mentioning another method that has enabled quantum simulators of gauge theories beyond building blocks, which is to use Gauss’s law to integrate out either the matter fields or the gauge fields [49,84,85].

To be more concrete, in what follows we consider the formulation of QED on a two-dimensional space lattice with lattice spacing a . Note that moving directly to the paragraph following Eq. (7) will not hinder the comprehension of the rest of this section. Since the Hamiltonian formalism is to be considered for its eventual application on quantum devices, an encoding needs to be applied to represent the fermionic and gauge degrees of freedom, which cannot be fully eliminated in $2 + 1$ dimensions. To deal with the fermionic *doubling problem* [86–88], i.e., the existence in d dimensions of 2^d flavors (or tastes) for each physical particle, many different discretizations have been considered. One of the most used is the Kogut-Susskind formulation [7], which separates fermionic and antifermionic degrees of freedom and assigns them to alternate sites of the lattice. Therefore, the fermions and antifermions are associated with a single component field operator $\hat{\phi}_{\vec{n}}$, with $\vec{n} = (n_x, n_y)$ as the coordinates of the lattice sites. The parity of the coordinate $n_x + n_y$ determines the type of matter associated with the site (i.e., with particles (antiparticles) placed on even (odd) sites).

The links of the lattice are identified by a site \vec{n} and a direction $\mu = x, y$ emanating from that site. The electric

field operators for each link $\hat{E}_{\vec{n},\mu}$ have integer eigenvalues, $\hat{E}_{\vec{n},\mu} |e_{\vec{n},\mu}\rangle = e_{\vec{n},\mu} |e_{\vec{n},\mu}\rangle$, with $e_{\vec{n},\mu} \in \mathbb{Z}$. On the links, we also define the unitary link operators

$$\hat{U}_{\vec{n},\mu} = e^{iag\hat{A}_{\vec{n},\mu}}, \quad (1)$$

where $\hat{A}_{\vec{n},\mu}$ is one of the spatial components of the vector field residing on the link emanating from vertex \vec{n} in direction μ , and g is the coupling constant. The operators $\hat{A}_{\vec{n},\mu}$ and $\hat{E}_{\vec{n},\mu}$ are canonical conjugates, resulting in the commutation relation

$$[\hat{E}_{\vec{n},\mu}, \hat{U}_{\vec{n}',\nu}] = \delta_{\vec{n},\vec{n}'} \delta_{\mu,\nu} \hat{U}_{\vec{n},\mu}. \quad (2)$$

Therefore, $\hat{U}_{\vec{n},\mu}$ acts as a raising operator on the electric field eigenstates—namely, $\hat{U}_{\vec{n},\mu} |e_{\vec{n},\mu}\rangle = |e_{\vec{n},\mu} + 1\rangle$. Physically, $\hat{U}_{\vec{n},\mu}$ measures the phase proportional to the coupling acquired by a unit charge moved along a link. The commutation relation in Eq. (2) together with the unitarity of $\hat{U}_{\vec{n},\mu}$ implies that the Hilbert spaces for the links are infinite dimensional. For practical simulations it is thus necessary to truncate the link Hilbert spaces to a finite dimension. After introduction of a proper discretization of the $U(1)$ group, it is possible to represent the gauge fields with a finite number of qubits. The truncation has to be chosen large enough to avoid noticeable effects for the parameter regime one intends to study.

The Hamiltonian can thus be written as [87]

$$\hat{H}_{\text{tot}} = \hat{H}_E + \hat{H}_B + \hat{H}_m + \hat{H}_{\text{kin}}, \quad (3)$$

where for the rest of the section we set the lattice spacing $a = 1$ without loss of generality. The first term in Eq. (3) is related to the electric interaction,

$$\hat{H}_E = \frac{g^2}{2} \sum_{\vec{n},\mu} \hat{E}_{\vec{n},\mu}^2, \quad (4)$$

where the first sum is over all lattice sites and the second sum is over the different directions of $\mu = x, y$ of the two-dimensional spatial lattice. The second term in Eq. (3) defines the magnetic interaction,

$$\hat{H}_B = -\frac{1}{2g^2} \sum_{\vec{n}} \left(\hat{P}_{\vec{n}} + \hat{P}_{\vec{n}}^\dagger \right), \quad (5)$$

where $\hat{P}_{\vec{n}} = \hat{U}_{\vec{n},x} \hat{U}_{\vec{n}+x,y} \hat{U}_{\vec{n}+y,x}^\dagger \hat{U}_{\vec{n},y}^\dagger$, and $\vec{n} + x$ and $\vec{n} + y$ are shorthand notation for $(n_x + 1, n_y)$ and $(n_x, n_y + 1)$. The operator $\hat{P}_{\vec{n}}$ is called the ‘‘plaquette operator’’ as it involves the product of link operators along a plaquette of the lattice. The third term corresponds to the fermionic mass

term,

$$\hat{H}_m = m \sum_{\vec{n}} (-1)^{n_x+n_y} \hat{\phi}_{\vec{n}}^\dagger \hat{\phi}_{\vec{n}}, \quad (6)$$

with m the bare fermion mass, and we have the sign factor taking into account the parity of the site, as in the Kogut-Susskind formulation the particles (antiparticles) are separated to even (odd) sites. The final term in Eq. (3) represents the kinetic energy of the fermions given by

$$\hat{H}_{\text{kin}} = \sum_{\vec{n},\mu} \frac{(-1)^{n_{xy}}}{2} \left(\hat{\phi}_{\vec{n}}^\dagger \hat{U}_{\vec{n},\mu} \hat{\phi}_{\vec{n}+x} + \text{H.c.} \right), \quad (7)$$

where for the links in the x direction $n_{xy} = 1$ and for those in the y direction $n_{xy} = (-1)^{n_x}$. The kinetic term corresponds to a fermionic hopping between neighboring sites while the gauge field is simultaneously changed on the link between the two sites.

In addition, the physical states $|\psi\rangle$ of the Hamiltonian in Eq. (3) have to fulfill Gauss’s law, for all \vec{n} , $\hat{G}_{\vec{n}} |\psi\rangle = q_{\vec{n}} |\psi\rangle$, where

$$\hat{G}_{\vec{n}} = \hat{E}_{\vec{n}-x,x} - \hat{E}_{\vec{n},x} + \hat{E}_{\vec{n}-y,y} - \hat{E}_{\vec{n},y} - \hat{Q}_{\vec{n}} \quad (8)$$

are the generators of time-independent gauge transformations, $\hat{Q}_{\vec{n}} = \hat{\phi}_{\vec{n}}^\dagger \hat{\phi}_{\vec{n}} - (1 - (-1)^{n_x+n_y})/2$ corresponds to the staggered charge operator, and $q_{\vec{n}} \in \mathbb{Z}$ represents static charges. Equation (8) corresponds to the lattice version of the divergence of the electric field being equal to the charge density.

An alternative to the Kogut-Susskind formulation is the *Wilson approach* [89,90]. It introduces a second-order derivative term in the Hamiltonian that vanishes linearly with the lattice spacing in the continuum limit. Compared with the Kogut-Susskind formulation, the Dirac spinor components of fermionic matter are not distributed to different sites, thus leading to a larger number of fermionic degrees of freedom on each vertex of the lattice. The main advantage of this approach is that the number of qubits needed to represent the gauge fields is lower than the number used in the Kogut-Susskind approach, and therefore it has a lower resource requirement [26].

One of the challenges of simulating the gauge theory with quantum computers is to find a resource-efficient mapping of all its degrees of freedom to qubits and gates. This holds, in particular, for the bosonic gauge degrees of freedom. Here several ansatzes exist in the literature [31,91–93] and it is important to test these approaches against each other, evaluate their advantages and shortcomings, and identify the most resource efficient discretization and truncation scheme.

Once we have developed the most suitable encoding, we must choose the most appropriate simulation technique depending on our goal. For example, to compute

the ground state energy (the low-lying spectrum) of our Hamiltonian, we can apply the variational quantum eigensolver (VQE) [94], variational quantum deflation [95], or the subspace-search variational quantum eigensolver [96]). Other approaches could be imaginary time evolution [97] or the creation of a suitable operator basis [98].

3. (2 + 1)D SU(2)

With the long-term goal of QCD in mind, it is important to consider non-Abelian gauge theories. A first step towards that direction can be taken by our studying the generalization of the previous lattice gauge model to the case of an SU(2) gauge group.

Below we present a brief summary of the Kogut-Susskind formulation for the case of an SU(2) LGT for the interested reader, in analogy to the discussion for the U(1) group in the previous subsection. However, skipping the upcoming paragraph will not hinder the comprehension of the remainder of this section. For a more detailed discussion, we refer the reader to Refs. [7,8]. The Kogut-Susskind Hamiltonian for the SU(2) LGT in 2 + 1 dimensions has the same structure as in the U(1) case shown in Eq. (3). Different from the case of U(1), for SU(2) we have two fermionic degrees of freedom $\hat{\phi}_{\vec{n},\alpha}$ on each vertex \vec{n} , representing the two “colors” of fermions, with the index $\alpha = 1, 2$ labeling the basis states of the fundamental representation of SU(2). Because of the non-Abelian structure of the group SU(2), the link operators $\hat{U}_{\vec{n},\mu}^{\alpha\beta}$ acting on the link emanating from vertex \vec{n} in direction μ carry now additional color indices α, β . With this notation, the kinetic term reads

$$\hat{H}_{\text{kin}} = \sum_{\vec{n},\mu} \frac{(-1)^{n_{xy}}}{2} \sum_{\alpha,\beta} \left(\hat{\phi}_{\vec{n},\alpha}^\dagger \hat{U}_{\vec{n},\mu}^{\alpha\beta} \hat{\phi}_{\vec{n}+\hat{\mu},\beta} + \text{H.c.} \right). \quad (9)$$

Compared with the U(1) case, we now have an additional sum over the color components $\alpha, \beta = 1, 2$. The mass term is given by

$$\hat{H}_m = m \sum_{\vec{n}} \sum_{\alpha} (-1)^{n_x+n_y} \hat{\phi}_{\vec{n},\alpha}^\dagger \hat{\phi}_{\vec{n},\alpha}, \quad (10)$$

where we again made the color indices explicit. The color-electric energy for the SU(2) LGT reads

$$\hat{H}_E = \frac{g^2}{2} \sum_{\vec{n},\mu} \sum_b \left(\hat{E}_{\vec{n},\mu}^b \right)^2, \quad (11)$$

where $\hat{E}_{\vec{n},\mu}^b$ is the color-electric field operator acting on the link emanating from vertex \vec{n} in direction μ . Note that $\hat{E}_{\vec{n},\mu}^b$ is given in the adjoint representation of SU(2), and the indices $b = 1, 2, 3$ label the different components of the color-electric field. In the above expression $\sum_b \left(\hat{E}_{\vec{n},\mu}^b \right)^2$ is

the Casimir operator of the group SU(2). Finally, the color-magnetic contribution to the energy is again given by the plaquette term

$$\begin{aligned} \hat{H}_B &= -\frac{1}{2g^2} \sum_{\vec{n}} \left(\hat{P}_{\vec{n}} + \hat{P}_{\vec{n}}^\dagger \right) \\ &= -\frac{1}{2g^2} \sum_{\vec{n}} \sum_{\alpha,\beta,\gamma,\delta} \left(\hat{U}_{\vec{n},x}^{\alpha\beta} \hat{U}_{\vec{n}+x,y}^{\beta\gamma} \hat{U}_{\vec{n}+y,x}^{\gamma\delta} \hat{U}_{\vec{n},y}^{\delta\alpha} + \text{H.c.} \right), \end{aligned} \quad (12)$$

where from the first line to the second line we made the plaquette operator explicit, $P_n = \sum_{\alpha,\beta,\gamma,\delta} \hat{U}_{\vec{n},x}^{\alpha\beta} \hat{U}_{\vec{n}+x,y}^{\beta\gamma} \hat{U}_{\vec{n}+y,x}^{\gamma\delta} \hat{U}_{\vec{n},y}^{\delta\alpha}$. Note that in all the Hamiltonian terms, the color indices are contracted, and thus the Hamiltonian is a color-neutral object and the physically relevant states have to be color singlets.

Again, the physical states have to fulfill Gauss’s law. In contrast to the case of U(1), for SU(2) Gauss’s law has three different components, $\hat{G}_{\vec{n}}^b$, $b = 1, 2, 3$, which do not commute among themselves, but each of them commutes with the Hamiltonian. The explicit form of Gauss’s law can be found, for example, in Refs. [29,42,48].

Compared with the case of U(1), the SU(2) LGT has a much richer structure: for example, there exist baryons, color-neutral bound states of the individual fermionic components within a single site that have no counterpart in the Abelian case [29]. Thus, the (2 + 1)D SU(2) LGT provides an ideal stepping stone towards more complicated non-Abelian theories.

The problem of simulating lattice gauge theories on a universal quantum computer using qubits as the basic degrees of freedom was defined in general terms in Ref. [24]. It was shown in Ref. [99] that, on quantum computers, lattice gauge theories in any spatial dimension scale polynomially with the number of lattice sites, the bosonic gauge field truncation threshold, and the total simulation time (i.e., number of time steps).

Other approaches use quantum simulators to emulate the physics of non-Abelian gauge theories. In these implementations, gauge invariance is a direct consequence of some underlying symmetry of the quantum simulator. For instance, angular momentum conservation is used to realize the SU(2) Yang-Mills model [39], and nuclear spin conservation in alkaline-earth atoms is used to mimic SU(N) models within the quantum link formulation [41]. In this respect, the quantum link formulation appears as a natural formulation for the quantum simulation of the non-Abelian model that was proposed within a Rydberg-based architecture [34] and within superconducting circuits [100].

The first quantum simulation of an SU(2) lattice gauge theory on IBM superconducting hardware was done

reported in Ref. [28]. Subsequently, exploratory computations were conducted for one-dimensional SU(2) on an IBM superconducting platform [29]. This implementation combined the fact that a one-dimensional theory with open boundary conditions allows one to rewrite all gauge field degrees of freedom as long-range interactions among fermions with the VQE to study both meson and baryon states. There have further been one-dimensional SU(3) quantum simulations [101–103], and error mitigation methods have been applied to study the time evolution of non-Abelian models [104].

In contrast to the one-dimensional case, studies of two-dimensional SU(2) gauge theory require both fermion and gauge field degrees of freedom. Several formulations have been proposed [105,106], and practical studies of each will provide valuable information for understanding their advantages and disadvantages.

The choice of basis for the local degrees of freedom in the implementation of a non-Abelian gauge model is important [107,108]. Usually, one needs to study the effect of discretization or truncation on the physical results of the models [109,110]. One option to discretize non-Abelian theories is to use finite-dimensional subgroups [111–113], which can be efficiently implemented within a Rydberg base architecture [114–117]. Early computations of SU(2) gauge fields on quantum hardware have used lattices with up to six plaquettes in total [28,118]. An initial study was also performed for SU(3) in Ref. [30].

Upcoming computations can build upon the lessons learned from these first steps, and grow in scale and scope alongside the continuing progress in quantum hardware deployment in the noisy intermediate-scale quantum era.

4. Quantum link models and D-theory

D-theory is an alternative formulation of lattice field theory in which continuous, classical fields are replaced by *discrete*, quantum degrees of freedom, which undergo *dimensional reduction* from an extra dimension of short extent [119]. In the D-theory approach, lattice gauge theories are realized via quantum link models [120–125]. Quantum links are generalized quantum spins endowed with an exact gauge symmetry, which is located on the links of a spatial lattice.

Quantum links reside in finite-dimensional irreducible representations of an embedding algebra. This is in contrast to the standard Wilson-type lattice gauge theory, which is based on an infinite-dimensional representation on each link. Quantum links with a U(N) or an SU(N) gauge group reside in the embedding algebra SU(2N). In particular, U(1) quantum link models are formulated with ordinary SU(2) quantum spins. SO(N) and Sp(N) quantum link models are realized with an SO(2N) and Sp(2N) embedding algebra, respectively. Since SU(2) = Sp(1), an

SU(2) quantum link model can be realized with a simple Sp(2) = SO(5) embedding algebra.

The simplest Abelian U(1) quantum link model is realized with ordinary quantum spins of 1/2, which can be embodied by individual qubits. These dynamics have already been represented by quantum circuits in a resource-efficient manner [126]. The implementation of the U(1) quantum link model on a triangular lattice is particularly simple, because it takes advantage, for instance, of the heavy hexagonal lattice topology underlying the 127-qubit IBM Eagle chip [127]. By use of manifestly gauge invariant height variables, which are embodied by qubits residing on a dual hexagonal lattice, the dynamics is realized with a rather short quantum circuit.

The simplest non-Abelian SU(2) quantum link model uses the embedding algebra Sp(2) = SO(5), which has a four-dimensional fundamental representation that can be embodied by a pair of qubits residing on each lattice link. By an exact duality transformation, this SU(2) quantum link model can be expressed in terms of Z(2)-valued height variables, which can even be embodied by individual qubits [128]. This model is also interesting from a condensed matter perspective, because it is closely related to the quantum dimer model on the kagome lattice, which has a rich, nontrivial phase structure. It would be very interesting to construct a quantum circuit, similar to the one for the U(1) quantum link model on the triangular lattice, to perform quantum computations of the real-time dynamics of SU(2) gauge theories. It is worth mentioning that while the proposed QED calculations will remain far from the continuum limit, they will nevertheless provide important feedback on how to efficiently tackle larger-scale simulations.

5. (1 + 1)D CP(N – 1) models from (2 + 1)D SU(N) quantum spin ladders

(1+1)D CP(N – 1) quantum field theories are toy models that share many important features with (3+1)D QCD: they are asymptotically free, have a nonperturbatively generated mass gap, and θ -vacua [129,130]. In addition, they have nontrivial phase structure at nonzero chemical potential, including Bose-Einstein condensates with and without ferromagnetism [131].

The standard lattice formulation of CP(N – 1) models at nonzero vacuum angle or at nonzero chemical potential suffers from similar sign and complex action problems as QCD itself. D-theory offers an alternative approach to standard lattice field theory, and uses discrete quantum (rather than continuous classical) degrees of freedom without compromising exact continuous symmetries, including gauge symmetry. In asymptotically free theories [including (1+1)D CP(N – 1) models and (3+1)D QCD], the continuum limit is reached naturally (i.e., without any fine-tuning) via dimensional reduction from a

higher-dimensional space-time, with a short extent of the extra dimension. Interestingly, the finite-density and θ -vacuum sign problems of the standard formulation have already been overcome by the alternative D-theory formulation, in which $\mathbb{CP}(N-1)$ models are regularized with use of $SU(N)$ quantum spin degrees of freedom [132]. This formulation is also amenable to analog quantum simulations with ultracold alkaline-earth atoms in optical lattices, which holds the promise to facilitate real-time simulations of their dynamics [133]. $\mathbb{CP}(N-1)$ models in the D-theory formulation are ideally suited as a testing ground for quantum computation, because, on the one hand, at least in some cases, advanced classical computational techniques are available for validation, and, on the other hand, similar methods can be developed for lattice gauge theories, ultimately aiming at QCD, in particular in the quantum link formulation. The strategy behind D-theory—namely, to formulate quantum field theory directly in terms of quantum degrees of freedom—is ideally suited for both quantum simulation and quantum computation.

The standard formulation of $\mathbb{CP}(N-1)$ models uses classical, Hermitean, idempotent $N \times N$ matrix fields $P(x)$,

$$P(x)^\dagger = P(x), \quad P(x)^2 = P(x), \quad \text{Tr}P(x) = 1, \quad (13)$$

with the Euclidean action

$$S[P] = \int d^2x \frac{1}{g^2} \text{Tr} [\partial_\mu P \partial_\mu P] + i\theta Q[P] \quad (14)$$

and the integer-valued topological charge

$$Q[P] = \frac{1}{\pi i} \int d^2x \epsilon_{\mu\nu} \text{Tr} [P \partial_\mu P \partial_\nu P] \\ \in \Pi_2[\mathbb{CP}(N-1)] = \mathbb{Z}. \quad (15)$$

The model is invariant under a global $SU(N)$ symmetry, $P(x)' = \Omega P(x) \Omega^\dagger$, $\Omega \in SU(N)$.

The alternative D-theory formulation replaces the classical field $P(x)$ by $SU(N)$ quantum spins T_x^a ($a \in \{1, 2, \dots, N^2 - 1\}$) that obey the commutation relation

$$[T_x^a, T_{x'}^b] = i\delta_{xx'} f_{abc} T_x^c \quad (16)$$

and reside on a two-dimensional spatial square lattice (of spacing a) with a long x_1 direction (of extent L with periodic boundary conditions) and a short x_2 -direction (of extent L' with open boundary conditions). The even-parity sites $x \in A$ (with even $x_1 + x_2$) carry the fundamental representation $\{N\}$, $T_x^a = \lambda^a/2$ (where the λ^a are Gell-Mann matrices), while the odd-parity sites $y \in B$ carry the anti-fundamental representation $\{\bar{N}\}$, $\bar{T}_y^a = -\lambda^{a*}/2$. An antiferromagnetic $SU(N)$ quantum spin ladder (with $J > 0$) is

then described by the nearest-neighbor Hamiltonian

$$H = J \sum_{\langle xy \rangle} T_x^a \otimes \bar{T}_y^a, \quad (17)$$

which commutes with the total $SU(N)$ spin $T^a = \sum_{x \in A} T_x^a + \sum_{y \in B} \bar{T}_y^a$. In the presence of chemical potentials μ_a at inverse temperature β , the grand canonical partition function then takes the form

$$Z = \text{Tr} \exp(-\beta(H - \mu_a T^a)). \quad (18)$$

Remarkably, this antiferromagnetic quantum spin ladder is a proper regularization for the (1+1)D $\mathbb{CP}(N-1)$ quantum field theory. An even extent L'/a of the short dimension corresponds to vacuum angle $\theta = 0$, while an odd extent implies $\theta = \pi$. For $L = L' = \beta = \infty$, the quantum antiferromagnet breaks the global $SU(N)$ symmetry down to $U(N-1)$ (at least for $N \leq 4$). This gives rise to dynamically generated, effective Goldstone boson fields $P(x)$ that reside in the coset space $SU(N)/U(N-1) = \mathbb{CP}(N-1)$. Once L' is made finite, the Mermin-Wagner theorem implies that $SU(N)$ can no longer break spontaneously. As a result, the previously massless Goldstone bosons pick up an exponentially small mass proportional to $\exp(-4\pi L' \rho_s/cN)$, where ρ_s is the spin stiffness and c is the spin-wave velocity. For moderately large $L'/a \gtrsim 4$, the corresponding correlation length $\exp(4\pi L' \rho_s/cN) \gg L'$ exceeds the extent of the short dimension and the system dimensionally reduces to the (1+1)D $\mathbb{CP}(N-1)$ model. These dynamics, which may seem complicated at first glance, have been verified in great detail in quantum Monte Carlo simulations using classical computers. Already at the level of classical computation, the use of discrete quantum, rather than continuous classical, fundamental degrees of freedom has led to numerous algorithmic advantages, which facilitated efficient numerical simulations of θ -vacua and dense matter systems [131, 132].

Analog quantum simulators for the $SU(N)$ quantum antiferromagnet have already been designed, with use of ultracold alkaline-earth atoms in an optical lattice, and are ready to be realized in the laboratory today [133]. This holds the promise to address the real-time dynamics, which remains inaccessible to classical simulation techniques. This would be the first time that an asymptotically free quantum field theory is studied with quantum simulation. The simple nature of the quantum spin degrees of freedom and the ultralocal form of their Hamiltonian strongly suggest one could also explore $\mathbb{CP}(N-1)$ models using digital quantum computation. In particular, in D-theory the $\mathbb{CP}(1)$ model with a global $SU(2)$ symmetry is regularized with ordinary $SU(2)$ quantum spins that can be embodied directly by individual qubits. Similarly, the $SU(3)$ quantum spins in the D-theory formulation of the $\mathbb{CP}(2)$ model are nothing but qutrits. The corresponding Hamiltonian dynamics can be realized with sequences

of single-qubit and two-qubit (or single-qutrit and two-qutrit) quantum gates. It is possible—and already quite interesting—to work with quantum spin chains (i.e., with $L'/a = 1$) rather than with quantum spin ladders ($L'/a > 1$). In particular, for $L'/a = 1$ the antiferromagnetic SU(2) quantum spin chain corresponds to the (1+1)D Wess-Zumino-Novikov-Witten conformal quantum field theory in the continuum limit. The corresponding SU(3) quantum spin system, although it is not in the continuum limit, describes a strongly coupled CP(2) model at a first-order phase transition with spontaneously broken charge conjugation symmetry. This would allow, for example, real-time studies of false vacuum decay.

6. Collective neutrino oscillations

Neutrinos play a central role in extreme astrophysical events such as core-collapse supernovae and neutron star binary mergers as they dominate the transport of energy, entropy, and lepton number. Because neutrinos have mass and because the mass basis, denoted by $\{| \nu_i \rangle\}_{i=1,2,3}$, is different from the flavor basis, neutrinos will experience oscillations in the population of the different flavors components (ν_e, ν_μ, ν_τ).

Given the importance of charge-current reactions, a detailed understanding of flavor oscillations in these settings is critical to predict their dynamical evolution. Given the high density of neutrinos in these environments, flavor oscillations are strongly affected by two-body neutrino-neutrino interactions, which render the neutrino cloud a strongly coupled many-body system. Direct solution of the evolution equations for general initial conditions can be exponentially hard with classical simulations, and the conventional approach is to rely on mean-field approximations [134–136], which, however, do not include direct scattering between neutrinos. Efforts to go beyond mean-field approximations with classical computers were recently reviewed in Ref. [137].

The complexity of neutrino physics persists even with the simplifying assumption that only two flavors (the electron flavor ν_e and one heavy flavor ν_x) participate in the oscillation. With this assumption, one can model each neutrino as a single two-level system and obtain the following Hamiltonian [138]:

$$H = \sum_{i=1}^N \mathbf{b}_i \cdot \boldsymbol{\sigma}_i + \lambda_e \sum_{i=1}^N \sigma_i^z + \frac{\mu}{2N} \sum_{i < j}^N (1 - \cos(\theta_{ij})) \boldsymbol{\sigma}_i \cdot \boldsymbol{\sigma}_j, \quad (19)$$

where $\boldsymbol{\sigma}_i = (\sigma_i^x, \sigma_i^y, \sigma_i^z)$ is a vector of Pauli matrices acting on the i th neutrino. The first term in Eq. (19) describes vacuum oscillations around the mass basis

with $\mathbf{b}_i = \delta m^2 / 4E_i (\sin(2\theta_v), 0, -\cos(2\theta_v))$, where $\delta m^2 = m_2^2 - m_1^2$ is the square mass difference between mass eigenstates, θ_v is the mixing angle, and E_i is the energy of the i th neutrino. The second term in Eq. (19) is generated by charge-current scattering with a background of electrons with coupling constant $\lambda_e = \sqrt{2}G_F n_e$, with G_F the Fermi constant and n_e the electron density. This is the term responsible for the Mikheyev-Smirnov-Wolfenstein (MSW) effect due to the interaction of electrons with neutrinos experienced by neutrinos traveling in dense matter. Finally, the third term in Eq. (19) is the neutrino-neutrino interaction generated by neutral-current weak reactions. Its coupling constant $\mu = \sqrt{2}G_F n_\nu$ is directly proportional to the local neutrino density n_ν , while the angular factor inside the sum encodes the spatial geometry of the problem through its dependence on the relative angle of propagation $\cos(\theta_{ij}) = \mathbf{p}_i \cdot \mathbf{p}_j / (\|\mathbf{p}_i\| \|\mathbf{p}_j\|)$, where \mathbf{p}_i is the momentum of the i th neutrino. This term prevents collinear neutrinos from interacting.

The Hamiltonian in Eq. (19) can be used to describe the flavor evolution of a homogeneous gas of neutrinos at fixed density. Most neutrinos, however, leave the explosion region of the emitter (neutron stars, etc.) where they were generated and thus experience different local conditions as they move out. This can be incorporated by one allowing the coupling constants λ_e and μ to change with the distance r from their emission, or equivalently with the time t since they left the neutrino sphere (neutrinos are considered as ultrarelativistic particles moving at approximately the speed of light). With this, we are left with describing the nonequilibrium evolution of a large number of fermions interacting through an eventually nonadiabatic two-body Hamiltonian. Several extensions are possible to account, for example, for the full three-flavor structure [139] or the presence of inhomogeneities [140] but are likely beyond the scope of hardware with about 100 qubits capable of executing several thousand two-qubit gates.

Current efforts to study the full many-body flavor dynamics generated by the Hamiltonian in Eq. (19) beyond the mean-field approximation have been made under a number of additional simplifying assumptions. A popular one is to consider an average interaction strength, effectively removing the angular dependence in the two-body interaction, turning it into a term proportional to the square of the total angular momentum. This has the effect that the system becomes integrable with use of the Bethe ansatz [138], and classical simulations were performed in the past exploiting directly this property up to $N = 9$ [141]. Use of more direct integration approaches allowed $N = 16$ to be reached [142], while with use of matrix product states together with the time-dependent variational principle systems up to $N = 20$ were studied while maintaining good convergence with the bond dimension [143]. The latter simulations used around 10^5 time steps for the entire calculation, and this leaves a direct comparison possibly

out of range of hardware with around 100 qubits that can run a few thousand two-qubit gates.

Another common assumption is to ignore the MSW term proportional to the electron density using the argument that this coupling constant greatly dominates in the interior regions, where many-body effects are expected to be important. The MSW term can be eliminated with use of a rotating-wave approximation that ultimately produces a lower effective mixing angle. In general, this is not necessary as this one-body term can be trivially fast-forwarded and included correctly, and efficiently, in the simulation by one resorting to interaction picture schemes such as the one proposed in Ref. [144]. In the absence of this term, the Hamiltonian enjoys a global $U(1)$ symmetry generated by rotations around the mass basis that can be used to reduce the implementation cost. This strategy was used in Ref. [145], together with the use of IBM QISKIT's isometry function to implement evolution in each sub-block to study flavor oscillations in systems of up to $N = 4$ neutrinos. The approach has the advantage that the circuit depth does not increase as a function of the time step, but for large system sizes it would require an exponentially large number of gates. Part of the difficulty in including the two-body interaction is its all-to-all nature, which naively does not fit well on devices with reduced connectivity. The problem can, however, be circumvented by the use of an appropriate SWAP network scheme producing a circuit with N layers of $N/2$ nearest-neighbor two-qubit gates each. This approach was proposed in Ref. [146], where a simulation with $N = 4$ neutrinos with a single Trotter step was performed on IBM devices and has been shown to be advantageous to allow classical simulations using matrix product states [147]. Platforms that allow all-to-all connectivity, such as trapped ions, allow more flexibility but require a similar number of two-qubit operations. Because of their current higher fidelity, simulations have been reported for up to ten time steps with $N = 4$ neutrinos and for one time step for up to $N = 12$ neutrinos [148,149]. Approaches using quantum annealers have also been proposed and applied for systems up to $N = 4$ [150].

The simplified neutrino oscillation problem described by Eq. (19) is encoded quite naturally on a digital quantum computer with one qubit per neutrino. Current attempts to describe neutrinos on these platforms are still restricted to small N values with rather simple initial conditions, usually wave functions describing noncorrelated neutrinos. Besides the description of larger neutrino number, challenges for future applications include the extension to more realistic initial conditions such as initially thermalized neutrinos, or the evolution of these correlated systems over longer time to extract, for instance, asymptotic entanglement between neutrinos or characterize the relaxation dynamics to thermal states [151]. Time evolution requires efficient algorithms to simulate the dynamics (see Sec. III A). A first-order product formula (PF) step

for N neutrinos costs $3N(N - 1)/2$ controlled NOT (CNOT) gate operations, while a second-order step will cost $3(N^2 - 3N/2 + 1)$ CNOT gates [148]. The depths are instead $3N$ and $6N - 3$, respectively (see also Table I).

The implementation can be performed in a more hardware efficient way by use of cross-resonance gates instead at the price of increasing the decomposition error. Furthermore, a hardware-friendly approach to multi-product formulas can further reduce circuit depth and increase simulation accuracy [152]. An additional possibility worth pursuing in the short term is the use of approaches based on variational time evolution (VTE), which allow for a circuit depth independent of the evolution time.

B. Selected applications for experiments

High-energy physics experiments are characterized by the need to process a large amount of complex, highly structured data. Historically, large collaborations have relied on massively parallel computing infrastructure and pioneered the field of distributed computing with the LHC Computing Grid. The need to search for processes with a small production cross section together with the use of next-generation detectors generates datasets of large size to analyze, which requires a new computing model, more efficient algorithms—including data-driven techniques such as artificial intelligence—and the integration of new hardware beyond the von Neumann architectures. It is in this context that investigations into the introduction of quantum computing in HEP experiments is framed: the community is looking into accelerating or improving the different steps of the data analysis and data processing chains. Currently most of the work is focused on the development and optimization of quantum machine learning (QML) algorithms implemented either as quantum neural networks (variational algorithms) or as kernel methods [153,154]. See Appendix E for a summary of these methods. The next section provides an overview of the range of algorithms under study as applied to HEP and their present limitations.

It is important to notice, however, that evaluation of the performance of QML algorithms on HEP data requires care: realistic applications have requirements that cannot be easily accommodated on quantum devices today. The most critical issue is related to the size of the data samples, together with their complexity. Indeed, studies on the introduction of quantum algorithms (and QML in particular) need to take into account both the total number of events that need to be analyzed (which can easily reach hundreds of thousands) and the large number of input features in each single event (typically on the order of tens or hundreds). The preferred approach today is a hybrid approach: A classical feature extraction and/or dimensionality reduction step is used to bring the classical input to a size that can be realistically embedded on noisy, near-term quantum hardware. Depending on the complexity of

both the dataset and the task, different methods are used, ranging from linear principal component analysis (PCA) to nonlinear trainable embedding or compression methods (autoencoders or other artificial intelligence–based techniques) [155]. The advantage of the latter is clearly their versatility and the possibility to train them together with the quantum algorithms for the specific task at hand.

In particular, trainable techniques allow an end-to-end optimization of the reduced data representation (often referred to as “latent representation”), their embedding in quantum states, and the quantum algorithm itself. A binary classification problem, such as the separation of signal versus uninteresting background, is a common example: simultaneously training an autoencoder for data compression together with the corresponding classifier ensures that the resulting latent representation exhibits maximal separation between the two classes. Multiple examples have already proven the advantage of this approach in both the classical domain and the quantum domain [156–161]. In addition, a critical part of the quantum algorithm design and optimization process is aimed at reducing the number of input features needed by the quantum algorithm in order to perform its task, together with the definition of a minimal training set, which still ensures convergence and generalization capabilities.

Finally, the compressed classical data are embedded, or loaded, onto quantum states for processing by the QML algorithm. This step is commonly referred to as the “state preparation step.” Different techniques have been studied [162] that are a compromise between an optimal use of qubit states, exploiting in full the potential exponential advantage, and the need to efficiently map state preparation circuits on noisy devices. In general, the choice of the data-embedding strategy has an effect both on the performance of the overall algorithm and on its interpretation (as, for example, in the kernel formalism) as mentioned in Sec. III.

Taken together, these steps have made possible the design and implementation of quantum algorithms for most of the tasks in the typical data processing chain, albeit at a reduced scale. Access to the $100 \otimes 100$ quantum hardware, combined with data reduction techniques, is likely to bring current prototypes to a much more realistic size. An overview of the proposed applications for data analysis in HEP experiments together with the associated quantum algorithms is given in the lower panel in Fig. 1.

1. Rare signal extraction

Extracting rare signals from background events is an essential part of data analysis in the search for new phenomena in HEP experiments. In this section we cover algorithms, methods, and limitations of this area of research, giving some references, which, for sure, do not represent a complete picture of the state of the art.

Posed as a classification task, rare signal extraction faces an imbalance problem in the number of samples belonging to the signal class versus the number of samples from the background class. Entry-level cases are the ones where a single feature is powerful enough to discriminate the process of interest, while more complicated cases rely on multivariate analysis of many features to get to a reasonable level of discrimination power.

In the machine learning community, techniques for learning from imbalanced data are well established, and for the HEP case, analysis methods developed in Refs. [163, 164] have been effectively implemented. An alternative approach to classification with imbalance techniques is anomaly detection [165,166]. In the following we touch upon some modern class imbalance techniques adopted in the community, focusing on novel loss functions and data resampling techniques. However, the main goal here is not merely the classification task but also the generation of predictions with their corresponding uncertainties. In particle physics, as in other scientific domains, if uncertainties are not presented, the picture is almost incomplete.

Use of the accuracy of a classifier as a metric for rare events can be misleading as it says nothing about the signal, in terms of distribution and feature importance. The receiver operating characteristic curve is a good general-purpose metric, providing information about the true and false positive rates across a range of thresholds, and the area under the receiver operating characteristic curve is a good general-purpose single-number metric. Nevertheless, when one is dealing with imbalanced data, the precision-recall curve is the preferred metric, where the recall represents a measure of how many true signal events have actually been identified as a signal and precision quantifies how likely an event is to truly be a signal and depends on how rare the signal is. Different strategies can be used, such as undersampling the majority class or oversampling the minority class, where the former is preferred because of the potential overfitting resulting from oversampling [167]. Moreover, the standard algorithm can be modified by one adjusting the hyperparameters of the loss and by adding an additional penalty for misclassification. For instance, following Ref. [168], a modified version of the cross-entropy loss function used for binary classification to differentiate between easy-to-classify and hard-to-classify samples is the focal loss function (LF):

$$L = -(1 - p_t)^\gamma \log_{10}(p_t), \quad (20)$$

where p_t is the model’s estimated probability that a given event belongs to the signal class and γ is the modulating parameter. As γ is increased, the rate at which easy-to-classify samples are down-weighted also increases. As pointed out previously, not only should the classification be efficient but also predict outcomes with low uncertainty. Current approaches for this include dropout training

in deep neural networks as approximate Bayesian inference, variance estimation across an ensemble of trained deep neural networks, and the probabilistic random forest algorithm [169]. For example, such techniques have been used in the measurement of the longitudinal polarization fraction in same-sign WW scattering [170] and for the decay of the Higgs boson to charm-quark pairs [171].

Same-sign WW production at the LHC is the vector boson scattering process with the largest ratio of electroweak-to-QCD production. As such it provides a great opportunity to study whether the discovered Higgs boson leads to unitary longitudinal vector boson scattering, and to search for physics beyond the Standard Model (BSM). Confirming or refuting the unitarity of vector boson scattering requires not just a measurement of $pp \rightarrow jjW \pm W \pm$ but also of the fraction of these events where both W bosons are longitudinally polarized (LL fraction). The fraction of longitudinally polarized events is predicted to be only a fraction (0.07) of the total number of events in the Standard Model at large dijet invariant mass (m_{jj}) [170], making this a challenging measurement. Common techniques for this kind of use case include a random forest with imbalanced implementation, a gradient-boosted decision tree, and deep learning models with a standard or focal loss function. Overall, all of the machine learning models significantly outperform the kinematic variables approach [172].

The second application of class imbalance techniques is the measurement of Higgs boson decays to charm-quark pairs. Searches for the decay of the Higgs boson to charm-quark pairs have produced only weak limits to date. Again, one of the reasons for this poor performance is that in the Standard Model the rate for $h \rightarrow b\bar{b}$ is about 20 times larger than the rate for $h \rightarrow c\bar{c}$. The standard approach relies on tagging the flavor of the jets, which involves discriminating charm-initiated jets from bottom jets, or vice versa. The primary technique used currently in this case is boosted decision trees, mainly structured as binary classification problem, where the community effort is devoted to the definition of *ad hoc* flavor tagging through the use of the class imbalance techniques instead of general-purpose ones [171].

It is natural to ask whether quantum computing algorithms could be used to support these complicated tasks. However, it is not evident where a quantum algorithm could provide a systematic advantage with respect to these classical approaches. Possible directions of research should answer the following questions: Can we overcome the problem of lack of density or insufficiency of information for these problems? Can we better explore and analyze the feature space that describes those problems? Could QML methods, which use quantum models to encode input data into a high-dimensional Hilbert space and extract physical properties of interest from the quantum state, be an alternative approach to signal detection? A particularly

intriguing direction for quantum approaches here could be the possibility of performing training directly on experimental data [173] that can be directly analyzed as quantum data.

Overall, in the absence of a clear hint of new physics in HEP experiments, a data-driven, model-agnostic search for rare signals has gained considerable interest. Anomaly detection, realized with use of unsupervised machine learning, is the most commonly used technique and will continuously become important in HEP analysis workflow. The feasibility of anomaly detection was investigated in Ref. [174] with a variational quantum algorithm (VQA)-based quantum autoencoder (QAE). With the benchmark process of $pp \rightarrow H \rightarrow t\bar{t}$ for the signal, the QAE performance for anomaly detection was compared with that from a classical autoencoder, showing faster convergence in the quantum case. Recently, Schuhmacher *et al.* [175] found that with the use of a quantum support vector classifier trained to identify the artificial anomalies, it is possible to identify realistic BSM events with high accuracy. In parallel, they also explored the potential of quantum algorithms for increasing the classification accuracy and provided plausible conditions for the best exploitation of this novel computational paradigm. Additionally, Wozniak *et al.* [159] found evidence that quantum anomaly detection with a quantum-enhanced support vector machine (QSVM) could outperform the best classical counterpart. In Ref. [176] an anomaly quantum generative adversarial network (QGAN) was introduced to identify anomalous events (BSM particles). Interestingly, this model can achieve the same anomaly detection accuracy as its classical counterpart using 10 times fewer training data points.

Overall, current quantum-classical hybrid QML for rare signal extraction is largely based on two algorithms: VQA [177] and QSVM with the kernel method [178,179]. The quantum kernel-based QSVM has the potential for good trainability due to a convex cost-function landscape, and this property could be beneficial for noisy quantum hardware. However, the kernel function would exponentially concentrate to a fixed value with the number of qubits unless the quantum feature map is properly designed [180], analogously to the barren plateau in the VQA.

VQA-based QML methods are generally known to be affected by the infamous barren plateau problem, where a nonconvex landscape of the cost function causes the gradients to vanish exponentially in the number of qubits, as detailed in Sec. III B 2. On current noisy hardware, overcoming barren plateaus may be critical for QML applications to signal extraction. The approach based on so-called geometrical quantum machine learning, which exploits prior knowledge of the problem, such as symmetry presented in the data at hand, will be promising for applications to HEP data analysis. However, experimental data are the result of a complex convoluted effect given

by different layers of interaction, from parton showers to detector effects. This would eventually destroy any desirable symmetry of the data. Alternatively, quantum models in an overparameterized regime may have a desirable cost landscape. This provides motivation for exploring geometrical quantum machine learning models and/or overparameterization in a realistic HEP data analysis flow. We should also pursue how efficiently a QML model can generalize to unseen test data with fewer trainable parameters or fewer training data, and also consider the possibility of reusing well-known techniques from classic machine learning, such as an ensemble, where, for instance, the effect of noise could be mediated by the structure of the algorithm [181].

2. Pattern recognition tasks: Reconstructing particle trajectories and particle jets

Multiple steps in experimental data processing can be categorized under pattern recognition. This involves associating a given set of measurements of an object (such as the raw energy measured by sensors in a detector or its spatial coordinates) with a specific instance. Examples include identifying a particle trajectory, determining a particle type, or linking a particle jet to the hadronization of a specific parton (jet). In HEP, this problem has high dimensionality, since the detector sensors are arranged in highly granular structures, the objects represent physics properties, and the object classes are typically exclusives (an energy deposition belongs to one and only one trajectory). Two examples are indeed represented by the reconstruction of charged particles and the reconstruction of jets, together with the identification of their properties.

The reconstruction of charged particle trajectories, *tracking*, is an essential ingredient in event reconstruction for HEP. Particle track candidates are built from space points corresponding to energy deposits left by charged particles—or *hits*—as they traverse the sensitive detector material. The track parameters (e.g., position and curvature) computed hereafter are used in subsequent processing steps throughout the reconstruction and analysis of data to compute physics observables.

In collider particle physics, a jet is a collection of stable particles collimated into a roughly cone-shaped region. Jets arise from the fragmentation of quarks and gluons produced in high-energy collisions. During the collision, the QCD confinement the quarks and gluons are subjected to is broken, yielding a spray of color-neutral particles that can be experimentally measured in particle detectors. Jets have played and are playing a fundamental role in collider physics. Events with three jets in e^+e^- collisions demonstrated the existence of the gluon. Nowadays jets produced by the fragmentation of heavy quarks—namely, b and c quarks—are crucial for several studies, in particular, to

determine the Higgs boson couplings. In recent years, tools have been developed to disentangle different kinds of jet.

a. Track reconstruction. Several current HEP experiments are exploring and several future HEP experiments will explore high-intensity scenarios going to extreme regimes with thousands of charged particles crossing a square centimeter of a sensitive detector. Furthermore, depending on the process under study and the detector layout, each track can consist of a variable number of measurements. The multiplicity of possible track candidates from the input space points scales quadratically or cubically with the number of hits. Therefore, tight selections on the input space points are required to narrow down the search space. Nevertheless, track reconstruction is one of the largest users of CPU time in HEP experiments, providing strong motivation for the research and development of novel approaches.

Several approaches have been proposed to address the tracking problem and can be roughly divided into global and local approaches. Global tracking methods approach track reconstruction as a clustering problem, thus considering all the space points at once, whereas local tracking methods generally consist of a series of steps executed sequentially. Several studies have been performed for the global [182,183] and the local [184] methods, finding a potential reduction of computational complexity for the latter.

The first proposals to solve the particle track reconstruction problem on a quantum computer focused on converting the problem to a quantum unconstrained binary optimization (QUBO) problem [185,186]. In this way, one can group two hits (doublets) or three hits (triplets) from consecutive detector layers, and binary values represent if a given doublet or triplet corresponds to a particle track. There have been several proposals in the literature on how to determine the coefficients of the QUBO based on either the geometry or the impact on the overall energy of the QUBO [182,183,187]. In its most general form, one can write such a QUBO Hamiltonian as

$$\hat{H} = \sum_{i < j}^N J_{ij} \hat{T}_i \hat{T}_j + \sum_{i=1}^N h_i \hat{T}_i$$

where in the case of triplets, \hat{T}_i represents the i th triplet and \hat{T}_i can be mapped to the Pauli \hat{Z} operator on the i th qubit. J_{ij} is the coupling coefficient between the i th and j th triplets, and h_i determines the strength of the field on the i th triplet. Then it is possible to use algorithms such as the quantum approximate optimization algorithm (QAOA), the VQE, or the Harrow-Hassidim-Lloyd algorithm find the ground state of the Hamiltonian, which corresponds to the desired solution. Although such a QUBO Hamiltonian

is sparse in general, it consists of at least 10'000 sites for a real-world problem, or about 500 in more favorable scenarios with smaller occupancies such as the LHCb Vertex Locator [188]. The limited number of qubits available currently restricts the Hamiltonian to a few tens of sites and therefore strategies to partition the Hamiltonian to many smaller pieces are needed.

Recently, Ducket *et al.* [189] proposed a method to solve the triplet classification using a QSVM-based approach. In this method, spatial coordinates of each hit from the triplet are encoded to quantum states, which results in a nine-qubit circuit. Quantum kernel methods promise an advantage for datasets with many features; therefore, a triplet-based approach might not provide a benefit. However, this method may outperform a classical kernel method in cases where considering a higher number of hits is useful.

Classical graph neural network (GNN) methods were shown to have linear scaling with respect to the number of input space points, which makes them a strong candidate for future implementations of particle track reconstruction algorithms [190]. Although there is no formal proof that this scaling is linear, the empirical evidence suggests it is so. It is likely that this improvement comes from the parallelization capacity of graphics processing units. This means that there is still a need for large graphics processing unit clusters. In a not too distant future, a quantum advantage could be achieved if GNNs with similar characteristics can be implemented on quantum computers. Recently, it was shown that a quantum-classical hybrid GNN approach is possible, and that it can perform similarly to the classical equivalent for up-to 16 qubits [191, 192]. However, understanding if this can be realized at large scale requires a larger number of qubits.

The availability of utility-scale devices would enable the study of larger local Hamiltonians with 100 sites and give researchers a tool to investigate if QUBO-based approaches are viable. Similarly, such a device would allow us to implement quantum-classical hybrid GNNs of sizes comparable to sizes of the classical state-of-the-art models.

Regarding local methods, although a full analysis chain is presently unreachable due to hardware limitations, we can nevertheless consider a complexity analysis to illustrate the general evolution of the classical and quantum approaches to the problem. It is not clear, in particular, whether all steps in the track or, in general, object reconstruction may benefit from a quantum algorithmic approach. This is the procedure originally followed, for instance, by Wei *et al.* [193], who estimated the classical and quantum computational scaling of a well-known (albeit unused) jet clustering algorithm. However, since this algorithm is not the current standard used at the LHC, it is much more informative to estimate the complexity of a current choice—namely, the combinatorial track finder algorithm [194], which is the tracking algorithm used by

the CMS collaboration [195]. The underlying structure of the combinatorial track finder algorithm, the combinatorial Kalman filter [196], is used by several current track reconstruction algorithms [197–199] and the analysis can easily be generalized to most presently available algorithms. This strategy has been followed by Magano *et al.* [184] using the algorithm as it is described in Ref. [194]. The conclusion is that it is possible to reconstruct the same tracks (up to bounded-error probability) with lower quantum complexity by an adequate use of quantum search routines.

A $100 \otimes 100$ machine may allow there to be some progress along the lines defined in Ref. [184], although it is necessary to investigate the number of qubits that can effectively be used for the implementation of the program. Moreover, since the approach of Ref. [184] is applicable to a hybrid quantum-classical approach it is possible to implement the program according to the available resources. In any case, it is important to bear in mind that in the short term track reconstruction algorithms will be quite limited by the input size, and investment in the QAOA or in jet clustering may be more rewarding.

b. Jet reconstruction and identification. Jet clustering algorithms aim at estimating the kinematics of the particle that initiated the jet. Usually, these algorithms are based on clustering schemes, which combine the observed particles into a jet for further study.

Clustering algorithms have different properties and characteristics that can make them more appropriate for a particular task, such as the extraction of observables or as a tool to extract specific properties of the final state. An essential property of an optimal jet clustering algorithm is infrared and collinear (IRC) safety. An observable is IRC safe if it remains unchanged in the limit of a collinear splitting or the emission of an infinitely soft (low momentum) particle.

Two main approaches have been pursued in clustering particles into a jet: cone and sequential recombination schemes. The first approach aims to find regions with a high-energy flow and thus define rigid conic boundaries. In sequential recombination algorithms, particles are clustered locally with use of a distance metric.

Jet clustering algorithms can be computationally expensive, as the execution time scales polynomially with the number of particles to be clustered. Speedups can be achieved by one considering the clustering problem from a geometrical point of view instead of combinatorially. In this way, sequential recombination algorithms can be executed in $\mathcal{O}(N^2)$ or even $\mathcal{O}(N \ln N)$ complexity rather than $\mathcal{O}(N^3)$ complexity. Cone algorithms could be implemented exactly (and therefore made IRC safe) with $\mathcal{O}(N^2 \ln N)$ complexity rather than the expected $\mathcal{O}(N2^N)$ complexity.

Quantum-assisted algorithms have been explored to reduce the computational overhead of these clustering routines. The first application of quantum-assisted algorithms to the task of clustering particles into a jet was introduced in Ref. [193]. Two clustering techniques were used for the particular case of electron-positron collisions and inspired by the calculation of *thrust* [200,201], an event shape quantity that allows the partition of event particles into two hemisphere jets. The first approach targeted the universal quantum computing setting based on Grover’s algorithm. In addition, a QUBO formulation for thrust was developed, suitable for quantum annealing. Classically, the calculation of thrust can be costly, scaling as $\mathcal{O}(N^3)$ [202] for an event with N particles, or with the improved method introduced in Ref. [203], as $\mathcal{O}(N^2 \log_{10} N)$. The thrust-based QUBO formulation was benchmarked in Ref. [204], with use of the D-Wave Advantage 1.1 quantum processing unit, and compared with classical QUBO-solving techniques such as simulated annealing and annealing optimization subroutines such as reverse annealing. Results from these studies revealed the limitations of current quantum annealing devices in terms of connectivity. QUBO formulations involving many spin variables and all-to-all connectivity, such as the thrust problem, perform poorly on currently available quantum annealers. An extension to the QUBO formulation for thrust calculation was presented in Ref. [205], and was based on the angular distance between two particles in a given event and penalizing the assignment of two particles located on the same hemisphere of the partition. Results from the hardware deployment in these studies were limited to a low number of annealing runs due to limited access to the quantum processing unit.

Algorithms based on digital quantum computing have also been proposed; however, the algorithms in Refs. [193, 206] are not suitable for implementation on noisy devices due to the need for a quantum-RAM-like architecture to access particle information in parallel. Another promising study [207] deals with the quantum version of three clustering algorithms found in the classical literature: the *k-means algorithm* [208] (a quantum version of this algorithm is used in Ref. [206]), *affinity propagation* [209], and the k_T jet clustering algorithm [210]. Two quantum subroutines are introduced: the first computes the Minkowski distance between particles, and the second tracks the maximum in a long-tailed distribution. For both subroutines, the authors prove polynomial speedups as compared with well-known classical algorithms. The quantum algorithms were applied to simulated data for a typical LHC collision setting and achieved efficiencies comparable to those of their classical counterparts. In particular, the quantum- k_T version is a conceptually more straightforward algorithm with a similar execution time compared with subroutines in the FastJet library [211].

Jet tagging, the identification of the flavor of the quark that originated the jet, is another aspect of jet physics that

experimental physicists are continuously improving. For example, in the determination of the Higgs boson couplings to b and c quarks, the jet tagging efficiency and purity determine the actual size of the dataset useful for the measurements and, therefore, their accuracy. Jet tagging is based on global jet characteristics and on each jet’s particle properties. In principle, it therefore requires a large number of features, which means a high-dimension dataset. The study reported in Ref. [212] limited the data representation to a few properties to cope with the low number of qubits available and short circuit depth. As already mentioned in the introduction to this section, this is the approach often used in experimental HEP, and therefore the performance of the QC algorithms is by definition limited and the comparison with classical methods is performed with use of the same dataset dimension. Two different feature encodings have been tested: angle encoding is used when a two-feature dataset is used, while for 16 features, amplitude encoding is used. Even though the exercise is quite simple, it showed that in the training phase, the QML method reaches optimal performance with a lower number of events with respect to the ML ones. The limited access to the hardware resources did not allow an extensive study of the noise impact, which was evaluated only for the two-qubit case. This study could largely benefit from much more powerful hardware, in particular the 100×100 IBM hardware. Instead of reproposing the same exercise, it would be possible to design a new circuit where the entanglement entropy can play an important role. Jet tagging feature correlation is considered as classical correlation, while in QML this can be understood and included in the circuit optimization, improving the classification performance. A further step forward could be to perform the jet classification study on data obtained in proton-proton collisions and in Monte Carlo-simulated events. Collider data may exhibit quantum characteristics not visible in simulations. That could happen due to the limited knowledge of jet formation and evolution, which is regulated by the nonperturbative QCD and described only by models in the simulation. Such effects, if present, are currently absorbed by the systematic errors in the jet reconstruction quantities.

3. Interpretable models and inference

In this section we review the use of quantum models as inference tools to extract the characteristic properties of a dataset in HEP. We give two examples of such models: characterizing the nonperturbative structure of hadrons through parton distribution functions (PDFs), and estimating the Wilson coefficients of effective field theories (EFTs) and their correlations. We emphasize the potential of these tools to enable precision modeling of physical phenomena and provide a first step towards being able to bridge the fields of quantum computing and quantum

information in extracting quantum descriptors of HEP processes from models learned from data.

In high-energy physics, perturbation theory is used to calculate particle interactions at high energies [213]. These perturbative methods allow the calculation of scattering amplitudes as a series expansion in powers of the coupling constant. However, as the energy of the interaction decreases, the coupling constant becomes large and the perturbative expansion breaks down [214]. This results in a nonperturbative regime where the underlying physical processes are not easily calculable, and must instead be obtained through experimental measurements or numerical simulations [215]. Characteristic functions that capture the essential features of the underlying physical process can be used to represent the relative probability of a particular physical process as a sum of simpler, more tractable functions. The choice of basis functions and coefficients is critical in constructing an accurate representation of the underlying physical process as they must be able to accurately characterize the process in both the perturbative regime and the nonperturbative regime, as well as any additional physical constraints that may be present.

PDFs are an example of nonperturbative effects that are necessarily characterized by such approximations from data [216]. PDFs describe the probability distribution of the momentum fraction carried by the quarks and gluons inside a proton. The need for PDFs arises from the fact that the proton is a composite particle made up of quarks and gluons that are constantly interacting, which makes it impossible to calculate the momentum distribution of these partons with use of perturbative methods alone. Nonetheless, there are known constraints on the form of PDFs that can be derived from the fundamental principles of QCD, and their predictions are highly constrained by experiments.

The accurate estimate of PDFs is vital to all measurements in experimental collider physics, as they are used to predict the rates and distributions of processes [217]. Uncertainties arise from the limited precision of how experimental data are used to constrain the PDFs, as well as from theoretical uncertainties in how to extract perturbative estimates from the fitted PDFs. Quantum computing affords us new avenues to address both shortcomings by providing characteristic functions that may better represent the nature of the process they are used to represent.

A recent study investigating an approach based on the use of a parameterized quantum circuit (PQC) was explored for estimating the functional form of PDFs [218] from data. The PQC approach aims to find an ansatz for representing the PDFs as a PQC, the parameters of which are estimated with use of a classical optimization algorithm to minimize the difference between the predicted data and the experimental data. This is a promising avenue for leveraging the expressive power of PQCs to efficiently learn solutions to classically intractable problems.

Preliminary results obtained with the PQC approach are encouraging, showing good agreement with existing PDF fits obtained through classical optimization techniques. This represents an exciting first step towards using quantum algorithms for PDF estimation and highlights the potential of quantum computing for solving problems in high-energy physics. However significant work is still needed to leverage the quantum nature of the problem. In this construction, the PDFs being estimated are still classical approximations to an inherently quantum system and therefore the possible advantages of such a method are purely computational. It is foreseeable that quantum functions that characterize classically intractable processes such as these are possible in a way that, although simplified with respect to a fully numerical model (e.g., from lattice QCD), would give a notable improvement over classical models when compared with data.

In contrast to experimental measurements in which the exact prediction of a given Standard Model process is computed, EFTs provide a framework for modeling complex physical processes in terms of a hierarchy of simplified interactions, characterized by a set of Wilson coefficients [219]. These coefficients represent the coupling strengths of various operators that encode the effects of high-energy physics and can be determined through a process of matching with experimentally measured observables. While the precise values of the Wilson coefficients cannot be computed exactly, they can be approximated through a process of functional approximation, in which an ansatz is made for the form of the EFT such that the coefficients can be estimated from experimental data. This EFT approach is similar in nature to the fitting of PDFs, as both involve characterizing complex physical phenomena in terms of a simplified set of parameterized functions. In a recent study, Criado *et al.* [220] proposed a new method for estimating Wilson coefficients using a quantum computer. The method involves the use of a quantum computer to encode the EFT predictions and experimental data into a QUBO [221] optimization problem, with coefficients of the cost function determined by a Hamiltonian representation of a set of given coefficients. The QUBO problem is then solved on a quantum annealer to obtain the best-fit values of the Wilson coefficients. A primary goal of this method is that the optimization of the problem on a quantum computer can provide a more efficient and more accurate way of estimating the Wilson coefficients than is possible with classical methods. The Hamiltonian is constructed using the parameterization of an effective field theory approach, which allows a systematic expansion in powers of the inverse of the mass scale of the new physics being probed. The Standard Model effective field theory framework [222] used in this example contains a large number of parameters, making it challenging to extract information about the underlying physics. In this case the predictions for a reduced set of parameters are computed classically, and

only the relationship between the coefficients and the measurements is modeled in the Hamiltonian, not the dynamics of the EFT operators themselves. Through a careful understanding of the Hamiltonian representation of this process and its solution using QML, it might be possible to reduce the number of parameters needed to describe the system by identifying a smaller set of effective parameters that capture the essential physics and to identify correlations between different observables and effective couplings.

While much of the development of quantum algorithms and in particular QML is focused on identifying and solving computational bottlenecks present in traditional methods, the goals identified in these selected benchmark applications are those that leverage properties of QML models to better interpret data from experimental high-energy physics in new ways. Several studies have begun towards this goal; however, these initial steps provide only hints at how a complete understanding of how QML can be used to leverage a quantum interpretation of the information contained in data from experimental particle physics.

4. Generative models for simulation

Other natural applications of generative modeling include detector simulation and event generation. Monte Carlo simulation of collider detector events is one of the most computationally expensive tasks within the experimental data processing chain. Recent estimates suggest that more than 50% of the LHC computing grid (Worldwide LHC Computing Grid) is spent on simulation tasks directly or on the reconstruction of simulated data, i.e., the extraction of high-level features from simulated data [223]. The next-generation detectors for the High Luminosity Large Hadron Collider and future colliders, with their larger sizes, higher sensor granularity, and increased complexity, will be even more demanding in terms of computing resources for data simulation and reconstruction [224]. This fact has sparked, over the years, intense research on alternative approaches, generally designated as fast simulation strategies, in contrast to highly accurate Monte Carlo-based simulation.

Fast simulation, typically trading some level of accuracy for speed, relies on parametric modeling of the detector response [225] or, more recently, on deep generative models [226–228] that learn multidimensional, conditional probability distributions. In most cases, the focus is on the detector response itself: the deep generative models are trained to reproduce the detector output, which is then processed in the same fashion as Monte Carlo-simulated data. This approach can produce very realistic output, both in terms of the quality of the individual events and in terms of sample diversity. In other cases, direct generation of high-level features, typically used at the analysis level, is preferred, thus skipping the entire reconstruction process [229]. This approach has the advantage of being

computationally lightweight and flexible since the deep learning models learn directly the particle features and correlations in the final state of interest, taking into account all experimental effects. Its main limitation is the fact that the output is inherently analysis specific, and it cannot be used outside the scope it was initially designed for.

At the same time, several studies have started investigating quantum (or hybrid quantum-classical) implementations of generative models. A few examples are described in Ref. [230]. In most cases quantum architectures inspired by classical models have been studied: for example, implementations of a QGAN or a QAE. Particularly interesting is the case of quantum circuit Born machines [231], which instead are quantum generative models that do not have a classical counterpart and leverage the Born measurement rule during the sampling process. As in the classical domain, quantum architectures have been used to address two main types of application: detector output simulation and final state generation. In both cases, but in particular for detector output simulation, the main limitation of the current models lies in the dimensionality of the simulated output. Realistic applications to particle physics detectors require generative models to learn distributions whose size scales with the number of detector sensors.

Current models can generate accurate simulations for very small (ten-sized) setups, using one qubit to represent a detector sensor. Typically, reversible data compression techniques, such as autoencoders, can be used to bring down the original simulation to a size that is manageable by the quantum system: the classical encoder network produces a reduced latent representation that is then learned by the quantum generative model. A classical decoder network is then used to transform the synthetic output from the latent dimension to the original one. The expected advantage of using a quantum algorithm in this task would come from a more accurate and more generalizable learning of the latent representation. It is clear, however that a most interesting development in this direction would require reducing the weight of the classical data dimensionality reduction step with respect to the quantum algorithm. In this context, a $100 \otimes 100$ machine would enable the simulation of far more realistic use cases.

Aside from the sheer detector size, the need for discretization also affects how realistic quantum generative model-based simulations can be. In most cases, our detectors produce continuous features, while qubits naturally map to discrete quantities, so the size of the qubit system can have an impact on the detector simulation resolution. These same problems can affect the direct generation of high-level features, albeit at a different scale: in this case quadrimomenta (and possibly angular correlations) of particles produced in scattering or decay processes are in the range of a few tens, instead of a few thousands, making the problem much more manageable on near-term quantum systems. In this case, extreme care should be

put into correctly describing cross-correlations among particles, and thus good connectivity and the possibility to reproduce complex entanglement patterns over multiple qubits become essential.

III. ALGORITHMS, METHODS, AND LIMITATIONS

A. Quantum algorithms for quantum dynamics

The development of quantum algorithms for the simulation of quantum dynamics is a very active field of research, with potential applications covering a broad spectrum across the physical sciences [232,233]. Many powerful methods have been developed over the past few years, which can generally be classified as either decomposition based or variational in nature [233]. Techniques belonging to the former category aim at realizing a target unitary evolution $U(t) = e^{-iHt}$ through a decomposition into elementary quantum logic operations. This approach typically yields rigorous scaling laws and *a priori* error bounds, and, most importantly, provides a systematic way of exchanging resources (i.e., circuit depth, gate counts, and auxiliary qubits) for accuracy. Examples of decomposition methods include product formulas (see below), linear combinations of unitaries [234], quantum signal processing [235], and qubitization [236]. On the other hand, variational strategies address the task of approximating $U(t)$ by resorting to parameterized quantum circuits, for example, implementing time-dependent ansatzes or learning effective partial representations of the dynamics. This often reduces the circuit complexity compared with decomposition methods, thus lowering the experimental requirements for implementations on current noisy quantum processors. However, such an advantage comes at the cost of some classical overhead (e.g., optimization and additional measurements) and within a more heuristic framework where accuracy guarantees are harder to obtain. Both decomposition-based and variational algorithms have been applied for specific dynamical studies in LGT on quantum computers [26,237].

1. Product formulas

Among decomposition methods, product formulas are the simplest and most widely adopted paradigm [52,238,239]. In their basic implementation, they rely on the general Trotter approximation rule [240]:

$$e^{-iHt} = \lim_{n \rightarrow \infty} \left(\prod_i^M e^{-iH_i t/n} \right)^n, \quad (21)$$

where $H = \sum_i^M H_i$. At first order and for every finite choice of n , one has

$$e^{-iHt} \simeq \left(\prod_i^M e^{-iH_i t/n} \right)^n + \mathcal{O}\left(\sum_{i>j}^M \| [H_i, H_j] \|^2 t^2/n\right), \quad (22)$$

i.e., the decomposition error amounts to $\mathcal{O}(M^2 t^2/n)$. This may be systematically reduced either by one choosing a larger n or by one using a higher-order PF, for which the error becomes $\mathcal{O}((M\tau)^{2k+1}/n^{2k})$ at order $2k$ ($k \geq 1$) (see also Sec. III A 3). In both cases, greater theoretical accuracy is obtained in return for an increased gate count. Further improvements are possible, based, for example, on randomization and adaptive techniques [241–244] or on the use of linear combinations of PFs (multi-product-formulas) [152,245], which can reduce Trotter errors. Importantly, PFs can also be used for simulation of time-dependent Hamiltonians [246–248].

2. Variational approaches

Parameterized quantum circuits can be used to tackle quantum dynamical problems by either one resorting to well-established variational principles or by one recasting them as optimization tasks. In the first case [249], one builds a time-dependent wave-function ansatz spanning a suitable manifold in the Hilbert space of the target system and propagates the parameters by solving a classical equation of motion. For sufficiently well-behaved dynamics, the trajectory of a specific quantum state in time can be approximated by parameters whose number is significantly smaller than the dimension of the full space. This, in principle, results in a simulation whose cost in terms of quantum resources—and specifically circuit depth—is constant, or increases only moderately, with time (in contrast to, e.g., PFs). As an example, for an ansatz $|\Phi(\theta(t))\rangle \equiv |\Phi\rangle$ evolving under the action of a Hamiltonian H , the application of McLachlan’s variational principle leads to a set of differential equations for the parameters of the form [249]

$$\mathcal{M}\dot{\theta} = \mathcal{V}, \quad (23)$$

where

$$\mathcal{M} = \text{Re} \left(\frac{\partial \langle \Phi |}{\partial \theta_i} \frac{\partial | \Phi \rangle}{\partial \theta_j} + \frac{\partial \langle \Phi |}{\partial \theta_i} | \Phi \rangle \frac{\partial \langle \Phi |}{\partial \theta_j} | \Phi \rangle \right) \quad (24)$$

and

$$\mathcal{V} = \text{Im} \left(\frac{\partial \langle \Phi |}{\partial \theta_i} H | \Phi \rangle - \frac{\partial \langle \Phi |}{\partial \theta_i} | \Phi \rangle \langle \Phi | H | \Phi \rangle \right). \quad (25)$$

The matrix elements of \mathcal{M} and \mathcal{V} have to be evaluated through measurements on the quantum processor where the ansatz is prepared, while Eq. (23) is integrated classically. Two main versions of the VTE algorithm have been devised and applied in quantum simulations: the variational quantum time evolution algorithm for real-time propagation, and the variational quantum imaginary time evolution algorithm for “dynamical” ground state preparation (for a review, see Ref. [233]).

The VTE algorithm is particularly attractive in those cases where a direct decomposition of unitary Hamiltonian evolution becomes quickly demanding with growing system size, for example, in first quantization [250] or when one is dealing with fermionic or bosonic degrees of freedom [251–254] and gauge fields [26,48]. In practice, one crucial ingredient is the choice of the ansatz, which ideally should incorporate physical intuition (e.g., respecting symmetries and/or conservation laws) and good mathematical properties (e.g., concerning the form of the tangent space associated with the parameterized manifold along time-evolution paths). While several promising strategies for ansatz construction have been proposed, including adaptive ones [255], it remains challenging, in general, to correlate in a systematic way ansatz expressivity with simulation accuracy and performances, if not with *a posteriori* error bounds [256]. The application of VTE is also limited by the high numerical sensitivity associated with the solution of Eq. (23) via matrix inversion and by the large number of measurements required to construct \mathcal{M} and \mathcal{V} [253,256].

In parallel to the standard VTE algorithm, numerous other approaches are being explored. For instance, variational quantum methods have been used to learn a (partial) diagonalization of the short-time evolution of a system [257–260] and to compress the circuits required to implement a short time step on a given state [261–264]. Additional proposals aimed at implementing near-term quantum simulations include quantum-assisted methods that perform all necessary quantum measurements at the start of the algorithm instead of using a classical-quantum feedback loop [265–267], methods based around Cartan decompositions [268,269], and approaches using Krylov theory [270].

3. Algorithmic limitations

Of the two approaches for performing time-evolution dynamics, it is considerably more straightforward to characterize the (near-term) simulation errors associated with Trotterization-based methods. For a fixed total time T , the discretization in n time intervals ($dt = T/n$) of the time-evolution operator according to Eq. (21) (i.e., with use of first-order Trotter expansion) will lead to a residual error ϵ of $\mathcal{O}(\alpha_c(T/n)^{p+1})$, with $p = 1$ and where $\alpha_c = \sum_{i,j} \|H_j, [H_j, H_i]\|$ (see Ref. [271]). This implies that one would require $n \times \mathcal{O}(M\alpha_{\text{comm}}(T/n)^2)$ gates to achieve the desired accuracy, where M is the number of Pauli strings building up the system Hamiltonian. On the other hand, a practical implementation of the Trotter expansion in near-term, noisy, quantum computers will need to face the additional errors arising from the gate infidelities. Assuming that we have only errors induced by the two-qubit CNOT operations, ϵ_{2g} , the overall Trotter error will scale as

$$\epsilon_{\text{Trotter}} \sim \mathcal{O}(\alpha_c(T/n)^2 + (n_0\epsilon_{2g})^n), \quad (26)$$

where n_0 is the number of two-qubit operations required for the circuit implementation of the operator e^{iHt} , for fixed t . We therefore conclude that for the Trotter formula there must be an optimal value of the discretization variable n , which we name n^* , that minimizes the overall error.

In the case of the VTE algorithm, the quantum circuit is of a constant depth, while the number of gates required for its implementation depends on the number of degrees of freedom necessary to produce a suitable representation of the subspace that spans the dynamics of the system. Assuming that we have knowledge of a variational form that can be systematically improved by one adding circuit layers, L , one can—in principle—achieve a desired accuracy as a function of the circuit depth. In the case of LGT, one could, for instance, use a recently proposed Hamiltonian-inspired variational ansatz [48], which has the advantage of combining a physically motivated variational circuit with the possibility of naturally enforce dynamical constraints, such as Gauss’s law. On the formal side, Zoufal *et al.* [256] investigated error bounds associated with VTE. However, unlike the Trotter expansion and similar methods, there seems to be no systematic way to assess *a priori* the scaling the variational error in the VTE algorithm as a function of the total simulation time T or number of circuit layers L . Preliminary studies [272] showed that in the case of QED calculations in $1 + 1$ dimensions the number of Hamiltonian-inspired layers to reach a desired accuracy increases rapidly with the dimensionality of the problem, approaching the number of gates required to implement the Trotter formula already with 10–15 sites. Finally, it is also important to mention that the quality of the VTE approach depends on the accuracy in the solution of the system of linear differential equations in Eq. (23).

B. Quantum machine learning

1. Opportunities for quantum speedup

QML is an area of particular interest in experimental particle physics encompassing many of the algorithms described in this section. In general terms, two main approaches have emerged in the development of quantum-enhanced machine learning: the role of the quantum computer as an accelerator of otherwise established classical learning methods and the design of genuinely quantum methods, which do not mimic classical algorithms. This first method includes the relatively straightforward application of QC methods to speed up an otherwise computationally costly training method [273]. Such approaches include classes of methods, dubbed “quantum linear algebra-based methods,” in which the principal goal is to represent high-dimensional data in states of just logarithmically many qubits. This approach may allow even

exponential speedups, but comes with numerous caveats [274], most notably requiring some means of generating the required data-bearing quantum states, which, if done naively, already nullifies any possible advantage. Solutions to this may exist, for example, by the use quantum RAM [275], but in any case these methods are mostly considered only in the context of large-scale fault-tolerant quantum computers.

In contrast, the design of genuinely quantum methods may yet offer advantages based on the idea of parameterized quantum circuits (PQC-based methods) as the key building block of the model. The basic examples here include the quantum support vector machine [178] and the closely related quantum kernel methods [179], and, more generally, so-called quantum neural network models.

In general, the quantum model attains the form $f_{\theta}(x) = \text{Tr}[\rho(x, \theta)O(x, \theta)]$, where the observable O is most often fixed and independent of data (x) or trainable parameters (θ), and $\rho(x, \theta)$ is prepared by one applying a parameterized circuit on some fiducial state, for example, $\rho(x, \theta) = U(x, \theta)|0\rangle\langle 0|U(x, \theta)$. In so-called linear models such as kernels and QSVMs, in contrast to data-reuploading models [276], the state depends only on x , and this constitutes the loading of the data. Note that the targeted advantage in these settings is not in the dimensionality or number of data points but is rather in the *quality* of learning that can be achieved.

The mapping $x \mapsto \rho(x, \theta)$, a process that is typically independent of the setting of the θ parameters, constitutes the data loading, in which the key questions here are in finding a suitable mapping that will allow favorable data processing. Unlike in the case of quantum linear algebra approaches, the dimensionality of the state $\rho(x)$ is typically independent of the data dimensionality. In particular, as was proven in Ref. [276], a single qubit line can express arbitrary multidimensional functions, given sufficient depth and data reuploading. This is analogous to how one-hidden-layer neural nets allow functional universality [277], but nonetheless the use of multiple layers allows more efficient access to useful function families. The use of more qubits allows more expressive function families at shallower circuit depths, and indeed qubit number scaling as a function of data dimension is necessary for any potential of a quantum utility or advantage (as constant-sized quantum circuits are simulatable in polynomial time in the depth).

Indeed, the minimum is superlogarithmic scaling of the qubit numbers in the dimension of x , and linear scalings can ensure the exponential cost of the classical simulation of the quantum model using the best known classical algorithms. This freedom also stymies any good approximations of how many qubits would be necessary to achieve good performance of quantum learning algorithms of this type; it is easy to construct models that are not classically simulatable, but currently, it is not known how the

increase in qubit numbers affects the quality of outcomes, and whether this can ultimately lead to a method that can outperform classical solutions. In practice, it has been suggested that a linear scaling between qubits and the input dimension may be a good starting point [179]; however, this necessitates the use of either classical dimensionality-reduction techniques or circuit-cutting techniques [278] for any real-world applications in this field.

We highlight that QML by construction inherits the heuristic feature of machine learning. As of today, there are no evident HEP use cases where a strict quantum advantage can be claimed. On the other hand, we have very clear reasons to believe that quantum models can lead to a learning advantage; this is the key point of Ref. [279]. In essence, it shows that any bounded-error quantum polynomial time (BQP)-hard problem, or more precisely any problem not in HeurBPP/poly (i.e., the class of decision problems that can be solved by a polynomial-time heuristic algorithm) but in BQP, allows there to be learning advantages. In a HEP context, potential examples include scattering in scalar field theories (BQP complete), and various problems related to hard variants of gauge field theories (essentially anything that we do not know how to simulate but that a QC could simulate is a candidate), can lead to a quantum advantage. How to reconcile these complexity theoretical arguments with the challenges posed by exponential concentration (see below) is an important and active area of research [280].

It is also worth highlighting that a quantum advantage could be claimed even for problems in HeurBPP/poly, but not BPP, if the poly advice needs to be collected with a quantum computer (i.e., if producing advice is in BQP but not BPP). In this manner, a quantum computer might prove valuable for producing data for quantum enhanced machine learning algorithms, for example, as explored in Ref. [281]. Again, such advantages could be imagined in any HEP scenario where a quantum simulation is expected to provide an advantage.

Another more indirect argument for an advantage for some HEP contexts comes by one combining the results on advantages from topological data analysis (TDA) with the duality between TDA and supersymmetric theories [282,283].

2. Algorithmic limitations

A fundamental limitation to the scaling up most PQC-based machine learning methods is the so-called barren plateau phenomenon, where the gradients [284] of the cost function vanish exponentially with n . On such barren plateau landscapes, the cost function exponentially concentrates about its mean, leading to an exponentially narrow minimum (a narrow gorge) [285]. Hence, on a barren plateau, exponential precision is required to detect a cost-minimizing direction and therefore to navigate through the landscape. Thus, minimization of the cost

typically requires an exponential number of shots, even if we use gradient-free [286] or higher-derivative [287] optimizers. While this phenomenon was originally identified in the context of variational quantum algorithms and quantum neural networks, it has recently been shown that exponential concentration is also a barrier to the scalability of quantum generative modeling [288] and quantum kernel methods [180].

A number of causes of barren plateaus have by now been identified, including the use of variational ansatzes that are too expressive [284,289–291] or too entangling [292–294]. However, even inexpressive and low-entangling quantum neural networks may exhibit barren plateaus if the cost function is “global” [295], i.e., relies on one measuring global properties of the system, or if the training dataset is too random or entangled [296–299]. Finally, barren plateaus can be caused by quantum error processes washing out all landscape features, leading to noise-induced barren plateaus [300,301].

Several methods to mitigate or avoid barren plateaus have been proposed. The simplest is perhaps to use a shallow ansatz along with a local cost function [284,295]; however, it is questionable whether physically interesting and classically intractable problems can be solved within this regime. More promising is the ongoing search for problem-inspired ansatzes [302–306], problem-inspired initialization strategies [307], pretraining strategies [308–313], or layerwise learning [314]. Of particular interest currently is the field of geometric quantum machine learning, which provides a group-theoretic strategy for building symmetries into quantum neural networks [315–318]. In the context of LGT simulations, this approach could be suitable since we can use the (local and global) gauge symmetry (see Ref. [48] for a gauge-invariant construction of the ansatz, although it is not clear if this ansatz can mitigate the barren plateau problem).

Beyond barren plateaus, there is a growing awareness of the problems induced by local minima [319–322]. Namely, it has been shown that quantum cost landscapes for a large class of problems can exhibit highly complex and non-convex landscapes that are resource intensive to optimize [319,320,322]. Thus, the construction of strategies to mitigate and avoid local minima [321] is another important research direction to ensure the successful scaling up of hybrid variational quantum algorithms.

3. Near-term applications

Given access to a noiseless 100-qubit system, assuming that we have the capacity to train the model, it is, in principle, possible to tackle very high-dimensional systems, and also learning problems where the underlying physics generating the data is very sophisticated. In essence, any system where a 100-qubit quantum simulation would be able to capture relevant physics could, in principle, be

captured by a 100-qubit learning model. In practice, as mentioned, this will be possible only if the PQC architecture is carefully tailored to the learning task to enable the trainability of the system.

As shown in Sec. II B, architectures inspired by the properties of classical deep neural networks have been successfully trained in the quantum context: quantum hierarchical classifiers, such as Tree Tensor Networks (TTN) and multi-scale entanglement renormalization ansatz (MERA), for example, have been successfully trained to reproduce two-dimensional images representing the output of a HEP detector [323–325], and quantum convolutions achieved optimal results for image analysis and image generation while mitigating the problem of barren plateaus [326]. A $100 \otimes 100$ machine could be used to understand to what extent a quantum convolutional neural network could reproduce the hierarchical learning of a classical convolutional neural network, before incurring the limitations mentioned in the next subsection.

While a graph-based interpretation of HEP data has been tested for a relatively small setup in the field of particle trajectory reconstruction, interesting quantum graph implementations have been proposed [327] and could be tested in conjunction with point-cloud interpretation of HEP data for applications ranging from tracking to jet reconstruction and jet tagging to event generation of matrix element calculations. Quantum equivariant neural networks are also under study. Examples implementing spatial symmetries (rotations or reflections) have shown great potential on image-related tasks and are being studied on HEP datasets as well. The case of physics symmetries, equally, if not more interesting, is also very promising, although for certain applications in classical data processing, a major challenge is represented by the difference existing between the original symmetries underlying the quantum process and the remnants accessible through measurements and observables. An appropriate choice of loss functions and learning processes will determine the task PQCs can be trained for.

As explained throughout this paper, generative models are among the most powerful and most versatile architectures that could be studied on a $100 \otimes 100$ machine: in particular, it should be possible to move from a hybrid version to a fully quantum version of the more complex topologies such as a QGAN or a QAE. Designing a mechanism for efficiently reproducing attention on quantum states could pave the way for the implementation of transformers, which are among the most powerful architectures existing today in the classical domain. Similar considerations can be made in the choice of feature maps and kernels for kernel-based methods such as quantum support vector machines, which together with variational algorithms are used for classification, clustering, or anomaly-detection problems in the frameworks of both supervised and unsupervised learning.

C. Resource estimation for the proposed use cases

1. Theoretical applications

We conclude this section with a rough estimation of the resources needed for the proposed applications. In the case of QED static calculations, we take ground state properties as our main target (e.g., targeting phase structure features for which high precision is not required). Similarly, for QED dynamics we are interested in the qualitative behavior of scattering particles (e.g., entanglement production). In the following we are concerned only with the number of qubits and layers required for the simulation of the relevant physical problems, which are also compatible with the noisy hardware at our disposal in the near term. Therefore, we will avoid mentioning the targeted precision of the solutions (the results must be qualitatively correct, in agreement with the best known classical approximations) or the execution time of the algorithms, which is limited by the machine runtime to a maximum of a few hours.

Table I reports preliminary resource estimates, i.e., the number of qubits and the number of CNOT gate layers, to execute the three selected topics discussed in this section on a near-term quantum device compatible with the utility-scale experiments targeted in this work—namely, hardware with about 100 qubits and capable of executing several thousand two-qubit gate operations. The values reported in Table I are based on state-of-the-art calculations performed recently by the authors or by other members of the community. In particular, the dimensions of the systems were motivated by the limits imposed by the available number of qubits and the minimal dimensions and sizes needed to obtain meaningful physical insights [328]. On the other hand, the number of qubits and gate counts required for the implementation of these minimal setups on a quantum register were estimated from recent studies on similar Hamiltonians [see, e.g., Refs. [26, 31, 329] for “(2 + 1)D QED static”, Refs. [26, 330] for “(1 + 1)D QED dynamics”, and Ref. [148] for “neutrino oscillations”], while the values given for the larger implementations (maximum values) are obtained from realistic

extrapolations based on these “minimum size” calculations and theoretical studies [26].

2. Experimental applications

Because of the difficulty in predicting trainability, convergence, and the quality of the final results for QML algorithms, we provide in Table II an outlook on the size of physical systems that could be studied by the different applications assuming a best case scenario for the data-embedding circuit. We assume linear scaling for the encoding circuit depth through angle (or dense angle) encoding. No assumption on the trainability of such a system can be made at this point. However, the possibility to implement such systems at the 100-qubit scale would provide valuable insights into the impact QML algorithms could make in the next few years. As an example, an anomaly-detection problem, such as the Higgs analysis described herein, could be implemented by one skipping entirely the classical data-compression step (currently based on a classical autoencoder): the quantum circuit could directly analyze the raw jet features without the introduction of any intermediate bias or loss of information. In this respect, recent work [331] showed the remarkable impact the data-compression step can have on the performance of a classifier. In the case of generative modeling, both for detector simulation and for event generation, access to a large number of qubits $\mathcal{O}(100)$ will allow the generation of two-dimensional detector images, albeit still limited in size. On the other hand, an event generator capable of generating hundreds of features could be used to generate an entire jet and study its substructure. Assuming that we have trainability and convergence, the pattern-recognition use cases are probably those that could show the greatest advantage. The possibility to input hundreds of features (space points in the case of particle trajectory reconstruction, or particles in the case of jet reconstruction and jet tagging) would allow us to overcome the iterative approach used by current implementations and enable reconstruction of large event fractions in one step.

TABLE I. For (2+1)D QED, we consider a minimum linear lattice size L of 4 and a maximum of 8; this leads to 8–16 qubits to describe the fermionic degrees of freedom and 10/15 gauge links, which leads—with truncation of the gauge fields $l = 2, 3$ —to 20/100 and 30/150 qubits, respectively. The final number of resources is reported in the table. For (1+1)D QED dynamics, we give a suitable number of lattice points that allows us to study the time evolution of scattering particles. For two flavor neutrinos we consider a direct mapping to qubits, where the cost is based on a first-order PF. For the largest system, with 40 neutrinos, the CNOT gate count would still be 2340 with depth 120 (for more details, see Ref. [148]). VQITE, variational quantum imaginary time evolution; VQTE, variational quantum time evolution.

Systems	Physical size (minimum/maximum)	No. of qubits (minimum/maximum)	Algorithm	No. of CNOT gate layers
(2+1)D QED static	$4 \times 4/8 \times 8$ sites	30/160	VQE/VQITE	$\sim 10/100$
(1+1)D QED dynamics	12/20 sites	30/100	VQTE/Trotter	20/100
Collective neutrino oscillations	10/40 neutrinos	10/40	VTE/PF	30/120

TABLE II. Tested QML applications. The last column shows the size of the problem that could be implemented with 100 qubits, assuming linear circuit depth scaling for the encoding circuit (as in the case of angle or dense angle encoding). QAG, quantum angle generator; QCBM, quantum circuit Born machine; QGNN, quantum-classical hybrid graph neural network.

Application	Algorithm	Features	No. of qubits	Circuit depth	F_{100} (projected)
Anomaly detection	QSVM	16 (latent features)	16	30	300
Detector simulation	QAG	8 (pixels)	8	16	100
Event generation	QCBM	16 (output features)	4	4	100
Event generation	QGAN	3 (output features)	3	1	100
Tracking	QGNN	2 (input space points)	8	9	200

IV. CONCLUSIONS AND OUTLOOK

In this paper we have described applications from experimental and theoretical high-energy physics where quantum computers have the potential to show a better performance than their classical counterparts. The selected applications were chosen for utility-scale noisy hardware, i.e., devices with approximately 100 qubits capable of executing several thousand two-qubit gates, and, where possible, a resource estimate was made. The given applications are by no means complete, and should serve as examples that are of very great interest for the high-energy physics community. We emphasize that this work should serve as an initial step by the present authors for exploring the potential of quantum computing for high-energy physics, and we expect that the community of high-energy physicists working on this will substantially grow in the future.

Concerning the quantum algorithms proposed for the applications outlined in Sec. II A, we have identified quantum dynamics as one of the main targets because of its relevance in the field of HEP, for example, in scattering phenomena, string breaking, quenching, or dynamical properties of phase transitions. The exponentially growing costs of the corresponding classical approaches combined with the availability of well-tuned quantum algorithms make quantum computing a very promising tool for tackling problems in quantum dynamics. As outlined in Sec. II A and Table I, such quantum dynamics applications are indeed compatible with utility-scale noisy hardware. Besides the dynamical aspects of the applications of theoretical HEP models, we have also described static situations where quantum computing could lead to better performance. These include Abelian and non-Abelian lattice gauge theories supplied with topological terms or nonzero fermion density or investigations of neutrino oscillations. While for these cases quantum computing has clearly an advantage over classical Markov Chain Monte Carlo methods, it remains to be seen whether it will have advantages over tensor network approaches, for example, when one is taking the continuum limit or close to a phase transition.

In this paper, we have identified and proposed concrete examples of $(1+1)$ D and $(2+1)$ D theoretical models of HEP (and, in particular, lattice gauge theory) that are

particularly hard classically due to the level of the entanglement produced, but still have a great physical relevance as prototypes for understanding fundamental dynamic but also static aspects of the laws of nature. In the path towards large-scale simulations, we propose the development of hybrid quantum-classical algorithms, which can optimally leverage the advantages offered by the two complementary computational paradigms; for instance, the combination of TNs with a quantum circuit representation of the system wave function can offer a unique opportunity for enabling simulations of strongly entangled systems for longer timescales or close to phase transitions. The models we consider are an intermediate step towards the $(3+1)$ D theories needed to study the Standard Model of HEP. These lower-dimensional models are of great interest by themselves. Investigating them with quantum computing can help develop algorithms and methods to study their $(3+1)$ D counterparts. A fascinating perspective would be to explore phases of QCD currently out of reach, such as the very early universe or when the strengths of a topological term becomes large. In addition, quantum computing may allow studies of scattering phenomena in a fully nonperturbative fashion, thereby providing completely new insight into particle collisions and shedding light on the transition from the confined phase of QCD to the quark-gluon plasma.

A wide variety of QC applications are anticipated in quantum simulations and experimental HEP workflows. Quantum simulations of simplified LGTs in the Standard Model, such as $(2+1)$ D QED or $(2+1)$ D SU(2) theory, are potential well-motivated applications for near-term quantum computers. In experiments, QML may improve, for example, signal processing and detector reconstruction. However, as mentioned in Sec. II B, encoding classical data into a quantum circuit is a big challenge, in particular for future colliders, which will produce an enormous amount of data. Moreover, this data encoding can also cause barren plateaus.

This provides motivation for the possibility of using *quantum data*, i.e., data generated by a quantum system, to directly exploit the quantum properties encoded in quantum simulations and HEP experimental data. Understanding how to learn quantum states has received much

attention. For instance, in tomography, a learner is given copies to an unknown n -qubit quantum state ρ and needs to learn ρ up to an ε -trace distance. Here, the sample complexity was pinned down to $\Theta(2^{2n}/\varepsilon^2)$ [332,333]. The exponential nature of learning an unknown quantum state is undesirable. However, certain restricted classes of states are learnable with use of polynomially many copies of the states, such as stabilizer states [334], Gibbs states of local Hamiltonians [335], and matrix product states [336]. Another body of work considers learning only certain properties of ρ instead of the entire unknown quantum state. For instance, (1) in probably approximately correct (PAC) learning, one has access to $(E_i, \text{Tr}(\rho E_i))$, where $\{E_i, \mathbb{I} - E_i\}$ is a uniformly random positive operator-valued measure element; (2) in shadow tomography, the goal is, given copies of an unknown ρ , to learn the expectation values of ρ with respect to a certain set of *fixed, a priori known* observables $\{E_1, \dots, E_m\}$; and (3) other models, such as classical shadows, online learning, and learning with differential privacy, have modified the models (1) and (2). In all these models the complexity of learning is $\mathcal{O}(n)$ [337–340], which is *exponentially* better than tomography. For a detailed survey of the complexity of learning quantum data, we refer the interested reader to Ref. [341].

Quantum data learning for HEP may help extract physical information from quantum states in quantum simulations. This was first proposed for condensed-matter physics [342] and was further explored in Refs. [84,343–348]. An example is the recognition of quantum phases. Here, the QML model learns pairs of a quantum state and its phase to predict the phase of unknown states. In HEP, we often encounter phase transitions that cannot be investigated by local order parameters, such as confinement-deconfinement transitions in QCD. Here, quantum data learning may help extract physical information.

In the long term, one may perform a quantum experiment, for example, with an analog quantum simulator, measure the final state with a quantum sensor, and then coherently transduce the states to a quantum computer to extract physical information via QML (see, e.g., Ref. [349]). This hybrid system could be extended to the concept of a quantum-enhanced HEP experiment. For instance, one could physically place quantum sensing devices in HEP experiments and directly feed the quantum states registered on the sensors into quantum computers. This involves many challenges; for example, detect particles or wavelike matter with quantum sensors, coherently transfer the generated state to another quantum system, and perform quantum operations to measure physical properties within coherence times. Such experiments provide an exciting opportunity to directly explore quantum phenomena observed in HEP experiments and extract dynamical properties of entangled quantum states.

A crucial success criterion in the era of noisy quantum devices is the codesign of error mitigation schemes that efficiently mitigate the different noise sources (e.g., gate errors, qubit decoherence, and crosstalk) to guarantee results of sufficient quality to extract the physics of interest. Several error mitigation schemes have been proposed in the past few years (see Appendix A), including zero-noise extrapolation [350], probabilistic error cancellation [351], and the probabilistic error amplification approach recently applied to the dynamics of the transverse field Ising model with more than 100 sites [2]. All these methods require an accurate description of the noise sources in the quantum device. This has become a very active and successful area of research [350–355]. Finally, the precision of most quantum algorithms depends on the quality of the measurement process. Accurate results can require a number of projective measurements that easily exceed what is currently affordable with current quantum computer clock speeds. These clock speeds are determined, in part, by the gate times, which currently range from a few tens of nanoseconds with superconducting qubits to a few hundred milliseconds with ion-based technologies. This urges the design of novel approaches to reduce this measurement overhead. Informationally complete positive operator-valued measures [356] and classical shadows [357] offer viable solutions to this problem, thereby opening new avenues to use quantum computers in large-scale simulations.

ACKNOWLEDGMENTS

A.D.M., M.G., and S.V. are supported by CERN through the CERN Quantum Technology Initiative. K.J.’s work is funded by the European Union’s Horizon Europe framework program under the ERA Chair scheme with Grant Agreement No. 101087126. A.C. and C.T. are supported in part by the Helmholtz Association—“Innopool Project Variational Quantum Computer Simulations.” K.J., A.C., C.T., and S.K. are supported by funds from the Ministry of Science, Research and Culture of the State of Brandenburg within the Centre for Quantum Technologies and Applications. A.R. is funded by the European Union. This project has received funding from the European Union’s Horizon Europe research and innovation program under Grant Agreement No. 101080086 – NeQST. E.R.O. is supported by Grant No. PID2021-126273NB-I00 and by the European Union via QuantERA project T-NiSQ Grant No. PCI2022-132984, QuantERA project QuantHEP, the project Euryqa, and PASQUANS2 funded by the European Union “NextGenerationEU”/PRTR, by the European Regional Development Fund (ERDF) – “A way of making Europe”, by MCIN/AEI/10.13039/501100011033, by the Italian National Center for HPC, Big Data and Quantum Computing, by the Basque Government through Grant No. IT1470-22. J.T. has received support from the

European Union’s Horizon Europe research and innovation program through the ERC starting grant FINE-TEA-SQUAD (Grant No. 101040729). J.T.B., V.D., and V.C. are supported by the Dutch National Growth Fund, as part of the Quantum Delta NL program. V.D. and V.C. also are supported by the Netherlands Organisation for Scientific Research (NWO/OCW), as part of the Quantum Software Consortium program (Project No. 024.003.037/3368). Z.H. acknowledges support from the Sandoz Family Foundation’s Monique de Meuron program. L.N. is supported by the IBM-UTokyo lab under the Japan–IBM Quantum Partnership. J.S. acknowledges the support of the Fundação para a Ciência e a Tecnologia (FCT) under Contracts No. CERN/FIS-COM/0036/2019 and No. UIDB/04540/2020 and the project QuantHEP supported by the European Union Horizon 2020 QuantERA ERA-NET Cofund in Quantum Technologies and by FCT (Contract No. QuantERA/0001/2019). E.F. acknowledges support by the Deutsche Forschungsgemeinschaft under Germany’s Excellence Strategy—EXC-2123 “Quantum-Frontiers”—390837967. J.C.H. acknowledges financial support by the Emmy Noether Programme of the Deutsche Forschungsgemeinschaft under Grant No. HA 8206/1-1. The IBM team acknowledges Jay Gambetta for his precious and constant support of the HEP working group.

The views and opinions expressed are those of the authors only and do not necessarily reflect those of the European Union or the European Commission. Neither the

European Union nor the granting authority can be held responsible for them.

APPENDIX A: IBM ROADMAP ON QUANTUM COMPUTING

In the last few years, we have observed the flourishing of many different quantum computing platforms, each with its own technological and scientific goals. Common to all these quantum computing efforts is the ambition to scale up their technology to empower scientific progress and foster innovation. In the following, we provide a summary of the IBM quantum computing Roadmap (see Fig. 2) based on superconducting qubits, which is the one most familiar to the authors. However, by no means should this be taken as a reference for the realization of our research program in HEP. A summary of the Roadmaps for the other main quantum computing platforms, including trapped ions, neutral atoms, quantum dots, photonics, and NMR, can be found in Ref. [358].

Bringing useful quantum computing to the scientific world, and in particular to the HEP community, is contingent on the development of quantum computing hardware and software that permits the execution of quantum algorithms at a scale that is capable of producing insights and results not accessible by classical computers. But more than requiring only a large-scale device, one requires that

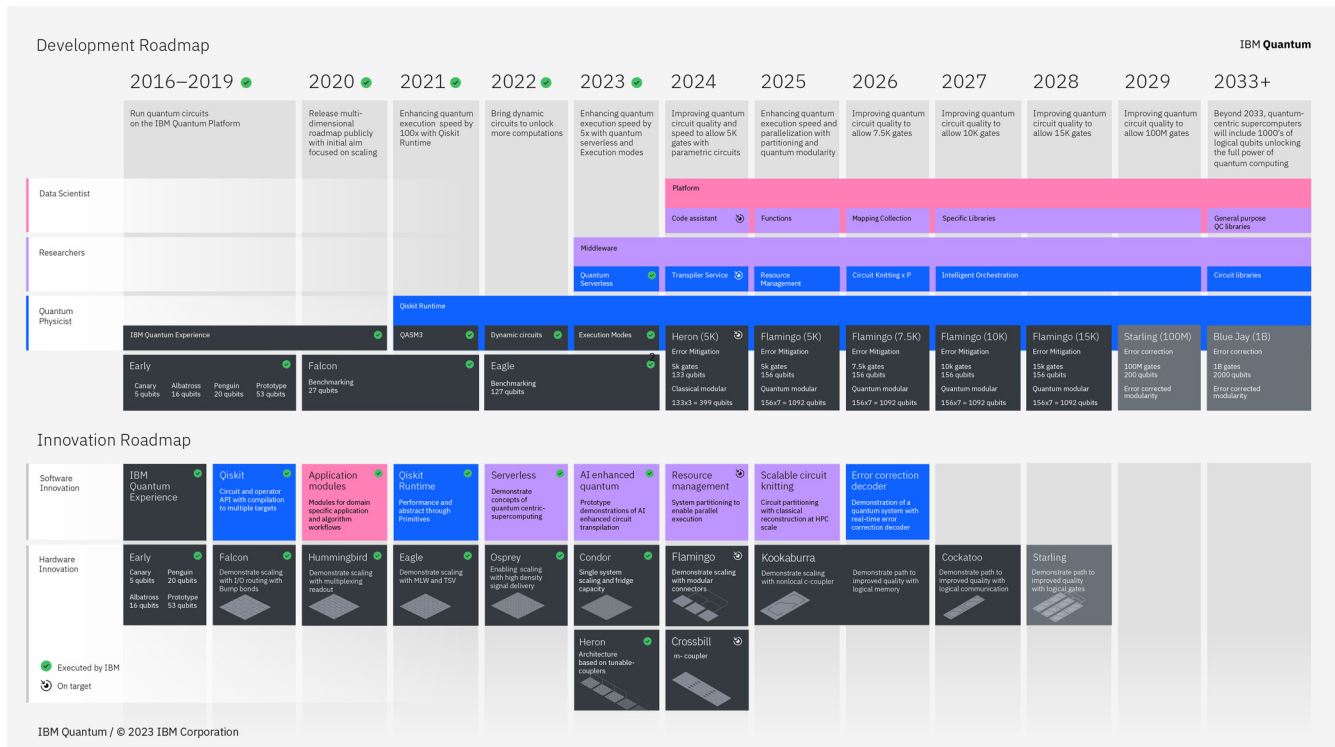


FIG. 2. IBM’s Roadmap for upcoming quantum computers, updated 2023.

the components are sufficiently reliable and have coherence times as well as gate parameters of high quality [359]. The IBM Quantum Roadmap proposes a list of stepping stones that progressively improve on the necessary requirements. The first development Roadmap was previewed in 2020 [360], laying out a progression of the then available 27-qubit Falcon devices to the Condor chip with 1121 qubits by the end of 2023. With the release of the 433-qubit Osprey chip at the end of 2022 [361] the Roadmap has been extended [362]. The new Roadmap now lays out a path to the newly introduced Kookaburra chip with 4105 qubits that uses interconnected chip designs with long-range couplers. Furthermore, the new Roadmap added new chip architectures, such as the Heron chip with 133 qubits incorporating recent advances from gate and qubit research.

The greatest adversary to the realization of large-scale quantum computers is noise. The components of quantum computers are considerably more sensitive to imperfections and external interactions than their classical counterparts, leading them to decohere and turn into classical mixtures [363]. For specific tasks such as quantum dynamical simulations it is reasonable to expect that useful insights may already be gathered from noisy quantum processors [2], for example, for gauge theories [79]—as the technology matures. However, other well-known quantum algorithms, such as Shor’s factoring procedure [364], quantum amplitude amplification [365,366] and quantum phase estimation [367] will almost certainly require some form of quantum error correction. The design plans for the progressively larger QC layouts are therefore aimed at providing a path to the long-term goal of realizing a fault-tolerant quantum computer. However, current error-correcting codes, which could be used to realize fault-tolerant quantum computing at a nontrivial scale, require system sizes that exceed the available hardware by several orders of magnitude [368,369]. Building a fault-tolerant computer, therefore, requires not only higher-quality and larger-scale devices but also research in error-correcting codes. Recent advances in the theory of error correction [370–374], including recent effort exploring the interplay between quantum error correction and gauge-fermionic theories [375–378], provide us with a reason to be optimistic about future progress. However, if we wait for the realization of a fault-tolerant quantum computer to run algorithms and do not actively explore the potential of near-term devices, we will forgo a promising opportunity to obtain a computational advantage in the near future.

We are observing remarkable progress in quantum hardware. As the Roadmap and the already completed milestones indicate, we are both building larger devices and can manufacture components with an order of magnitude improvement in two-qubit gate fidelities [379]. A quantum processing unit at the scale of the 65-qubit Hummingbird chip could implement circuits with a few thousand gates

to a reasonable degree of accuracy without resorting to error correction when two-qubit gate fidelities of 99.99% become available. Circuits of such a size can arguably no longer be simulated by exact methods on a classical computer. This suggests an alternative path of utilizing current and impending quantum devices [380]. Here, one is restricted to computations with only shallow-depth quantum circuits, where the size of the circuit is determined by hardware parameters such as coherence times and gate fidelities. As these hardware characteristics improve, the circuit sizes that become accessible increase, ultimately leading to circuits that provide a computational advantage over classical approaches. This path lays out a gradual progression to obtaining quantum advantage one hardware improvement at a time, ultimately driving the hardware evolution to progressively better and larger devices until error correction methods can be applied to provide us with access to circuits no longer limited by the device noise.

Early experiments [381] demonstrated that despite the restriction to shallow-depth circuits, noise and decoherence lead to a bias in the estimates of expectation values. For this approach to provide an advantage over classical approximation methods, this bias has to be mitigated. These observations have motivated the development of error mitigation tools such as zero-noise extrapolation [350,382] and probabilistic error cancellation [350]. The goal of these methods is to reduce, or even fully remove, the noise-induced bias from expectation values measured in shallow-depth circuits. This is achieved by one slightly modifying the circuits in different ways and combining measurement outcomes in postprocessing to produce noise-free estimates. The protocols introduce an additional computational and sampling overhead that will ultimately grow exponentially in the noise strength, illustrating that these protocols do not extend the circuit depth beyond the device-specific parameters, but ensure only that accurate values are produced within the allotted circuit size. The zero-noise extrapolation method was experimentally implemented for the first time on small-scale chips [355]. There it was shown that the effect of noise in earlier experiments [381] could be removed. Recently it was demonstrated [239] that this method could be scaled to larger circuit sizes on improved quantum hardware, such as the recent version of the 27-qubit Falcon processor, by combination of the method with error suppression techniques including dynamical decoupling [383,384] and Pauli twirling [352,353,385]. Advances in learning and modeling correlated noise on quantum processors have enabled the implementation of probabilistic error cancellation [351] to fully remove the noise bias for even the highest-weight observables on larger devices.

To enable the scientific community to utilize these advances, IBM Quantum has announced a challenge to both internal developers and the community: the 100 × 100 Challenge [1]. In 2024, IBM Quantum is planning

to offer a quantum computing chip capable of calculating unbiased observables of circuits with 100 qubits and a depth of 100 gate operations in a reasonable runtime, i.e., within 1 day. This new tool is to challenge the community towards proposing quantum algorithms that use this hardware to solve interesting problems that are notoriously hard for classical computers.

The HEP community plays a pivotal role here since the field is one of the driving sources for challenging computational problems inherent to quantum mechanics. This community is ideally equipped to propose problem-relevant heuristics [386,387] that stand to benefit from early demonstrations on quantum hardware.

APPENDIX B: EXECUTION ON QUANTUM HARDWARE

To give readers an overview of how a quantum computation is done, we briefly summarize the steps required to go from a HEP problem to an execution on hardware. First, the problem is mapped to a language understandable by a digital quantum computer. For instance, continuous fermionic fields are discretized on a lattice, resulting in creation and annihilation operators $a_{i,\sigma}^\dagger$ and $a_{i,\sigma}$ with spin σ at lattice site i . Next, the discretized operators are mapped to Pauli spin operators, such that the initial statistics of the model are preserved. For instance, the anticommutation rules of fermions are preserved with the Jordan-Wigner or Bravyi-Kitaev mappings [388]. This results in a set of Pauli operators $\{P_i\}$ that a quantum computer can work with. Here, each P_i is a tensor product of Pauli spin matrices $\{I, X, Y, Z\}$. Typically, a quantum computation will then act with exponentials of the P_i 's—resulting in unitary operators $U_i = \exp\{-i\theta P_i\}$ —on the corresponding qubit register. Most digital quantum computers support a universal hardware native basis gate set built from a two-qubit gate (e.g., a CNOT gate or a controlled Z gate) and single-qubit rotations. Therefore, they cannot directly implement an arbitrary U_i . To overcome this, a transpiler decomposes the U_i 's into the hardware native basis gate set. While general results such as the Solovay-Kitaev theorem exist [389], efficiently transpiling unitary operators is an active area of research [390]. Once the circuit is transpiled to the hardware native basis gate set, it can be executed by the device.

The transmon is a popular superconducting qubit built from a Josephson junction in parallel with a capacitor [391,392]. This system forms a nonlinear resonator engineered such that the ground state and the first excited state are split by an energy $\hbar\omega_{01}$, where the qubit transition frequency $\omega_{01}/2\pi$ is engineered to lie close to 5 GHz. On IBM Quantum hardware, single-qubit \sqrt{X} and X gates are engineered by microwave pulses, close to Gaussians in shape [393], modulated at ω_{01} . Arbitrary rotations $R_Z(\theta)$ around the Z axis of the qubit are virtual and implemented

by one changing the phase of all subsequent microwave pulses [394]. Two-qubit gates are typically more complex than single-qubit gates and have a larger error. For instance, a CNOT gate can be created by one driving one qubit at the frequency of another qubit [395], while controlled Z gates can be created by one carefully modulating a frequency-tunable element that couples two qubits [396]. Finally, the state of the qubits is read out, which requires one driving a microwave resonator whose resonance frequency depends on the state of the qubit to which it is coupled. The transmission and reflection of this resonator is then converted to a 0 or a 1 [392].

APPENDIX C: ILLUSTRATION OF A QUANTUM SIMULATION: THE CASE OF THE SCHWINGER MODEL

Let us consider the Schwinger model, i.e., QED in $1 + 1$ dimensions, to illustrate how to obtain a lattice formulation and how to address it with a quantum device. The continuum Lagrangian for the massive Schwinger model reads [397]

$$\mathcal{L} = \bar{\psi}(i\gamma^\mu \partial_\mu - g\gamma^\mu A_\mu - m)\psi - \frac{1}{4}F_{\mu\nu}F^{\mu\nu}, \quad (\text{C1})$$

where $\psi = (\psi_1, \psi_2)^T$ denotes a two-component Dirac spinor describing the fermions, m is the bare fermion mass, A_μ is the gauge field with coupling constant g , $F_{\mu\nu} = \partial_\mu A_\nu - \partial_\nu A_\mu$ corresponds to the field strength tensor, and γ^μ are the Dirac matrices for two dimensions. The indices μ and ν in Eq. (C1) take the values 0 and 1, corresponding to the temporal and spatial components of the gauge field, and the Einstein summation convention is implied.

Choosing temporal gauge, $A_0 = 0$, performing a negative Legendre transformation of \mathcal{L} , and integrating it over space, one can obtain the Hamiltonian

$$H = \int dx \left(-i\bar{\psi}\gamma^1(\partial_1 - igA_1)\psi + m\bar{\psi}\psi + \frac{1}{2}\mathcal{F}^2 \right), \quad (\text{C2})$$

where $\mathcal{F} = -\dot{A}^1$ corresponds to the electric field. The physical states of the Hamiltonian have to fulfill an additional constraint in the form of Gauss's law,

$$\partial_1 \mathcal{F} = g\psi^\dagger \psi, \quad (\text{C3})$$

which is a consequence of the choice of gauge and corresponds to the equation of motion for A_0 .

At first glance, a discretization of the Hamiltonian in Eq. (C2) seems straightforward: after the introduction of a spatial lattice, the fields can be discretized and the derivatives can be approximated as finite differences. However, such a naive approach fails to produce the correct continuum limit in the sense that observables extracted from

the lattice theory do not converge to their continuum values as the lattice spacing is taken to zero. The origin of this problem can be traced back to additional low-energy contributions in the first Brillouin zone of the lattice theory [87,88]. In general, discretization of the Hamiltonian of a fermionic theory in d spatial dimensions yields $2^d - 1$ unwanted contributions. Since the number of detrimental contributions doubles with each dimension, this is commonly referred to as “fermion doubling” [88].

To avoid fermion doubling, one has to counteract these additional low-energy contributions arising from the lattice discretization. There are various ways to remove the doublers; the two most commonly used ones for quantum simulation are Wilson fermions and Kogut-Susskind staggered fermions. Wilson’s approach, also mentioned in Sec. II A 2, adds a lattice version of the second derivative of the fermion fields to the Hamiltonian that lifts the additional low-energy contributions and vanishes as the lattice spacing is taken to zero [46,88,90]. The Kogut-Susskind staggered fermions correspond to distributing the different spinor components of the Dirac spinor to different lattice sites. This technique effectively doubles the lattice spacing, thus avoiding fermion doubling [7,87]. While the Kogut-Susskind approach allows one to fully avoid fermion doubling in one spatial dimension, in higher spatial dimensions it reduces only the number of doublers [87]. So far, most quantum simulation experiments for LGT with fermions have used the Kogut-Susskind staggered fermions; hence, we focus on the lattice discretization of the Schwinger Hamiltonian using these in the following.

The Hamiltonian lattice formulation of the Schwinger Hamiltonian in Eq. (C2) with Kogut-Susskind staggered fermions reads

$$\hat{H}_{\text{SM}} = \sum_{\ell} \left[-\frac{\kappa}{2a} (\hat{\phi}_{\ell}^{\dagger} \hat{U}_{\ell,\ell+1} \hat{\phi}_{\ell+1} + \text{H.c.}) + m(-1)^{\ell} \hat{\phi}_{\ell}^{\dagger} \hat{\phi}_{\ell} + \frac{ag^2}{2} \hat{E}_{\ell,\ell+1}^2 \right], \quad (\text{C4})$$

where m is the bare fermion mass, a is the lattice spacing, g is the coupling, and we have introduced an additional parameter κ in front of the kinetic term. The matter degrees of freedom are represented by the single-component fermionic fields $\hat{\phi}_{\ell}, \hat{\phi}_{\ell}^{\dagger}$ on site ℓ . The gauge degrees of freedom are represented by the link operators $\hat{U}_{\ell,\ell+1} = \exp(i\hat{\theta}_{\ell})$ and the electric field operators $\hat{E}_{\ell,\ell+1}$, both acting on the gauge link between sites ℓ and $\ell + 1$. The operator $\hat{\theta}_{\ell}$ is the canonical conjugate of the electric field operator, $[\hat{\theta}_{\ell}, \hat{E}_{\ell'}] = i\delta_{\ell\ell'}$, and takes values in $[0, 2\pi]$. Hence, one finds for the commutation relations

$$[\hat{E}_{\ell,\ell+1}, \hat{U}_{\ell',\ell'+1}] = \delta_{\ell,\ell'} \hat{U}_{\ell,\ell+1}, \quad (\text{C5a})$$

$$[\hat{U}_{\ell,\ell+1}, \hat{U}_{\ell',\ell'+1}^{\dagger}] = 0. \quad (\text{C5b})$$

This implies that the unitary operator $\hat{U}_{\ell,\ell+1}$ acts as a shift operator for the electric field on the gauge link joining sites ℓ and $\ell + 1$, lowering the electric flux by one unit. The physical states $|\psi\rangle$ of the Hamiltonian in Eq. (C4) must fulfill the lattice version of Gauss’s law, which is given by for all ℓ , $\hat{G}_{\ell} |\psi\rangle = 0$, where

$$\hat{G}_{\ell} = \hat{E}_{\ell,\ell+1} - \hat{E}_{\ell-1,\ell} - \hat{Q}_{\ell}. \quad (\text{C6})$$

The operators \hat{G}_{ℓ} are the generators of time-independent gauge transformations, and $\hat{Q}_{\ell} = \hat{\phi}_{\ell}^{\dagger} \hat{\phi}_{\ell} - (1 - (-1)^{\ell})/2$ is the staggered charge on site ℓ .

For $\kappa = 1$, the continuum limit, $ag \rightarrow 0$, of Eq. (C4) converges to the continuum Hamiltonian for (1+1)D QED. In particular, one has the correspondence

$$\frac{\hat{\phi}_{\ell}}{\sqrt{a}} \rightarrow \begin{cases} \psi_1(\ell a) & \text{for } \ell \text{ even,} \\ \psi_2(\ell a) & \text{for } \ell \text{ odd} \end{cases} \quad (\text{C7})$$

for the fermion fields and

$$\hat{\theta}_{\ell}/ag \rightarrow A_1(\ell a), \quad g\hat{E}_{\ell,\ell+1} \rightarrow \mathcal{F}(\ell a) \quad (\text{C8})$$

for the gauge fields. Using the fact that the gauge connection shows only a small change along the link between neighboring lattice sites in the limit of small lattice spacing, one can expand $\hat{U}_{\ell,\ell+1} \approx 1 + iagA_1 + \mathcal{O}((ag)^2)$, which together with the correspondence above allows one to recover the continuum Hamiltonian.

The fermionic degrees of freedom in the Schwinger Hamiltonian can, in principle, be realized in an analog quantum simulator. However, they do not readily translate on digital devices. With a Jordan-Wigner transformation, we can replace the fermionic degrees of freedom with Pauli operators:

$$\hat{\phi}_{\ell} = \prod_{n<\ell} (i\hat{\sigma}_n^z) \hat{\sigma}_{\ell}^{-}, \quad \hat{\phi}_{\ell}^{\dagger} = \prod_{n<\ell} (-i\hat{\sigma}_n^z) \hat{\sigma}_{\ell}^{+}, \quad (\text{C9})$$

where $\sigma_{\ell}^{\pm} = (\hat{\sigma}_{\ell}^x \pm i\hat{\sigma}_{\ell}^y)/2$. Moreover, the commutation relations in Eq. (C5) imply that the Hilbert spaces on the gauge links are infinitely dimensional, which makes them challenging for numerical simulations and experimental implementations.

In the case of open boundary conditions, the problem of infinite-dimensional gauge links can be avoided by one integrating out the gauge links. After the electric field value l_0 on the left boundary has been fixed, a recursive application of Gauss’s law in Eq. (C6) allows the reconstruction of the electric field purely from the charge content of the sites, $\hat{E}_{\ell,\ell+1} = \sum_{k<\ell+1} Q_k + l_0$. By substituting this into Eq. (C4), applying a unitary to the fermionic fields [90,398], and translating the resulting expression to

spin language with the Jordan-Wigner transformation, we obtain

$$\begin{aligned} \hat{H}_{\text{SM}} = & -\frac{\kappa}{2a} \sum_{\ell=0}^{N-2} (\hat{\sigma}_{\ell}^x \hat{\sigma}_{\ell+1}^x + \hat{\sigma}_{\ell}^y \hat{\sigma}_{\ell+1}^y) \\ & + m \sum_{\ell=0}^{N-1} (-1)^{\ell} \hat{\sigma}_{\ell}^z + \frac{ag^2}{2} \sum_{\ell=0}^{N-2} \left(\sum_{k=0}^{\ell} Q_k + l_0 \right)^2, \end{aligned} \quad (\text{C10})$$

where $Q_{\ell} = (\hat{\sigma}_{\ell}^z + (-1)^{\ell})/2$ is the staggered charge operator in the spin representation, and l_0 corresponds to a topological θ term [90,399]. We also dropped all constant terms in the Hamiltonian.

Another way to address the infinite-dimensional links in practical simulations is to truncate them to a finite dimension. While there are various ways of truncating the gauge degrees of freedom [91,92,105,106], the *quantum link model* formulation [121,122,124] has been successfully used in many experiments and simulations. QLMs replace the infinite-dimensional link operators with finite spin operators:

$$\hat{U}_{\ell,\ell+1} \rightarrow \frac{\hat{s}_{\ell,\ell+1}^+}{\sqrt{S(S+1)}}, \quad (\text{C11a})$$

$$\hat{E}_{\ell,\ell+1} \rightarrow \hat{s}_{\ell,\ell+1}^z, \quad (\text{C11b})$$

where $\hat{s}_{\ell,\ell+1}^{\pm} = (\hat{s}_{\ell,\ell+1}^x \pm i\hat{s}_{\ell,\ell+1}^y)/2$ and $\hat{s}_{\ell,\ell+1}^x, \hat{s}_{\ell,\ell+1}^y, \hat{s}_{\ell,\ell+1}^z$ are the spin operators of the chosen spin representation S acting on the link between sites ℓ and $\ell+1$. This renders the commutation relations from Eqs. (C5) of the form

$$[\hat{E}_{\ell,\ell+1}, \hat{U}_{\ell',\ell'+1}] \rightarrow \delta_{\ell,\ell'} \frac{\hat{s}_{\ell,\ell+1}^+}{\sqrt{S(S+1)}}, \quad (\text{C12a})$$

$$[\hat{U}_{\ell,\ell+1}, \hat{U}_{\ell',\ell'+1}^{\dagger}] \rightarrow 2\delta_{\ell,\ell'} \frac{\hat{s}_{\ell,\ell+1}^z}{S(S+1)}. \quad (\text{C12b})$$

In the limit $S \rightarrow \infty$, the QLM representation converges to the commutation relations in Eqs. (C5). The spin- S U(1) QLM Hamiltonian reads

$$\begin{aligned} \hat{H}_{\text{QLM}} = & \sum_{\ell} \left[-\frac{\kappa}{2a\sqrt{S(S+1)}} (\hat{\sigma}_{\ell}^+ \hat{s}_{\ell,\ell+1}^+ \hat{\sigma}_{\ell+1}^- + \text{H.c.}) \right. \\ & \left. + \frac{m}{2} (-1)^{\ell} \hat{\sigma}_{\ell}^z + \frac{g^2 a}{2} (\hat{s}_{\ell,\ell+1}^z)^2 \right]. \end{aligned} \quad (\text{C13})$$

1. Analog quantum simulation

We illustrate the concept of analog quantum simulation with the simplest case of $S = 1/2$, which renders the gauge

and electric field operators as two-level systems. This gives rise to the spin-1/2 U(1) QLM with Hamiltonian

$$\hat{H}_{\text{QLM}} = \sum_{\ell} \left[-\frac{\kappa}{2} (\hat{\sigma}_{\ell}^+ \hat{s}_{\ell,\ell+1}^+ \hat{\sigma}_{\ell+1}^- + \text{H.c.}) + \frac{m}{2} (-1)^{\ell} \hat{\sigma}_{\ell}^z \right], \quad (\text{C14})$$

where we omitted a trivial factor in the kinetic term for notational brevity. We also set the lattice spacing to unity, $a = 1$. Importantly, the electric energy term $\propto g^2$ becomes an inconsequential constant for $S = 1/2$, which is why it is omitted in Eq. (C14).

We seek to map the target model (C14) onto an analog quantum simulator that is feasible to implement in the laboratory. To this end, we use an optical superlattice of bosons, with the shallow sites representing the sites of the QLM, and deep sites representing the links of the QLM; see Fig. 3. We would like to engineer our quantum simulator such that on a shallow superlattice site only one or zero bosons can live, while on a deep site only two or zero bosons can reside, which can faithfully map the allowed configurations based on Gauss's law (see Fig. 3). In this gauge-invariant subspace, the QLM operators can be represented by bosonic operators as

$$\hat{s}_{\ell,\ell+1}^+ = \frac{(\hat{b}_{\ell,\ell+1}^{\dagger})^2}{\sqrt{2}}, \quad \hat{s}_{\ell,\ell+1}^z = \frac{\hat{b}_{\ell,\ell+1}^{\dagger} \hat{b}_{\ell,\ell+1} - 1}{2}, \quad (\text{C15a})$$

$$\hat{\sigma}_{\ell}^+ = \hat{b}_{\ell}^{\dagger}, \quad \hat{\sigma}_{\ell}^z = 2\hat{b}_{\ell}^{\dagger} \hat{b}_{\ell} - 1, \quad (\text{C15b})$$

where $\hat{b}_{\ell,\ell+1}^{\dagger}$ ($\hat{b}_{\ell,\ell+1}$) are bosonic creation (annihilation) operators acting on the link between site ℓ and site $\ell+1$. Yang *et al.* [78] showed that this mapping can be achieved in second-order degenerate perturbation theory

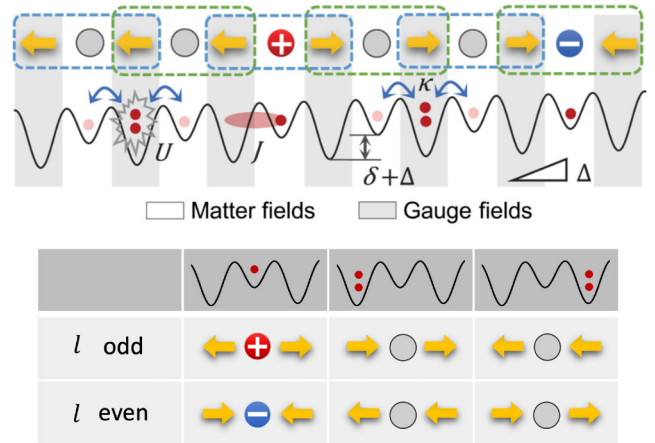


FIG. 3. Mapping of a QLM onto a Bose-Hubbard model quantum simulator (adapted from Ref. [78]).

using the Bose-Hubbard superlattice Hamiltonian (Bose-Hubbard model),

$$\begin{aligned} \hat{H}_{\text{BH}} = & -J \sum_{j=1}^{L-1} (\hat{b}_j^\dagger \hat{b}_{j+1} + \text{H.c.}) + \frac{U}{2} \sum_{j=1}^L \hat{n}_j (\hat{n}_j - 1) \\ & + \frac{1}{2} \sum_{j=1}^L [(-1)^j \delta + 2j \Delta] \hat{n}_j, \end{aligned} \quad (\text{C16})$$

in the regime of $U, \delta \gg J, \Delta$. Here J is the bosonic tunneling constant, U is the on-site repulsion strength, δ is a staggering potential (between the shallow and deep sites), Δ is a global tilt, and $\hat{n}_j = \hat{b}_j^\dagger \hat{b}_j$; see Fig. 3. The parameters of the QLM are related to those of the Bose-Hubbard model as $m \approx \delta - U/2$ and $\kappa \approx 8\sqrt{2}J^2/U$.

Subleading terms arise in this perturbative mapping that explicitly break Gauss's law, but the corresponding violations are reliably and controllably suppressed by a leading-order linear gauge protection term proportional to $\sum_j j \Delta (-1)^j \hat{G}_j$, where \hat{G}_j is the generator of Gauss's law [400].

2. Digital quantum simulations

A typical quantum simulation of the Schwinger Hamiltonian in Eq. (C10) will start with the optimization of the ground state. To this end, one can implement a variational quantum circuit, which preserves the desired symmetries of the Hamiltonian (see, e.g., Ref. [48]) and then perform a hybrid VQE calculation to obtain the set of circuit parameters that characterizes the ground state wave function.

To perform quantum dynamics, one first decompose the time-evolution operator corresponding to the Hamiltonian in Eq. (C10) using the Suzuki-Trotter formula as

$$e^{-iH_{\text{SM}}\Delta t} \approx e^{-iH_{\text{kin}}\Delta t} e^{-iH_m\Delta t} e^{-iH_E\Delta t}, \quad (\text{C17})$$

where H_{kin} , H_m , and H_E are the kinetic, the mass and the electric energy terms of the Hamiltonian, and Δt is the time step. The latter two factors, $e^{-iH_m\Delta t}$ and $e^{-iH_E\Delta t}$, are easily

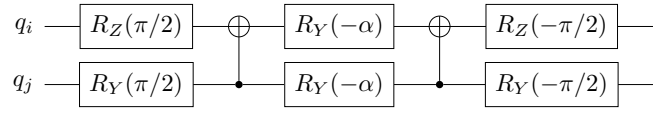


FIG. 4. Quantum circuit for $e^{-i(X_i X_j + Y_i Y_j)(\alpha/2)}$ on qubits i and j .

implemented with use of R_Z single-qubit rotations, while the first factor $e^{-iH_{\text{kin}}\Delta t}$ can be implemented by a quantum circuit as shown in Fig. 4.

APPENDIX D: RESOURCE REQUIREMENTS FOR QUANTUM SIMULATION OF LATTICE QED

In this appendix we assess the resource requirements for the implementation of the quantum link model formulation of U(1) lattice gauge theories with dynamical Wilson fermions in arbitrary dimension d . In Ref. [26], we assessed the number of qubits required to capture all degrees of freedom. Then we also reported the number of Pauli strings that are required to implement the different terms in the QED Hamiltonian, and finally we touched upon how this translates into the number of required quantum gates. We express all scalings in terms of a combination of the following model parameters:

- (1) n_s , the number of lattice sites.
- (2) n_e , the number of lattice edges (scales linearly with n_s in regular lattices).
- (3) n_p , the number of lattice plaquettes (scales linearly with n_s in regular lattices).
- (4) n_{spinor} , the number of spinor components.
- (5) d , the number of spatial lattice dimensions.
- (6) d_S , the dimension of the spin- S system in the quantum link model.
- (7) $n_{\text{nonzero}}(A)$, the number of nonzero elements of the matrix A .
- (8) $n_{\text{Pauli}}(\hat{O})$, the total number of Pauli strings in the encoding of the operator \hat{O} .
- (9) $n_{\text{real}}(\hat{O})$, the number of Pauli strings with real coefficients in the encoding of \hat{O} .

TABLE III. Scaling relations for the number of Pauli terms for the terms in the lattice QED Hamiltonian shown for different encodings of the truncated gauge operators. These relations do not depend on whether the Jordan-Wigner, Bravyi-Kitaev, or parity mapping is used for the fermions.

Term	Number of Pauli strings		
	Logarithmic encoding	Logarithmic encoding (perfect)	Linear encoding
H_{mass}	$\mathcal{O}(n_s n_{\text{spinor}})$	$\mathcal{O}(n_s n_{\text{spinor}})$	$\mathcal{O}(n_s n_{\text{spinor}})$
H_{hopp}	$\mathcal{O}(n_s d n_{\text{spinor}}^2 d_S^2)$	$\mathcal{O}(n_s d n_{\text{spinor}}^2 d_S)$	$\mathcal{O}(n_s d n_{\text{spinor}}^2 d_S)$
H_{Wilson}	$\mathcal{O}(n_s d n_{\text{spinor}}^2 d_S^2)$	$\mathcal{O}(n_s d n_{\text{spinor}}^2 d_S)$	$\mathcal{O}(n_s d n_{\text{spinor}}^2 d_S)$
H_{elec}	$\mathcal{O}(n_s d d_S)$	$\mathcal{O}(n_s d d_S)$	$\mathcal{O}(n_s d d_S^2)$
H_{plaq}	$\mathcal{O}(n_s d d_S^2)$	$\mathcal{O}(n_s d d_S^4)$	$\mathcal{O}(n_s d d_S^4)$

- (10) $n_{\text{imag}}(\hat{O})$, the number of Pauli strings with imaginary coefficients in the encoding of \hat{O} .
- (11) $n_{\text{mix}}(\hat{O})$, the number of Pauli strings with neither purely real nor purely imaginary coefficients in the expansion of \hat{O} .

Table III provides a summary of this analysis. For the exact formulas for the number of Pauli terms, we refer to the respective sections above.

The analysis shows that the dominant term with respect to the number of required Pauli strings is the plaquette term H_{plaq} , due to its strong scaling with d_S . For this reason, even for small values of d_S , the plaquette term contributes by far the highest number of Pauli strings of all the terms in the Hamiltonian.

The best overall scaling, and thus the lowest number of required Pauli terms, is achieved by use of a logarithmic encoding for a quantum link model with a perfectly representable spin- S system. The logarithmic encoding is also more favorable in terms of the number of required qubits. The downside of perfectly representable S is that the eigenvalue $S_z = 0$ is not contained in the spectrum as d_S is a power of 2, resulting in a degenerate ground state.

APPENDIX E: ALGORITHMS AND THEIR LIMITATIONS

In this appendix we provide an overview of various classical and quantum algorithms relevant for the field of high-energy physics and highlight their capabilities as well as their limitations.

1. VQE and variational quantum deflation

The variational quantum eigensolver is a hybrid quantum-classical approach to obtain an approximation for the ground state of a (quantum) system [94]. The algorithm uses the quantum device to prepare an ansatz state in the form of a parametric quantum circuit. On the basis of the measurement outcome of the expectation value of the Hamiltonian, a classical minimization algorithm is used to obtain a new set of parameters. Running the feedback loop between the classical computer and the quantum device until convergence, one obtains an approximation for the ground state and its energy, provided the ansatz chosen is expressive enough and the optimization did not converge to a local minimum. The main limitations of the VQE are barren plateaus (see Sec. III B 2) and the large number of measurements needed to solve problems of interest. Wang *et al.* [401] have provided a potential approach for minimizing estimation runtime on noisy quantum computers.

Variational quantum deflation is an extension of the VQE allowing the computation of low-lying excitations by running a VQE looking for a low-energy state that is

orthogonal to all previous states [95]. The subspace-search variational quantum eigensolver is another approach used to compute excited states. This algorithm searches for a low-energy subspace by supplying orthogonal input states to the variational ansatz [96]. All the variational algorithms can be applied to Hamiltonians in both theoretical models and experimental analysis.

2. Tensor networks

Tensor networks are a family of entanglement-based ansatzes providing an efficient parameterization of the physically relevant moderately entangled states [11,13]. TN algorithms allow the computation of ground states, low-lying excitations, thermal states, and to a certain extent real-time dynamics. While TNs are extremely successful in situations with moderate entanglement, they cease to work for highly entangled scenarios such as out-of-equilibrium dynamics. Moreover, in higher dimensions, the numerical algorithms are computationally challenging but have a polynomial scaling in tensor size, thus allowing the first proof-of-principle demonstrations for LGTs [22,57].

3. Quantum approximate optimization algorithm

The quantum approximate optimization algorithm is a hybrid quantum-classical approach, originally designed to tackle combinatorial optimization problems [402]. The problem is encoded in an Ising-type Hamiltonian whose ground state is the optimal solution to the combinatorial optimization problem. The QAOA can be seen as a special type of VQE, where the initial state is given by $\bigotimes |+\rangle$ and the parametric ansatz circuit in its plain vanilla form consists of a series of two alternating types of layer, each one containing a single real parameter. The first one is the exponential of the problem Hamiltonian, $\exp(-i\gamma\mathcal{H})$, followed by a mixing layer corresponding to $R_X(\beta_i)$ gates applied to each qubit. In the limit of infinitely many layers, the QAOA can be interpreted as an adiabatic evolution of an eigenstate of the X operator to the eigenstate of the problem Hamiltonian. From a theoretical point of view, the performance of the QAOA is not entirely clear; it seems to depend on various factors and does not necessarily outperform classical algorithms [403–405]. Dalzell *et al.* [406] gave some estimates on the number of qubits needed for a quantum advantage with QAOA circuits. Furthermore, the resulting quantum circuits can be deep, making them hard to implement on noisy hardware [301,407]. However, some of these issues may be alleviated by algorithmic advances such as warm starts [408] and counteradiabatic driving [409]. Alternatives to the standard QAOA are also described in the literature, including the expressive QAOA [410], the multiangle QAOA [411], and the recursive QAOA [412].

4. Quantum k -means algorithm

The classical k -means algorithm is an efficient algorithm to classify data into k clusters on the basis of an unlabeled set of training vectors. It belongs to the family of unsupervised machine learning algorithms. The number k of clusters must be known *a priori*, which somewhat limits the range of its application in HEP. The algorithm is iterative and assigns at each step a training vector to the nearest centroid. The centroid location is then updated according to the average over the cluster of vectors associated at the current step to the centroid. The most time-consuming and resource-consuming part of the algorithm is the calculation of the distance. In the classical version, with Lloyd's version of the algorithm, the time complexity is $\mathcal{O}(NM)$, where N is the number of features and M is the number of training examples [413–415]. The quantum version of the k -means algorithm provides an exponential speedup for very large dimensions of a training vector. This is achieved through the introduction of two quantum subroutines, *SwapTest* and *DistCalc*, for the distance calculation [416] and the quantum subroutine *GroverOptim* to assign a vector to the closest centroid cluster [417].

5. Quantum kernels

Quantum kernels are a supervised quantum machine learning algorithm for classification and regression. The inputs can either be quantum (i.e., quantum states with an associated classical label) or fully classical (i.e., input-output data pairs). For the latter, the input classical data are first embedded into quantum states. For a quantum speedup over classical algorithms, it is important to use an embedding (also called a “quantum feature map”) that is capable of recognizing classically intractable features [281,418,419]. For a given input pair of inputs, one then evaluates a similarity measure between two encoded quantum states on a quantum computer. Formally, this function corresponds to an inner product of data states, and is known as a “quantum kernel” [178,281,420]. The fidelity quantum kernel [178,420] and the projected quantum kernel [281] are two common choices of kernels.

6. Quantum generative modeling

Quantum systems, as inherently probabilistic systems, are naturally tailored to generative modeling tasks [421]. The aim of generative modeling is to use training samples from a given target distribution to learn a model distribution that can then be used to generate new samples. As well as providing an efficient means of generating samples, it has been shown that quantum generative models can encode probability distributions that cannot be modeled efficiently classically [422–424]. A number of different architectures and training strategies are being explored for quantum generative modeling. The quantum circuit Born machine [425] encodes a probability distribution in

an n -qubit pure state. The quantum Boltzmann machine [426] is based on the Boltzmann distribution of a quantum Hamiltonian. A QGAN [427] uses the interplay of a generative quantum neural network and a classical or quantum discriminative model for a target distribution. In all cases the quantum generative model is generally trained by optimization of a cost function that estimates the distance between the model distribution and the training distribution. Commonly used costs include the Kullback-Leibler divergence [428], the Jensen-Shannon divergence [429], the (quantum) Rényi divergence [430,431], and the maximum mean discrepancy [432].

7. Quantum reinforcement learning

Reinforcement learning is an interactive mode of machine learning well suited for sequential decision and control tasks, and its objective is identifying the optimal policy (specification of what a learner does in a given situation) for a task environment. Current state-of-art methods include policy gradient methods, where the optimal policy is parameterized, and the performance is optimized in the policy space with use of interactions with the task environment, and deep Q -learning methods, where the optimal value functions, which evaluate the “value” of a given state-action pair under a given policy, are approximated. Other approaches combine features of policy-based and value function-based methods. In quantum reinforcement learning, i.e., in quantum approaches to reinforcement learning, the policies (in policy gradients), or value functions (in value function-based methods) are expressed with use of parameterized quantum circuits, instead of, for example, neural networks, which are conventionally used. The first quantum policy methods that achieved successful performances in OpenAI Gym benchmarking environments were reported in Ref. [433], and the same paper proved the existence of task environments that can be learned only with quantum learners. In Ref. [434] the quantum approach was extended to value-based approaches (deep Q learning), and analogous proofs of learning separations were given. Jerbi *et al.* [435] studied the use of quantum methods to speed up neural network-based deep energy models. Follow-up studies include the analysis of the performance of simple unentangled quantum learners [436], learning in partially observable environments [437], and applications in combinatorial optimization [438]. Quantum reinforcement learning was also used in the work reported in Ref. [439], where free energy-based reinforcement learning is extended to multidimensional continuous state-action space environments to open the door for a broader range of real-world applications. A hybrid actor-critic scheme for continuous state-action spaces was developed on the basis of the deep deterministic policy gradient algorithm combining a classical actor network with a quantum Boltzmann

machine-based critic. The environments used throughout represent the existing particle accelerator beam line of the Advanced Plasma Wakefield Experiment (AWAKE) at CERN. Quantum reinforcement learning with parameterized circuits suffers from barren plateaus as well (as it contains conventional supervised learning as a special case), although it is not known whether the phenomenon is exacerbated. In recent work [440], the effect of noise was studied as well, and the results suggest that the models could be somewhat resistant to noise, but more studies are required for conclusive findings.

8. Topological data analysis

TDA is an increasingly studied technique for extracting robust topological features from complex datasets, and has in recent times also been used in high-energy physics problems [441]. The principal computational task in TDA is the extraction of so-called (persistent) Betti numbers, which can be used to distinguish the underlying topological spaces of data. In Ref. [442], a quantum algorithm for this problem was proposed, and it was suggested it may offer exponential speedups over conventional methods. In Refs. [283,443] it was proven that certain generalizations of the TDA problem are deterministic quantum computation with one-clean-qubit (DQC1) hard (and thus likely offer exponential speedups), and Ref. [444] showcases how persistent features can be extracted as well. References [282,445,446] provide streamlined versions of the original algorithm, where up-to-exponential savings in the qubit numbers were achieved, and Ref. [282] has showcased a concrete family of datasets where concrete superpolynomial speedups over the best conventional methods are achieved. In Refs. [283,447], based on Ref. [448], a deep connection between TDA and supersymmetric theories was established that may lead to new applications of (quantum) TDA in not only analyzing experimental data but also exploring theoretical spaces beyond the Standard Model. However it is important to note that it remains to be determined if quantum TDA offers guaranteed speedups or if it can be “dequantized” with use of a new class of classical methods. Further, it is still an open question whether the regimes where quantum dramatic speedups kick in (i.e., when the desired homology, or Betti number, is high) have wide application.

[1] I. Quantum, Quantum-centric supercomputing: The next wave of computing (), <https://research.ibm.com/blog/next-wave-quantum-centric-supercomputing>.

[2] Y. Kim, A. Eddins, S. Anand, K. X. Wei, E. van den Berg, S. Rosenblatt, H. Nayfeh, Y. Wu, M. Zaletel, K. Temme, and A. Kandala, Evidence for the utility of quantum computing before fault tolerance, *Nature* **618**, 500 (2023).

- [3] S. Dürr, Z. Fodor, J. Frison, C. Hoelbling, R. Hoffmann, S. D. Katz, S. Krieg, T. Kurth, L. Lellouch, T. Lippert, K. K. Szabo, and G. Vulvert, Ab initio determination of light hadron masses, *Science* **322**, 1224 (2008).
- [4] C. Alexandrou, Recent progress on the study of nucleon structure from lattice QCD and future perspectives, *SciPost Phys. Proc.* **3**, 015 (2020).
- [5] K. Fukushima and T. Hatsuda, The phase diagram of dense QCD, *Rep. Prog. Phys.* **74**, 014001 (2011).
- [6] M. Troyer and U.-J. Wiese, Computational complexity and fundamental limitations to fermionic quantum Monte Carlo simulations, *Phys. Rev. Lett.* **94**, 170201 (2005).
- [7] J. Kogut and L. Susskind, Hamiltonian formulation of Wilson’s lattice gauge theories, *Phys. Rev. D* **11**, 395 (1975).
- [8] J. B. Kogut, An introduction to lattice gauge theory and spin systems, *Rev. Mod. Phys.* **51**, 659 (1979).
- [9] P. Silvi, E. Rico, T. Calarco, and S. Montangero, Lattice gauge tensor networks, *New J. Phys.* **16**, 103015 (2014).
- [10] M. Dalmonte and S. Montangero, Lattice gauge theory simulations in the quantum information era, *Contemp. Phys.* **57**, 388 (2016).
- [11] M. C. Bañuls and K. Cichy, Review on novel methods for lattice gauge theories, *Rep. Prog. Phys.* **83**, 024401 (2020).
- [12] M. C. Bañuls, R. Blatt, J. Catani, A. Celi, J. I. Cirac, M. Dalmonte, L. Fallani, K. Jansen, M. Lewenstein, S. Montangero, C. A. Muschik, B. Reznik, E. Rico, L. Tagliacozzo, K. Van Acoleyen, F. Verstraete, U.-J. Wiese, M. Wingate, J. Zakrzewski, and P. Zoller, Simulating lattice gauge theories within quantum technologies, *Eur. Phys. J. D* **74**, 165 (2020).
- [13] M. C. Bañuls, K. Cichy, J. I. Cirac, K. Jansen, and S. Kühn, Tensor networks and their use for lattice gauge theories, PoS(LATTICE 2018)022, (2019).
- [14] B. Buyens, J. Haegeman, K. Van Acoleyen, H. Verschelde, and F. Verstraete, Matrix product states for gauge field theories, *Phys. Rev. Lett.* **113**, 091601 (2014).
- [15] S. Kühn, E. Zohar, J. Cirac, and M. C. Bañuls, Non-Abelian string breaking phenomena with matrix product states, *J. High Energy Phys.* **2015**, 130 (2015).
- [16] T. Pichler, M. Dalmonte, E. Rico, P. Zoller, and S. Montangero, Real-time dynamics in U(1) lattice gauge theories with tensor networks, *Phys. Rev. X* **6**, 011023 (2016).
- [17] B. Buyens, J. Haegeman, F. Hebenstreit, F. Verstraete, and K. Van Acoleyen, Real-time simulation of the Schwinger effect with matrix product states, *Phys. Rev. D* **96**, 114501 (2017).
- [18] M. C. Bañuls, M. P. Heller, K. Jansen, J. Knaute, and V. Svensson, From spin chains to real-time thermal field theory using tensor networks, *Phys. Rev. Res.* **2**, 033301 (2020).
- [19] M. Rigobello, S. Notarnicola, G. Magnifico, and S. Montangero, Entanglement generation in (1+1)D QED scattering processes, *Phys. Rev. D* **104**, 114501 (2021).
- [20] M. C. Bañuls, K. Cichy, J. I. Cirac, K. Jansen, and S. Kühn, Density induced phase transitions in the Schwinger model: A study with matrix product states, *Phys. Rev. Lett.* **118**, 071601 (2017).
- [21] P. Silvi, E. Rico, M. Dalmonte, F. Tschirsich, and S. Montangero, Finite-density phase diagram of a (1+1)-d

- non-abelian lattice gauge theory with tensor networks, *Quantum* **1**, 9 (2017).
- [22] T. Felser, P. Silvi, M. Collura, and S. Montangero, Two-dimensional quantum-link lattice quantum electrodynamics at finite density, *Phys. Rev. X* **10**, 041040 (2020).
- [23] P. Silvi, Y. Sauer, F. Tschirsich, and S. Montangero, Tensor network simulation of an SU(3) lattice gauge theory in 1D, *Phys. Rev. D* **100**, 074512 (2019).
- [24] T. Byrnes and Y. Yamamoto, Simulating lattice gauge theories on a quantum computer, *Phys. Rev. A* **73**, 022328 (2006).
- [25] S. P. Jordan, K. S. M. Lee, and J. Preskill, Quantum algorithms for quantum field theories, *Science* **336**, 1130 (2012).
- [26] S. V. Mathis, G. Mazzola, and I. Tavernelli, Toward scalable simulations of lattice gauge theories on quantum computers, *Phys. Rev. D* **102**, 094501 (2020).
- [27] R. P. Feynman, Simulating physics with computers, *Int. J. Theor. Phys.* **21**, 467 (1982).
- [28] N. Klco, J. R. Stryker, and M. J. Savage, SU(2) non-Abelian gauge field theory in one dimension on digital quantum computers, *Phys. Rev. D* **101**, 074512 (2020).
- [29] Y. Atas, J. Zhang, R. Lewis, A. Jahanpour, J. F. Haase, and C. A. Muschik, SU(2) hadrons on a quantum computer via a variational approach, *Nat. Commun.* **12**, 6499 (2021).
- [30] A. Ciavarella, N. Klco, and M. J. Savage, Trailhead for quantum simulation of SU(3) Yang-Mills lattice gauge theory in the local multiplet basis, *Phys. Rev. D* **103**, 094501 (2021).
- [31] G. Clemente, A. Crippa, and K. Jansen, Strategies for the determination of the running coupling of (2+1)-dimensional QED with quantum computing, *Phys. Rev. D* **106**, 114511 (2022).
- [32] D. Banerjee, M. Dalmonte, M. Müller, E. Rico, P. Stebler, U.-J. Wiese, and P. Zoller, Atomic quantum simulation of dynamical gauge fields coupled to fermionic matter: From string breaking to evolution after a quench, *Phys. Rev. Lett.* **109**, 175302 (2012).
- [33] L. Tagliacozzo, A. Celi, A. Zamora, and M. Lewenstein, Optical Abelian lattice gauge theories, *Ann. Phys.* **330**, 160 (2013).
- [34] L. Tagliacozzo, A. Celi, P. Orland, M. W. Mitchell, and M. Lewenstein, Simulation of non-Abelian gauge theories with optical lattices, *Nat. Commun.* **4**, 2615 (2013).
- [35] H. P. Büchler, M. Hermele, S. D. Huber, M. P. A. Fisher, and P. Zoller, Atomic quantum simulator for lattice gauge theories and ring exchange models, *Phys. Rev. Lett.* **95**, 040402 (2005).
- [36] E. Zohar and B. Reznik, Confinement and lattice quantum-electrodynamic electric flux tubes simulated with ultracold atoms, *Phys. Rev. Lett.* **107**, 275301 (2011).
- [37] E. Zohar, J. I. Cirac, and B. Reznik, Simulating compact quantum electrodynamics with ultracold atoms: Probing confinement and nonperturbative effects, *Phys. Rev. Lett.* **109**, 125302 (2012).
- [38] P. Hauke, D. Marcos, M. Dalmonte, and P. Zoller, Quantum simulation of a lattice Schwinger model in a chain of trapped ions, *Phys. Rev. X* **3**, 041018 (2013).
- [39] E. Zohar, J. I. Cirac, and B. Reznik, Cold-atom quantum simulator for SU(2) Yang-Mills lattice gauge theory, *Phys. Rev. Lett.* **110**, 125304 (2013).
- [40] E. Zohar, J. I. Cirac, and B. Reznik, Simulating (2 + 1)-dimensional lattice QED with dynamical matter using ultracold atoms, *Phys. Rev. Lett.* **110**, 055302 (2013).
- [41] D. Banerjee, M. Bögli, M. Dalmonte, E. Rico, P. Stebler, U.-J. Wiese, and P. Zoller, Atomic quantum simulation of U(N) and SU(N) non-Abelian lattice gauge theories, *Phys. Rev. Lett.* **110**, 125303 (2013).
- [42] E. Zohar, J. I. Cirac, and B. Reznik, Quantum simulations of lattice gauge theories using ultracold atoms in optical lattices, *Rep. Prog. Phys.* **79**, 014401 (2016).
- [43] C. Laflamme, W. Evans, M. Dalmonte, U. Gerber, H. Mejía-Díaz, W. Bietenholz, U.-J. Wiese, and P. Zoller, CP(N - 1) quantum field theories with alkaline-earth atoms in optical lattices, *Ann. Phys.* **370**, 117 (2016).
- [44] D. González-Cuadra, E. Zohar, and J. I. Cirac, Quantum simulation of the Abelian-Higgs lattice gauge theory with ultracold atoms, *New J. Phys.* **19**, 063038 (2017).
- [45] E. Rico, M. Dalmonte, P. Zoller, D. Banerjee, M. Bögli, P. Stebler, and U.-J. Wiese, SO(3) “nuclear physics” with ultracold gases, *Ann. Phys.* **393**, 466 (2018).
- [46] T. V. Zache, F. Hebenstreit, F. Jendrzejewski, M. K. Oberthaler, J. Berges, and P. Hauke, Quantum simulation of lattice gauge theories using Wilson fermions, *Quantum Sci. Technol.* **3**, 034010 (2018).
- [47] N. Klco, E. F. Dumitrescu, A. J. McCaskey, T. D. Morris, R. C. Pooser, M. Sanz, E. Solano, P. Lougovski, and M. J. Savage, Quantum-classical computation of Schwinger model dynamics using quantum computers, *Phys. Rev. A* **98**, 032331 (2018).
- [48] G. Mazzola, S. V. Mathis, G. Mazzola, and I. Tavernelli, Gauge-invariant quantum circuits for U(1) and Yang-Mills lattice gauge theories, *Phys. Rev. Res.* **3**, 043209 (2021).
- [49] E. A. Martinez, C. A. Muschik, P. Schindler, D. Nigg, A. Erhard, M. Heyl, P. Hauke, M. Dalmonte, T. Monz, P. Zoller, and R. Blatt, Real-time dynamics of lattice gauge theories with a few-qubit quantum computer, *Nature* **534**, 516 (2016).
- [50] C. Kokail, C. Maier, R. van Bijnen, T. Brydges, M. K. Joshi, P. Jurcevic, C. A. Muschik, P. Silvi, R. Blatt, C. F. Roos, and P. Zoller, Self-verifying variational quantum simulation of the lattice Schwinger model, *Nature* **569**, 355 (2019).
- [51] C. W. Bauer, *et al.*, Quantum simulation for high-energy physics, *PRX Quantum* **4**, 027001 (2023).
- [52] S. Lloyd, Universal quantum simulators, *Science* **273**, 1073 (1996).
- [53] U. Schollwöck, The density-matrix renormalization group in the age of matrix product states, *Ann. Phys.* **326**, 96 (2011).
- [54] S. Montangero, *Introduction to Tensor Network Methods* (Springer International Publishing, Cham, 2018).
- [55] P. Silvi, F. Tschirsich, M. Gerster, J. Jünemann, D. Jaschke, M. Rizzi, and S. Montangero, The tensor networks anthology: Simulation techniques for many-body quantum lattice systems, *SciPost Phys. Lect. Notes* **8**, 8 (2019).

- [56] J. I. Cirac, D. Pérez-García, N. Schuch, and F. Verstraete, Matrix product states and projected entangled pair states: Concepts, symmetries, theorems, *Rev. Mod. Phys.* **93**, 045003 (2021).
- [57] G. Magnifico, T. Felser, P. Silvi, and S. Montangero, Lattice quantum electrodynamics in (3+1)-dimensions at finite density with tensor networks, *Nat. Commun.* **12**, 3600 (2021).
- [58] M. Van Damme, L. Vanderstraeten, J. De Nardis, J. Haegeman, and F. Verstraete, Real-time scattering of interacting quasiparticles in quantum spin chains, *Phys. Rev. Res.* **3**, 013078 (2021).
- [59] F. Barratt, J. Dborin, M. Bal, V. Stojevic, F. Pollmann, and A. G. Green, Parallel quantum simulation of large systems on small NISQ computers, *npj Quantum Inf.* **7**, 79 (2021).
- [60] M. Meth, V. Kuzmin, R. van Bijnen, L. Postler, R. Stricker, R. Blatt, M. Ringbauer, T. Monz, P. Silvi, and P. Schindler, Probing phases of quantum matter with an ion-trap tensor-network quantum eigensolver, *Phys. Rev. X* **12**, 041035 (2022).
- [61] M. C. Banuls, M. P. Heller, K. Jansen, J. Knaute, and V. Svensson, A quantum information perspective on meson melting, *Phys. Rev. D* **108**, 076016 (2023).
- [62] Y. Aoki, *et al.*, (Flavour Lattice Averaging Group (FLAG)), FLAG review 2021, *Eur. Phys. J. C* **82**, 869 (2022).
- [63] S. Schaefer, R. Sommer, and F. Virotta, (ALPHA), Critical slowing down and error analysis in lattice QCD simulations, *Nucl. Phys. B* **845**, 93 (2011).
- [64] C. Alexandrou, A. Athenodorou, K. Hadjiyiannakou, and A. Todaro, Neutron electric dipole moment using lattice QCD simulations at the physical point, *Phys. Rev. D* **103**, 054501 (2021).
- [65] T. Bhattacharya, V. Cirigliano, R. Gupta, E. Mereghetti, and B. Yoon, Contribution of the QCD Θ -term to the nucleon electric dipole moment, *Phys. Rev. D* **103**, 114507 (2021).
- [66] I. M. Georgescu, S. Ashhab, and F. Nori, Quantum simulation, *Rev. Mod. Phys.* **86**, 153 (2014).
- [67] A. Acín, I. Bloch, H. Buhрман, T. Calarco, C. Eichler, J. Eisert, D. Esteve, N. Gisin, S. J. Glaser, F. Jelezko, *et al.*, The quantum technologies roadmap: A European community view, *New J. Phys.* **20**, 080201 (2018).
- [68] W. S. Bakr, J. I. Gillen, A. Peng, S. Fölling, and M. Greiner, A quantum gas microscope for detecting single atoms in a Hubbard-regime optical lattice, *Nature* **462**, 74 (2009).
- [69] W. S. Bakr, A. Peng, M. E. Tai, R. Ma, J. Simon, J. I. Gillen, S. Foelling, L. Pollet, and M. Greiner, Probing the superfluid-to-Mott insulator transition at the single-atom level, *Science* **329**, 547 (2010).
- [70] C. Gross and W. S. Bakr, Quantum gas microscopy for single atom and spin detection, *Nat. Phys.* **17**, 1316 (2021).
- [71] I. Bloch, Quantum coherence and entanglement with ultracold atoms in optical lattices, *Nature* **453**, 1016 (2008).
- [72] A. Browaeys and T. Lahaye, Many-body physics with individually controlled Rydberg atoms, *Nat. Phys.* **16**, 132 (2020).
- [73] M. Aidelsburger, L. Barbiero, A. Bermudez, T. Chanda, A. Dauphin, D. González-Cuadra, P. R. Grzybowski, S. Hands, F. Jendrzejewski, J. Jünemann, *et al.*, Cold atoms meet lattice gauge theory, *Philos. Trans. R. Soc. A* **380**, 20210064 (2022).
- [74] S. D. Bass and E. Zohar, Quantum technologies in particle physics, *Philos. Trans. R. Soc. A* **380**, 20210072 (2022).
- [75] C. Schweizer, F. Grusdt, M. Berngruber, L. Barbiero, E. Demler, N. Goldman, I. Bloch, and M. Aidelsburger, Floquet approach to \mathbb{Z}_2 lattice gauge theories with ultracold atoms in optical lattices, *Nat. Phys.* **15**, 1168 (2019).
- [76] A. Mil, T. V. Zache, A. Hegde, A. Xia, R. P. Bhatt, M. K. Oberthaler, P. Hauke, J. Berges, and F. Jendrzejewski, A scalable realization of local $U(1)$ gauge invariance in cold atomic mixtures, *Science* **367**, 1128 (2020).
- [77] J. C. Halimeh and P. Hauke, Reliability of lattice gauge theories, *Phys. Rev. Lett.* **125**, 030503 (2020).
- [78] B. Yang, H. Sun, R. Ott, H.-Y. Wang, T. V. Zache, J. C. Halimeh, Z.-S. Yuan, P. Hauke, and J.-W. Pan, Observation of gauge invariance in a 71-site Bose-Hubbard quantum simulator, *Nature* **587**, 392 (2020).
- [79] Z.-Y. Zhou, G.-X. Su, J. C. Halimeh, R. Ott, H. Sun, P. Hauke, B. Yang, Z.-S. Yuan, J. Berges, and J.-W. Pan, Thermalization dynamics of a gauge theory on a quantum simulator, *Science* **377**, 311 (2022).
- [80] H.-Y. Wang, W.-Y. Zhang, Z.-Y. Yao, Y. Liu, Z.-H. Zhu, Y.-G. Zheng, X.-K. Wang, H. Zhai, Z.-S. Yuan, and J.-W. Pan, Interrelated thermalization and quantum criticality in a lattice gauge simulator, *Phys. Rev. Lett.* **131**, 050401 (2023).
- [81] G.-X. Su, H. Sun, A. Hudomal, J.-Y. Desaulles, Z.-Y. Zhou, B. Yang, J. C. Halimeh, Z.-S. Yuan, Z. Papić, and J.-W. Pan, Observation of many-body scarring in a Bose-Hubbard quantum simulator, *Phys. Rev. Res.* **5**, 023010 (2023).
- [82] J. Osborne, I. P. McCulloch, B. Yang, P. Hauke, and J. C. Halimeh, Large-scale 2 + 1D $U(1)$ gauge theory with dynamical matter in a cold-atom quantum simulator, [ArXiv:2211.01380](https://arxiv.org/abs/2211.01380).
- [83] J. Osborne, B. Yang, I. P. McCulloch, P. Hauke, and J. C. Halimeh, Spin- S $U(1)$ quantum link models with dynamical matter on a quantum simulator, [ArXiv:2305.06368](https://arxiv.org/abs/2305.06368).
- [84] H. Bernien, S. Schwartz, A. Keesling, H. Levine, A. Omran, H. Pichler, S. Choi, A. S. Zibrov, M. Endres, M. Greiner, *et al.*, Probing many-body dynamics on a 51-atom quantum simulator, *Nature* **551**, 579 (2017).
- [85] G. Semeghini, H. Levine, A. Keesling, S. Ebadi, T. T. Wang, D. Bluvstein, R. Verresen, H. Pichler, M. Kalinowski, R. Samajdar, A. Omran, S. Sachdev, A. Vishwanath, M. Greiner, V. Vuletic, and M. D. Lukin, Probing topological spin liquids on a programmable quantum simulator, *Science* **374**, 1242 (2021).
- [86] H. Nielsen and M. Ninomiya, A no-go theorem for regularizing chiral fermions, *Phys. Lett. B* **105**, 219 (1981).
- [87] L. Susskind, Lattice fermions, *Phys. Rev. D* **16**, 3031 (1977).
- [88] H. J. Rothe, *Lattice Gauge Theories: An Introduction* (World Scientific Publishing Company, Singapore, 2012).
- [89] K. G. Wilson, Confinement of quarks, *Phys. Rev. D* **10**, 2445 (1974).

- [90] T. Angelides, L. Funcke, K. Jansen, and S. Kühn, Computing the mass shift of Wilson and staggered fermions in the lattice Schwinger model with matrix product states (2023).
- [91] C. W. Bauer and D. M. Grabowska, Efficient representation for simulating U(1) gauge theories on digital quantum computers at all values of the coupling, *Phys. Rev. D* **107**, L031503 (2023).
- [92] J. F. Haase, L. Dellantonio, A. Celi, D. Paulson, A. Kan, K. Jansen, and C. A. Muschik, A resource efficient approach for quantum and classical simulations of gauge theories in particle physics, *Quantum* **5**, 393 (2021).
- [93] C. Kane, D. M. Grabowska, B. Nachman, and C. W. Bauer, Efficient quantum implementation of 2+1 U(1) lattice gauge theories with Gauss law constraints, [ArXiv:2211.10497](https://arxiv.org/abs/2211.10497).
- [94] A. Peruzzo, J. McClean, P. Shadbolt, M.-H. Yung, X.-Q. Zhou, P. J. Love, A. Aspuru-Guzik, and J. L. O'Brien, A variational eigenvalue solver on a photonic quantum processor, *Nat. Commun.* **5**, 1 (2014).
- [95] O. Higgott, D. Wang, and S. Brierley, Variational quantum computation of excited states, *Quantum* **3**, 156 (2019).
- [96] K. M. Nakanishi, K. Mitarai, and K. Fujii, Subspace-search variational quantum eigensolver for excited states, *Phys. Rev. Res.* **1**, 033062 (2019).
- [97] S. McArdle, T. Jones, S. Endo, Y. Li, S. C. Benjamin, and X. Yuan, Variational ansatz-based quantum simulation of imaginary time evolution, *npj Quantum Inf.* **5**, 75 (2019).
- [98] P. J. Ollitrault, A. Kandala, C.-F. Chen, P. K. Barkoutsos, A. Mezzacapo, M. Pistoia, S. Sheldon, S. Woerner, J. M. Gambetta, and I. Tavernelli, Quantum equation of motion for computing molecular excitation energies on a noisy quantum processor, *Phys. Rev. Res.* **2**, 043140 (2020).
- [99] A. Kan and Y. Nam, Lattice quantum chromodynamics and electrodynamics on a universal quantum computer, [ArXiv:2107.12769](https://arxiv.org/abs/2107.12769).
- [100] A. Mezzacapo, E. Rico, C. Sabín, I. L. Egusquiza, L. Lamata, and E. Solano, Non-Abelian SU(2) lattice gauge theories in superconducting circuits, *Phys. Rev. Lett.* **115**, 240502 (2015).
- [101] R. C. Farrell, I. A. Chernyshev, S. J. M. Powell, N. A. Zemlevskiy, M. Illa, and M. J. Savage, Preparations for quantum simulations of quantum chromodynamics in 1 + 1 dimensions. I. Axial gauge, *Phys. Rev. D* **107**, 054512 (2023).
- [102] Y. Y. Atas, J. F. Haase, J. Zhang, V. Wei, S. M. L. Pfaendler, R. Lewis, and C. A. Muschik, Simulating one-dimensional quantum chromodynamics on a quantum computer: Real-time evolutions of tetra- and pentaquarks, [ArXiv:2207.03473](https://arxiv.org/abs/2207.03473).
- [103] R. C. Farrell, I. A. Chernyshev, S. J. M. Powell, N. A. Zemlevskiy, M. Illa, and M. J. Savage, Preparations for quantum simulations of quantum chromodynamics in 1 + 1 dimensions. II. Single-baryon β -decay in real time, *Phys. Rev. D* **107**, 054513 (2023).
- [104] S. A. Rahman, R. Lewis, E. Mendicelli, and S. Powell, Self-mitigating trotter circuits for SU(2) lattice gauge theory on a quantum computer, *Phys. Rev. D* **106**, 074502 (2022).
- [105] I. Raychowdhury and J. R. Stryker, Loop, string, and hadron dynamics in SU(2) Hamiltonian lattice gauge theories, *Phys. Rev. D* **101**, 114502 (2020).
- [106] Z. Davoudi, I. Raychowdhury, and A. Shaw, Search for efficient formulations for Hamiltonian simulation of non-Abelian lattice gauge theories, *Phys. Rev. D* **104**, 074505 (2021).
- [107] Z. Davoudi, A. F. Shaw, and J. R. Stryker, General quantum algorithms for Hamiltonian simulation with applications to a non-Abelian lattice gauge theory, *Quantum* **7**, 1213 (2023).
- [108] Y. Tong, V. V. Albert, J. R. McClean, J. Preskill, and Y. Su, Provably accurate simulation of gauge theories and bosonic systems, *Quantum* **6**, 816 (2022).
- [109] T. Hartung, T. Jakobs, K. Jansen, J. Ostmeyer, and C. Urbach, Digitising SU(2) gauge fields and the freezing transition, *Eur. Phys. J. C* **82**, 1 (2022).
- [110] T. Jakobs, M. Garofalo, T. Hartung, K. Jansen, J. Ostmeyer, D. Rolfes, S. Romiti, and C. Urbach, Canonical momenta in digitized SU(2) lattice gauge theory: Definition and free theory, *Phys. J. C* **83**, 669 (2023).
- [111] E. J. Gustafson, H. Lamm, F. Lovelace, and D. Musk, Primitive quantum gates for an SU(2) discrete subgroup: Binary tetrahedral, *Phys. Rev. D* **106**, 114501 (2022).
- [112] E. Zohar, A. Farace, B. Reznik, and J. I. Cirac, Digital lattice gauge theories, *Phys. Rev. A* **95**, 023604 (2017).
- [113] J. Bender, E. Zohar, A. Farace, and J. I. Cirac, Digital quantum simulation of lattice gauge theories in three spatial dimensions, *New J. Phys.* **20**, 093001 (2018).
- [114] D. González-Cuadra, T. V. Zache, J. Carrasco, B. Kraus, and P. Zoller, Hardware efficient quantum simulation of non-Abelian gauge theories with qudits on Rydberg platforms, *Phys. Rev. Lett.* **129**, 160501 (2022).
- [115] D. González-Cuadra, D. Bluvstein, M. Kalinowski, R. Kaubruegger, N. Maskara, P. Naldesi, T. V. Zache, A. M. Kaufman, M. D. Lukin, H. Pichler, *et al.*, Fermionic quantum processing with programmable neutral atom arrays, *Proc. Natl. Acad. Sci.* **120**, e2304294120 (2023).
- [116] T. V. Zache, D. González-Cuadra, and P. Zoller, Quantum and classical spin network algorithms for q -deformed Kogut-Susskind gauge theories, *Phys. Rev. Lett.* **131**, 171902 (2023).
- [117] T. V. Zache, D. González-Cuadra, and P. Zoller, Fermion-qudit quantum processors for simulating lattice gauge theories with matter, *Quantum* **7**, 1140 (2023).
- [118] S. A. Rahman, R. Lewis, E. Mendicelli, and S. Powell, SU(2) lattice gauge theory on a quantum annealer, *Phys. Rev. D* **104**, 034501 (2021).
- [119] R. Brower, S. Chandrasekharan, S. Riederer, and U.-J. Wiese, D-theory: Field quantization by dimensional reduction of discrete variables, *Nucl. Phys. B* **693**, 149 (2004).
- [120] D. Horn, Finite matrix models with continuous local gauge invariance, *Phys. Lett. B* **100**, 149 (1981).
- [121] P. Orland and D. Rohrlich, Lattice gauge magnets: Local isospin from spin, *Nucl. Phys. B* **338**, 647 (1990).
- [122] S. Chandrasekharan and U.-J. Wiese, Quantum link models: A discrete approach to gauge theories, *Nucl. Phys. B* **492**, 455 (1997).

- [123] R. Brower, S. Chandrasekharan, and U.-J. Wiese, QCD as a quantum link model, *Phys. Rev. D* **60**, 094502 (1999).
- [124] U.-J. Wiese, Ultracold quantum gases and lattice systems: Quantum simulation of lattice gauge theories, *Ann. Phys.* **525**, 777 (2013).
- [125] U.-J. Wiese, Towards quantum simulating QCD, *Nucl. Phys. A* **931**, 246 (2014).
- [126] U.-J. Wiese, From quantum link models to D-theory: A resource efficient framework for the quantum simulation and computation of gauge theories, *Philos. Trans. R. Soc. A* **380**, 20210068 (2022).
- [127] D. Banerjee, S. Caspar, F.-J. Jiang, J.-H. Peng, and U.-J. Wiese, Nematic confined phases in the U(1) quantum link model on a triangular lattice: Near-term quantum computations of string dynamics on a chip, *Phys. Rev. Res.* **4**, 023176 (2022).
- [128] D. Banerjee, F.-J. Jiang, T. Olesen, P. Orland, and U.-J. Wiese, From the SU(2) quantum link model on the honeycomb lattice to the quantum dimer model on the kagome lattice: Phase transition and fractionalized flux strings, *Phys. Rev. B* **97**, 205108 (2018).
- [129] A. d'Adda, M. Lüscher, and P. Di Vecchia, A In expandable series of non-linear σ models with instantons, *Nucl. Phys. B* **146**, 63 (1978).
- [130] H. Eichenherr, SU(N) invariant non-linear σ models, *Nucl. Phys. B* **146**, 215 (1978).
- [131] W. Evans, U. Gerber, M. Hornung, and U.-J. Wiese, SU(3) quantum spin ladders as a regularization of the CP(2) model at non-zero density: From classical to quantum simulation, *Ann. Phys.* **398**, 94 (2018).
- [132] B. Beard, M. Pepe, S. Riederer, and U.-J. Wiese, Study of CP($N - 1$) θ -vacua by cluster simulation of SU(N) quantum spin ladders, *Phys. Rev. Lett.* **94**, 010603 (2005).
- [133] C. Laflamme, W. Evans, M. Dalmonte, U. Gerber, H. Mejía-Díaz, W. Bietenholz, U.-J. Wiese, and P. Zoller, CP($N - 1$) quantum field theories with alkaline-earth atoms in optical lattices, *Ann. Phys.* **370**, 117 (2016).
- [134] H. Duan, G. M. Fuller, J. Carlson, and Y.-Z. Qian, Simulation of coherent nonlinear neutrino flavor transformation in the supernova environment: Correlated neutrino trajectories, *Phys. Rev. D* **74**, 105014 (2006).
- [135] H. Duan, G. M. Fuller, and Y.-Z. Qian, Collective neutrino oscillations, *Annu. Rev. Nucl. Part. Sci.* **60**, 569 (2010).
- [136] I. Tamborra and S. Shalgar, New developments in flavor evolution of a dense neutrino gas, *Annu. Rev. Nucl. Part. Sci.* **71**, 165 (2021).
- [137] A. V. Patwardhan, M. J. Cervia, E. Rrapaj, P. Siwach, and A. Balantekin, in *Handbook of Nuclear Physics*, edited by I. Tanihata, H. Toki, and T. Kajino (Springer Nature, Singapore, 2022).
- [138] Y. Pehlivan, A. B. Balantekin, T. Kajino, and T. Yoshida, Invariants of collective neutrino oscillations, *Phys. Rev. D* **84**, 065008 (2011).
- [139] P. Siwach, A. M. Suliga, and A. B. Balantekin, Entanglement in three-flavor collective neutrino oscillations, *Phys. Rev. D* **107**, 023019 (2023).
- [140] T. Stirner, G. Sigl, and G. Raffelt, Liouville term for neutrinos: Flavor structure and wave interpretation, *J. Cosmol. Astropart. Phys.* **2018**, 016 (2018).
- [141] M. J. Cervia, A. V. Patwardhan, A. B. Balantekin, S. N. Coppersmith, and C. W. Johnson, Entanglement and collective flavor oscillations in a dense neutrino gas, *Phys. Rev. D* **100**, 083001 (2019).
- [142] A. V. Patwardhan, M. J. Cervia, and A. B. Balantekin, Spectral splits and entanglement entropy in collective neutrino oscillations, *Phys. Rev. D* **104**, 123035 (2021).
- [143] M. J. Cervia, P. Siwach, A. V. Patwardhan, A. B. Balantekin, S. N. Coppersmith, and C. W. Johnson, Collective neutrino oscillations with tensor networks using a time-dependent variational principle, *Phys. Rev. D* **105**, 123025 (2022).
- [144] A. Rajput, A. Roggero, and N. Wiebe, Hybridized methods for quantum simulation in the interaction picture, *Quantum* **6**, 780 (2022).
- [145] K. Yeter-Aydeniz, S. Bangar, G. Siopsis, and R. C. Pooser, Collective neutrino oscillations on a quantum computer, *Quantum Inf. Process.* **21**, 1 (2022).
- [146] B. Hall, A. Roggero, A. Baroni, and J. Carlson, Simulation of collective neutrino oscillations on a quantum computer, *Phys. Rev. D* **104**, 063009 (2021).
- [147] A. Roggero, Entanglement and many-body effects in collective neutrino oscillations, *Phys. Rev. D* **104**, 103016 (2021).
- [148] V. Amitrano, A. Roggero, P. Luchi, F. Turro, L. Vespucci, and F. Pederiva, Trapped-ion quantum simulation of collective neutrino oscillations, *Phys. Rev. D* **107**, 023007 (2023).
- [149] M. Illa and M. J. Savage, Multi-neutrino entanglement and correlations in dense neutrino systems, *Phys. Rev. Lett.* **130**, 221003 (2023).
- [150] M. Illa and M. J. Savage, Basic elements for simulations of standard-model physics with quantum annealers: Multigrad and clock states, *Phys. Rev. A* **106**, 052605 (2022).
- [151] J. D. Martin, A. Roggero, H. Duan, and J. Carlson, Many-body neutrino flavor entanglement in a simple dynamic model, *ArXiv:2301.07049*.
- [152] A. Carrera Vazquez, D. J. Egger, D. Ochsner, and S. Woerner, Well-conditioned multi-product formulas for hardware-friendly Hamiltonian simulation, *Quantum* **7**, 1067 (2023).
- [153] W. Guan, G. Perdue, A. Pesah, M. Schuld, K. Terashi, S. Vallecorsa, and J.-R. Vlimant, Quantum machine learning in high energy physics, *Mach. Learn.: Sci. Technol.* **2**, 011003 (2021).
- [154] A. Delgado, K. E. Hamilton, J.-R. Vlimant, D. Magano, Y. Omar, P. Bargassa, A. Francis, A. Gianelle, L. Sestini, D. Lucchesi, *et al.*, Quantum computing for data analysis in high-energy physics, *ArXiv:2203.08805*.
- [155] K. Albertsson, *et al.*, Machine learning in high energy physics community white paper, *J. Phys.: Conf. Ser.* **1085**, 022008 (2018).
- [156] J. H. Collins, Y. Huang, S. Knapen, B. Nachman, and D. Whiteson, Machine-learning compression for particle physics discoveries, *ArXiv:2210.11489*.
- [157] M. Farina, Y. Nakai, and D. Shih, Searching for new physics with deep autoencoders, *Phys. Rev. D* **101**, 075021 (2020).

- [158] T. Cheng, J.-F. M. C. Arguin, J. Leissner-Martin, J. Pilette, and T. Golling, Variational autoencoders for anomalous jet tagging, *Phys. Rev. D* **107**, 016002 (2023).
- [159] K. A. Wozniak, V. Belis, E. Puljak, P. Barkoutsos, G. Dissertori, M. Grossi, M. Pierini, F. Reiter, I. Tavernelli, and S. Vallecorsa, Quantum anomaly detection in the latent space of proton collision events at the LHC, [ArXiv:2301.10780](https://arxiv.org/abs/2301.10780).
- [160] K. A. Wozniak, V. Belis, M. Pierini, S. Vallecorsa, G. Dissertori, P. Barkoutsos, and I. Tavernelli, Quantum machine learning in the latent space of high energy physics events, *J. Phys.: Conf. Ser.* **2438**, 012115 (2023).
- [161] V. Belis, S. González-Castillo, C. Reissel, S. Vallecorsa, E. F. Combarro, G. Dissertori, and F. Reiter, Higgs analysis with quantum classifiers, *EPJ Web Conf.* **251**, 03070 (2021).
- [162] S. Lloyd, M. Schuld, A. Ijaz, J. Izaac, and N. Killoran, Quantum embeddings for machine learning, [ArXiv:2001.03622](https://arxiv.org/abs/2001.03622).
- [163] M. Britsch, N. Gagunashvili, and M. Schmelling, Application of the rule-growing algorithm RIPPER to particle physics analysis, *PoS ACAT08*, 086 (2008).
- [164] M. Britsch, N. Gagunashvili, and M. Schmelling, Classifying extremely imbalanced data sets, [ArXiv:1011.6224](https://arxiv.org/abs/1011.6224).
- [165] J. P. Edelen and N. M. Cook, in *Proceedings of the 2021 Improving Scientific Software*, edited by W. Hu, D. Del Vento, and S. Su (2021).
- [166] J. H. Collins, K. Howe, and B. Nachman, Extending the search for new resonances with machine learning, *Phys. Rev. D* **99**, 014038 (2019).
- [167] H. M. Nguyen, E. W. Cooper, and K. Kamei, Borderline over-sampling for imbalanced data classification, *Int. J. Knowl. Eng. Soft Data Paradigms* **3**, 4 (2009).
- [168] T.-Y. Lin, P. Goyal, R. Girshick, K. He, and P. Dollár, Focal loss for dense object detection, [ArXiv:1708.02002](https://arxiv.org/abs/1708.02002).
- [169] J. Vazquez-Escobar, J. Hernandez, and M. Cardenas-Montes, Estimation of machine learning model uncertainty in particle physics event classifiers, *Comput. Phys. Commun.* **268**, 108100 (2021).
- [170] A. Ballestrero, *et al.*, Precise predictions for same-sign W-boson scattering at the LHC, *Eur. Phys. J. C* **78**, 671 (2018).
- [171] M. Aaboud, *et al.*, (ATLAS Collaboration), Search for the decay of the Higgs boson to charm quarks with the ATLAS experiment, *Phys. Rev. Lett.* **120**, 211802 (2018).
- [172] M. Grossi, J. Novak, B. Kerševan, and D. Rebuzzi, Comparing traditional and deep-learning techniques of kinematic reconstruction for polarization discrimination in vector boson scattering, *Eur. Phys. J. C* **80**, 1144 (2020).
- [173] E. M. Metodiev, B. Nachman, and J. Thaler, Classification without labels: Learning from mixed samples in high energy physics, *J. High Energy Phys.* **2017**, 174 (2017).
- [174] V. S. Ngairangbam, M. Spannowsky, and M. Takeuchi, Anomaly detection in high-energy physics using a quantum autoencoder, *Phys. Rev. D* **105**, 095004 (2022).
- [175] J. Schuhmacher, L. Boggia, V. Belis, E. Puljak, M. Grossi, M. Pierini, S. Vallecorsa, F. Tacchino, P. Barkoutsos, and I. Tavernelli, Unravelling physics beyond the standard model with classical and quantum anomaly detection, *Mach. Learn.: Sci. Technol.* **4**, 045031 (2023).
- [176] E. Bermot, C. Zoufal, M. Grossi, J. Schuhmacher, F. Tacchino, S. Vallecorsa, and I. Tavernelli, in *2023 IEEE International Conference on Quantum Computing and Engineering (QCE)* (IEEE Computer Society, Los Alamitos, CA, USA, 2023), p. 331.
- [177] M. Cerezo, A. Arrasmith, R. Babbush, S. C. Benjamin, S. Endo, K. Fujii, J. R. McClean, K. Mitarai, X. Yuan, L. Cincio, *et al.*, Variational quantum algorithms, *Nat. Rev. Phys.* **3**, 625 (2021).
- [178] V. Havlíček, A. D. Córcoles, K. Temme, A. W. Harrow, A. Kandala, J. M. Chow, and J. M. Gambetta, Supervised learning with quantum-enhanced feature spaces, *Nature* **567**, 209 (2019).
- [179] M. Schuld and N. Killoran, Quantum machine learning in feature Hilbert spaces, *Phys. Rev. Lett.* **122**, 040504 (2019).
- [180] S. Thanasilp, S. Wang, M. Cerezo, and Z. Holmes, Exponential concentration and untrainability in quantum kernel methods, [ArXiv:2208.11060](https://arxiv.org/abs/2208.11060).
- [181] M. Incudini, M. Grossi, A. Ceschini, A. Mandarino, M. Panella, S. Vallecorsa, and D. Windridge, Resource saving via ensemble techniques for quantum neural networks, *Quantum Mach. Intell.* **5**, 39 (2023).
- [182] L. Funcke, T. Hartung, B. Heinemann, K. Jansen, A. Kropf, S. Kühn, F. Meloni, D. Spataro, C. Tüysüz, and Y. C. Yap, in *20th International Workshop on Advanced Computing and Analysis Techniques in Physics Research: AI Decoded—Towards Sustainable, Diverse, Performant and Effective Scientific Computing* (IBS Science Culture Center, Daejeon, South Korea, 2022).
- [183] A. Crippa, *et al.*, Quantum algorithms for charged particle track reconstruction in the LUXE experiment, [ArXiv:2304.01690](https://arxiv.org/abs/2304.01690).
- [184] D. Magano, *et al.*, Quantum speedup for track reconstruction in particle accelerators, *Phys. Rev. D* **105**, 076012 (2022).
- [185] F. Bapst, W. Bhimji, P. Calafiura, H. Gray, W. Lavrijsen, L. Linder, and A. Smith, A pattern recognition algorithm for quantum annealers, *Comput. Softw. Big Sci.* **4**, 1 (2019).
- [186] A. Zlokapa, A. Anand, J.-R. Vlimant, J. M. Duarte, J. Job, D. Lidar, and M. Spiropulu, Charged particle tracking with quantum annealing optimization, *Quantum Mach. Intell.* **3**, 1 (2021).
- [187] T. Schwägerl, C. Issever, K. Jansen, T. J. Khoo, S. Kühn, C. Tüysüz, and H. Weber, Particle track reconstruction with noisy intermediate-scale quantum computers, [ArXiv:2303.13249](https://arxiv.org/abs/2303.13249).
- [188] D. Nicotra, M. L. Martinez, J. A. de Vries, M. Merk, K. Driessens, R. L. Westra, D. Dibeneditto, and D. H. C. Pérez, A quantum algorithm for track reconstruction in the LHCb vertex detector, [ArXiv:2308.00619](https://arxiv.org/abs/2308.00619).
- [189] P. Duckett, G. Facini, M. Jastrzebski, S. Malik, S. Rettie, and T. Scanlon, Reconstructing charged particle track segments with a quantum-enhanced support vector machine, *Phys. Rev. D* **109**, 052002 (2024).
- [190] X. Ju, *et al.*, Performance of a geometric deep learning pipeline for HL-LHC particle tracking, *Eur. Phys. J. C* **81**, 876 (2021).

- [191] C. Tüysüz, C. Rieger, K. Novotny, B. Demirköz, D. Dobos, K. Potamianos, S. Vallecorsa, J.-R. Vlimant, and R. Forster, Hybrid quantum classical graph neural networks for particle track reconstruction, *Quantum Mach. Intell.* **3**, 29 (2021).
- [192] Carla Rieger, Cenk Tüysüz, Kristiane Novotny, Sofia Vallecorsa, Bilge Demirköz, Karolos Potamianos, Daniel Dobos, and Jean-Roch Vlimant, Embedding of particle tracking data using hybrid quantum-classical neural networks, *EPJ Web Conf.* **251**, 03065 (2021).
- [193] A. Y. Wei, P. Naik, A. W. Harrow, and J. Thaler, Quantum algorithms for jet clustering, *Phys. Rev. D* **101**, 094015 (2020).
- [194] (CMS Collaboration), Description and performance of track and primary-vertex reconstruction with the CMS tracker, *J. Instrum.* **9**, 10009 (2014).
- [195] New versions have been published [449], but the general analysis should hold also in this case.
- [196] R. Frühwirth, Application of Kalman filtering to track and vertex fitting, *Nucl. Instrum. Methods Phys. Res. Section A: Accel. Spectr. Detectors Assoc. Equip.* **262**, 444 (1987).
- [197] G. Sguazzoni, Track reconstruction in CMS high luminosity environment, *Nucl. Part. Phys. Proc.* **273–275**, 2497 (2016).
- [198] T. A. Collaboration, Performance of the ATLAS track reconstruction algorithms in dense environments in LHC Run 2, *Eur. Phys. J. C* **77**, 673 (2017).
- [199] N. Braun, *Combinatorial Kalman Filter and High Level Trigger Reconstruction for the Belle II Experiment*, Springer Theses (Springer International Publishing, Cham, 2019).
- [200] S. Brandt, C. Peyrou, R. Sosnowski, and A. Wroblewski, The principal axis of jets—An attempt to analyse high-energy collisions as two-body processes, *Phys. Lett.* **12**, 57 (1964).
- [201] E. Farhi, Quantum chromodynamics test for jets, *Phys. Rev. Lett.* **39**, 1587 (1977).
- [202] H. Yamamoto, An efficient algorithm for calculating thrust in high multiplicity reactions, *J. Comput. Phys.* **52**, 597 (1983).
- [203] G. P. Salam and G. Soyez, A practical seedless infrared-safe cone jet algorithm, *J. High Energy Phys.* **2007**, 086 (2007).
- [204] A. Delgado and J. Thaler, Quantum annealing for jet clustering with thrust, *Phys. Rev. D* **106**, 094016 (2022).
- [205] D. Pires, Y. Omar, and J. Seixas, Adiabatic quantum algorithm for multijet clustering in high energy physics, *Phys. Lett. B* **843**, 138000 (2023).
- [206] D. Pires, P. Bargassa, J. Seixas, and Y. Omar, A digital quantum algorithm for jet clustering in high-energy physics, *ArXiv:2101.05618*.
- [207] J. J. M. de Lejarza, L. Cieri, and G. Rodrigo, Quantum clustering and jet reconstruction at the LHC, *Phys. Rev. D* **106**, 036021 (2022).
- [208] J. B. MacQueen, in *Proceedings of the Fifth Berkeley Symposium on Mathematical Statistics and Probability*, Vol. 1, edited by L. M. L. Cam and J. Neyman (University of California Press, Berkeley, 1967), p. 281.
- [209] B. J. Frey and D. Dueck, Clustering by passing messages between data points, *Science* **315**, 972 (2007).
- [210] S. D. Ellis and D. E. Soper, Successive combination jet algorithm for hadron collisions, *Phys. Rev. D* **48**, 3160 (1993).
- [211] M. Cacciari, G. P. Salam, and G. Soyez, FastJet user manual, *Eur. Phys. J. C* **72**, 1896 (2012).
- [212] A. Gianelle, P. Koppenburg, D. Lucchesi, D. Nicotra, E. Rodrigues, L. Sestini, J. de Vries, and D. Zuliani, Quantum machine learning for b -jet charge identification, *J. High Energy Phys.* **2022**, 14 (2022).
- [213] D. J. Gross and F. Wilczek, Ultraviolet behavior of non-Abelian gauge theories, *Phys. Rev. Lett.* **30**, 1343 (1973).
- [214] D. J. Gross and F. Wilczek, Asymptotically free gauge theories—I, *Phys. Rev. D* **8**, 3633 (1973).
- [215] M. A. Shifman, A. I. Vainshtein, and V. I. Zakharov, QCD and resonance physics. Theoretical foundations, *Nucl. Phys. B* **147**, 385 (1979).
- [216] J. Collins, *Foundations of Perturbative QCD*, Cambridge Monographs on Particle Physics, Nuclear Physics and Cosmology (Cambridge University Press, 2011).
- [217] A. Buckley, C. White, and M. White, *Practical Collider Physics* (IOP Publishing, Bristol, 2021), p. 2053.
- [218] A. Pérez-Salinas, J. Cruz-Martinez, A. A. Alhajri, and S. Carrazza, Determining the proton content with a quantum computer, *Phys. Rev. D* **103**, 034027 (2021).
- [219] J. Lang, S. Liebler, H. Schäfer-Siebert, and D. Zeppenfeld, Effective field theory versus UV-complete model: Vector boson scattering as a case study, *Eur. Phys. J. C* **81**, 659 (2021).
- [220] J. C. Criado, R. Kogler, and M. Spannowsky, Quantum fitting framework applied to effective field theories, *Phys. Rev. D* **107**, 015023 (2023).
- [221] G. Kochenberger, J.-K. Hao, F. Glover, M. Lewis, Z. Lü, H. Wang, and Y. Wang, The unconstrained binary quadratic programming problem: A survey, *J. Comb. Optim.* **28**, 58 (2014).
- [222] I. Brivio and M. Trott, The Standard Model as an effective field theory, *Phys. Rep.* **793**, 1 (2019).
- [223] Johannes Albrecht, *et al.*, (The HEP Software Foundation), A roadmap for HEP software and computing R&D for the 2020s, *Comput. Softw. Big Sci.* **3**, 7 (2019).
- [224] B. Schmidt, The high-luminosity upgrade of the LHC: Physics and technology challenges for the accelerator and the experiments, in *Journal of Physics: Conference Series*, Vol. 706 (IOP Publishing, 2016), p. 022002.
- [225] S. Ovin, X. Rouby, and V. Lemaitre, Delphes, a framework for fast simulation of a generic collider experiment, *ArXiv:0903.2225*.
- [226] G. R. Khattak, S. Vallecorsa, F. Carminati, and G. M. Khan, Fast simulation of a high granularity calorimeter by generative adversarial networks, *Eur. Phys. J. C* **82**, 386 (2022).
- [227] C. Krause and D. Shih, CaloFlow: Fast and accurate generation of calorimeter showers with normalizing flows, *Phys. Rev. D* **107**, 113003 (2023).
- [228] E. Buhmann, S. Diefenbacher, E. Eren, F. Gaede, G. Kasieczka, A. Korol, and K. Krüger, Getting high: High fidelity simulation of high granularity calorimeters with high speed, *Comput. Softw. Big Sci.* **5**, 13 (2021).
- [229] B. Hashemi, N. Amin, K. Datta, D. Olivito, and M. Pierini, LHC analysis-specific datasets with generative adversarial networks, *ArXiv:1901.05282*.

- [230] A. Delgado, *et al.*, Quantum computing for data analysis in high energy physics, [ArXiv:2203.08805](#).
- [231] Z.-Y. Han, J. Wang, H. Fan, L. Wang, and P. Zhang, Unsupervised generative modeling using matrix product states, [Phys. Rev. X](#) **8**, 031012 (2018).
- [232] F. Tacchino, A. Chiesa, S. Carretta, and D. Gerace, Quantum computers as universal quantum simulators: State-of-the-art and perspectives, [Adv. Quantum Technol.](#) **3**, 1900052 (2020).
- [233] A. Miessen, P. J. Ollitrault, F. Tacchino, and I. Tavernelli, Quantum algorithms for quantum dynamics, [Nat. Comput. Sci.](#) **3**, 25 (2023).
- [234] D. W. Berry, A. M. Childs, R. Cleve, R. Kothari, and R. D. Somma, Simulating Hamiltonian dynamics with a truncated Taylor series, [Phys. Rev. Lett.](#) **114**, 090502 (2015).
- [235] G. H. Low and I. L. Chuang, Optimal Hamiltonian simulation by quantum signal processing, [Phys. Rev. Lett.](#) **118**, 010501 (2017).
- [236] G. H. Low and I. L. Chuang, Hamiltonian simulation by qubitization, [Quantum](#) **3**, 163 (2019).
- [237] L. Nagano, A. Bapat, and C. W. Bauer, Quench dynamics of the Schwinger model via variational quantum algorithms, [Phys. Rev. D](#) **108**, 034510 (2023).
- [238] A. Chiesa, F. Tacchino, M. Grossi, P. Santini, I. Tavernelli, D. Gerace, and S. Carretta, Quantum hardware simulating four-dimensional inelastic neutron scattering, [Nat. Phys.](#) **15**, 455 (2019).
- [239] Y. Kim, C. J. Wood, T. J. Yoder, S. T. Merkel, J. M. Gambetta, K. Temme, and A. Kandala, Scalable error mitigation for noisy quantum circuits produces competitive expectation values, [Nat. Phys.](#) **549**, 1 (2023).
- [240] H. F. Trotter, On the product of semi-groups of operators, [Proc. Am. Math. Soc.](#) **10**, 545 (1959).
- [241] C. Zhang, in *Monte Carlo and Quasi-Monte Carlo Methods 2010*, edited by L. Ploskota and H. Wozniakowski (Springer, Heidelberg, 2012), p. 709.
- [242] A. M. Childs, A. Ostrander, and Y. Su, Faster quantum simulation by randomization, [Quantum](#) **3**, 182 (2019).
- [243] E. Campbell, Random compiler for fast Hamiltonian simulation, [Phys. Rev. Lett.](#) **123**, 070503 (2019).
- [244] Z.-J. Zhang, J. Sun, X. Yuan, and M.-H. Yung, Low-depth Hamiltonian simulation by an adaptive product formula, [Phys. Rev. Lett.](#) **130**, 040601 (2023).
- [245] S. A. Chin, Multi-product splitting and Runge-Kutta-Nyström integrators, [Celest. Mech. Dyn. Astron.](#) **106**, 391 (2010).
- [246] N. Wiebe, D. Berry, P. Høyer, and B. C. Sanders, Higher order decompositions of ordered operator exponentials, [J. Phys. A: Math. Theor.](#) **43**, 065203 (2010).
- [247] D. Poulin, A. Qarry, R. Somma, and F. Verstraete, Quantum simulation of time-dependent Hamiltonians and the convenient illusion of Hilbert space, [Phys. Rev. Lett.](#) **106**, 170501 (2011).
- [248] J. Watkins, N. Wiebe, A. Roggero, and D. Lee, Time-dependent Hamiltonian simulation using discrete clock constructions, [ArXiv:2203.11353](#).
- [249] X. Yuan, S. Endo, Q. Zhao, Y. Li, and S. C. Benjamin, Theory of variational quantum simulation, [Quantum](#) **3**, 191 (2019).
- [250] P. J. Ollitrault, S. Jandura, A. Miessen, I. Burghardt, R. Martinazzo, F. Tacchino, and I. Tavernelli, Quantum algorithms for grid-based variational time evolution, [Quantum](#) **7**, 1139 (2023).
- [251] A. Macridin, P. Spentzouris, J. Amundson, and R. Harnik, Digital quantum computation of fermion-boson interacting systems, [Phys. Rev. A](#) **98**, 042312 (2018).
- [252] S. Endo, I. Kurata, and Y. O. Nakagawa, Calculation of the Green's function on near-term quantum computers, [Phys. Rev. Res.](#) **2**, 033281 (2020).
- [253] A. Miessen, P. J. Ollitrault, and I. Tavernelli, Quantum algorithms for quantum dynamics: A performance study on the spin-boson model, [Phys. Rev. Res.](#) **3**, 043212 (2021).
- [254] F. Libbi, J. Rizzo, F. Tacchino, N. Marzari, and I. Tavernelli, Effective calculation of the Green's function in the time domain on near-term quantum processors, [Phys. Rev. Res.](#) **4**, 043038 (2022).
- [255] N. Gomes, D. B. Williams-Young, and W. A. de Jong, Computing the many-body Green's function with adaptive variational quantum dynamics, [ArXiv:2302.03093](#).
- [256] C. Zoufal, D. Sutter, and S. Woerner, Error bounds for variational quantum time evolution, [Phys. Rev. Appl.](#) **20**, 044059 (2023).
- [257] K. Heya, K. M. Nakanishi, K. Mitarai, and K. Fujii, Subspace variational quantum simulator, [ArXiv:1904.08566](#).
- [258] C. Cirstoiu, Z. Holmes, J. Iosue, L. Cincio, P. J. Coles, and A. Sornborger, Variational fast forwarding for quantum simulation beyond the coherence time, [npj Quantum Inf.](#) **6**, 1 (2020).
- [259] J. Gibbs, K. Gili, Z. Holmes, B. Commeau, A. Arrasmith, L. Cincio, P. J. Coles, and A. Sornborger, Long-time simulations with high fidelity on quantum hardware, [ArXiv:2102.04313](#).
- [260] J. Gibbs, Z. Holmes, M. C. Caro, N. Ezzell, H.-Y. Huang, L. Cincio, A. T. Sornborger, and P. J. Coles, Dynamical simulation via quantum machine learning with provable generalization, [Phys. Rev. Res.](#) **6**, 013241 (2024).
- [261] M. Otten, C. L. Cortes, and S. K. Gray, Noise-resilient quantum dynamics using symmetry-preserving ansatzes, [ArXiv:1910.06284](#).
- [262] S.-H. Lin, R. Dilip, A. G. Green, A. Smith, and F. Pollmann, Real- and imaginary-time evolution with compressed quantum circuits, [PRX Quantum](#) **2**, 010342 (2021).
- [263] S. Barison, F. Vicentini, and G. Carleo, An efficient quantum algorithm for the time evolution of parameterized circuits, [Quantum](#) **5**, 512 (2021).
- [264] M. Benedetti, M. Fiorentini, and M. Lubasch, Hardware-efficient variational quantum algorithms for time evolution, [Phys. Rev. Res.](#) **3**, 033083 (2021).
- [265] K. Bharti and T. Haug, Quantum-assisted simulator, [Phys. Rev. A](#) **104**, 042418 (2021).
- [266] J. W. Z. Lau, K. Bharti, T. Haug, and L. C. Kwek, Quantum assisted simulation of time dependent Hamiltonians, [ArXiv:2101.07677](#).
- [267] T. Haug and K. Bharti, Generalized quantum assisted simulator, [Quantum Sci. Technol.](#) **7**, 045019 (2022).
- [268] E. Kökcü, T. Steckmann, Y. Wang, J. K. Freericks, E. F. Dumitrescu, and A. F. Kemper, Fixed depth Hamiltonian

- simulation via Cartan decomposition, *Phys. Rev. Lett.* **129**, 070501 (2022).
- [269] T. Steckmann, T. Keen, A. F. Kemper, E. F. Dumitrescu, and Y. Wang, Simulating the Mott transition on a noisy digital quantum computer via Cartan-based fast-forwarding circuits, *Phys. Rev. Res.* **5**, 023198 (2023).
- [270] F. Jamet, A. Agarwal, C. Lupo, D. E. Browne, C. Weber, and I. Rungger, Krylov variational quantum algorithm for first principles materials simulations, [ArXiv:2105.13298](https://arxiv.org/abs/2105.13298).
- [271] A. M. Childs, Y. Su, M. C. Tran, N. Wiebe, and S. Zhu, Theory of trotter error with commutator scaling, *Phys. Rev. X* **11**, 011020 (2021).
- [272] N. Quadri, Master thesis (2021), ETH Zurich.
- [273] H. Neven, V. S. Denchev, G. Rose, and W. G. Macready, Training a binary classifier with the quantum adiabatic algorithm, [ArXiv:0811.0416](https://arxiv.org/abs/0811.0416).
- [274] S. Aaronson, Read the fine print, *Nat. Phys.* **11**, 291 (2015).
- [275] V. Giovannetti, S. Lloyd, and L. Maccone, Quantum random access memory, *Phys. Rev. Lett.* **100**, 160501 (2008).
- [276] A. Pérez-Salinas, A. Cervera-Lierta, E. Gil-Fuster, and J. I. Latorre, Data re-uploading for a universal quantum classifier, *Quantum* **4**, 226 (2020).
- [277] G. V. Cybenko, Approximation by superpositions of a sigmoidal function, *Math. Control Signals Syst.* **2**, 303 (1989).
- [278] S. C. Marshall, C. Gyurik, and V. Dunjko, High dimensional quantum machine learning with small quantum computers, *Quantum* **7**, 1078 (2023).
- [279] C. Gyurik and V. Dunjko, On establishing learning separations between classical and quantum machine learning with classical data, [ArXiv:2208.06339](https://arxiv.org/abs/2208.06339).
- [280] M. Cerezo, M. Larocca, D. Garcia-Martín, N. L. Diaz, P. Braccia, E. Fontana, M. S. Rudolph, P. Bermejo, A. Ijaz, S. Thanasilp, *et al.*, Does provable absence of barren plateaus imply classical simulability? or, why we need to rethink variational quantum computing, [ArXiv:2312.09121](https://arxiv.org/abs/2312.09121).
- [281] H.-Y. Huang, M. Broughton, M. Mohseni, R. Babbush, S. Boixo, H. Neven, and J. R. McClean, Power of data in quantum machine learning, *Nat. Commun.* **12**, 1 (2021).
- [282] D. W. Berry, Y. Su, C. Gyurik, R. King, J. Basso, A. D. T. Barba, A. Rajput, N. Wiebe, V. Dunjko, and R. Babbush, Quantifying quantum advantage in topological data analysis, *PRX Quantum* **5**, 010319 (2024).
- [283] C. Cade and P. M. Crichigno, Complexity of supersymmetric systems and the cohomology problem, *Quantum* **8**, 1325 (2024).
- [284] J. R. McClean, S. Boixo, V. N. Smelyanskiy, R. Babbush, and H. Neven, Barren plateaus in quantum neural network training landscapes, *Nat. Commun.* **9**, 4812 (2018).
- [285] A. Arrasmith, Z. Holmes, M. Cerezo, and P. J. Coles, Equivalence of quantum barren plateaus to cost concentration and narrow gorges, *Quantum Sci. Technol.* **7**, 045015 (2022).
- [286] A. Arrasmith, M. Cerezo, P. Czarnik, L. Cincio, and P. J. Coles, Effect of barren plateaus on gradient-free optimization, *Quantum* **5**, 558 (2021).
- [287] M. Cerezo and P. J. Coles, Higher order derivatives of quantum neural networks with barren plateaus, *Quantum Sci. Technol.* **6**, 035006 (2021).
- [288] M. S. Rudolph, S. Lerch, S. Thanasilp, O. Kiss, S. Vallecorsa, M. Grossi, and Z. Holmes, Trainability barriers and opportunities in quantum generative modeling, [ArXiv:2305.02881](https://arxiv.org/abs/2305.02881).
- [289] Z. Holmes, K. Sharma, M. Cerezo, and P. J. Coles, Connecting ansatz expressibility to gradient magnitudes and barren plateaus, *PRX Quantum* **3**, 010313 (2022).
- [290] M. Larocca, P. Czarnik, K. Sharma, G. Muraleedharan, P. J. Coles, and M. Cerezo, Diagnosing barren plateaus with tools from quantum optimal control, *Quantum* **6**, 824 (2022).
- [291] J. Tangpanitanon, S. Thanasilp, N. Dangniam, M.-A. Lemonde, and D. G. Angelakis, Expressibility and trainability of parametrized analog quantum systems for machine learning applications, *Phys. Rev. Res.* **2**, 043364 (2020).
- [292] C. Ortiz Marrero, M. Kieferová, and N. Wiebe, Entanglement-induced barren plateaus, *PRX Quantum* **2**, 040316 (2021).
- [293] K. Sharma, M. Cerezo, L. Cincio, and P. J. Coles, Trainability of dissipative perceptron-based quantum neural networks, *Phys. Rev. Lett.* **128**, 180505 (2022).
- [294] T. L. Patti, K. Najafi, X. Gao, and S. F. Yelin, Entanglement devised barren plateau mitigation, *Phys. Rev. Res.* **3**, 033090 (2021).
- [295] M. Cerezo, A. Sone, T. Volkoff, L. Cincio, and P. J. Coles, Cost function dependent barren plateaus in shallow parametrized quantum circuits, *Nat. Commun.* **12**, 1791 (2021).
- [296] Z. Holmes, A. Arrasmith, B. Yan, P. J. Coles, A. Albrecht, and A. T. Sornborger, Barren plateaus preclude learning scramblers, *Phys. Rev. Lett.* **126**, 190501 (2021).
- [297] S. Thanasilp, S. Wang, N. A. Nghiem, P. J. Coles, and M. Cerezo, Subtleties in the trainability of quantum machine learning models, *Quantum Mach. Intell.* **5**, 21 (2023).
- [298] G. Li, R. Ye, X. Zhao, and X. Wang, in *Advances in Neural Information Processing Systems* (2022), Vol. 35, pp. 19456–19469, https://proceedings.neurips.cc/paper_files/paper/2022/hash/7b2d0730df1edd8c97df4bf83696025d-Abstract-Conference.html.
- [299] L. Leone, S. F. E. Oliviero, L. Cincio, and M. Cerezo, On the practical usefulness of the hardware efficient ansatz, *Quantum* **8**, 1395 (2024).
- [300] S. Wang, E. Fontana, M. Cerezo, K. Sharma, A. Sone, L. Cincio, and P. J. Coles, Noise-induced barren plateaus in variational quantum algorithms, *Nat. Commun.* **12**, 6961 (2021).
- [301] D. Stilck França and R. Garcia-Patron, Limitations of optimization algorithms on noisy quantum devices, *Nat. Phys.* **17**, 1221 (2021).
- [302] A. Pesah, M. Cerezo, S. Wang, T. Volkoff, A. T. Sornborger, and P. J. Coles, Absence of barren plateaus in quantum convolutional neural networks, *Phys. Rev. X* **11**, 041011 (2021).
- [303] Z. Liu, L.-W. Yu, L.-M. Duan, and D.-L. Deng, Presence and absence of barren plateaus in tensor-network based machine learning, *Phys. Rev. Lett.* **129**, 270501 (2022).
- [304] E. Cervero Martín, K. Plekhanov, and M. Lubasch, Barren plateaus in quantum tensor network optimization, *Quantum* **7**, 974 (2023).

- [305] K. Zhang, M.-H. Hsieh, L. Liu, and D. Tao, Toward trainability of quantum neural networks, [ArXiv:2011.06258](#).
- [306] R. Wiersema, C. Zhou, Y. de Sereville, J. F. Carrasquilla, Y. B. Kim, and H. Yuen, Exploring entanglement and optimization within the Hamiltonian variational ansatz, *PRX Quantum* **1**, 020319 (2020).
- [307] E. Grant, L. Wossnig, M. Ostaszewski, and M. Benedetti, An initialization strategy for addressing barren plateaus in parametrized quantum circuits, *Quantum* **3**, 214 (2019).
- [308] W. Huggins, P. Patil, B. Mitchell, K. B. Whaley, and E. M. Stoudenmire, Towards quantum machine learning with tensor networks, *Quantum Sci. Technol.* **4**, 024001 (2019).
- [309] J. Dborin, F. Barratt, V. Wimalaweera, L. Wright, and A. Green, Matrix product state pre-training for quantum machine learning, *Quantum Sci. Technol.* (2022).
- [310] M. S. Rudolph, J. Miller, J. Chen, A. Acharya, and A. Perdomo-Ortiz, Synergistic pretraining of parametrized quantum circuits via tensor networks, *Nat. Commun.* **14**, 8367 (2023).
- [311] M. S. Rudolph, J. Chen, J. Miller, A. Acharya, and A. Perdomo-Ortiz, Decomposition of matrix product states into shallow quantum circuits, *Quantum Sci. Technol.* **9**, 015012 (2023).
- [312] M. Cheng, K. Khosla, C. Self, M. Lin, B. Li, A. Medina, and M. Kim, Clifford circuit initialisation for variational quantum algorithms, [ArXiv:2207.01539](#).
- [313] Y.-F. Niu, S. Zhang, and W.-S. Bao, Warm starting variational quantum algorithms with near Clifford circuits, *Electronics* **12**, 347 (2023).
- [314] A. Skolik, J. R. McClean, M. Mohseni, P. van der Smagt, and M. Leib, Layerwise learning for quantum neural networks, *Quantum Mach. Intell.* **3**, 5 (2021).
- [315] M. Larocca, F. Sauvage, F. M. Sbahi, G. Verdon, P. J. Coles, and M. Cerezo, Group-invariant quantum machine learning, *PRX Quantum* **3**, 030341 (2022).
- [316] J. J. Meyer, M. Mularski, E. Gil-Fuster, A. A. Mele, F. Arzani, A. Wilms, and J. Eisert, Exploiting symmetry in variational quantum machine learning, *PRX Quantum* **4**, 010328 (2023).
- [317] F. Sauvage, M. Larocca, P. J. Coles, and M. Cerezo, Building spatial symmetries into parameterized quantum circuits for faster training, *Quantum Sci. Technol.* **9**, 015029 (2024).
- [318] Q. T. Nguyen, L. Schatzki, P. Braccia, M. Ragone, P. J. Coles, F. Sauvage, M. Larocca, and M. Cerezo, Theory for equivariant quantum neural networks, *PRX Quantum* **5**, 020328 (2024).
- [319] L. Bittel and M. Kliesch, Training variational quantum algorithms is np-hard, *Phys. Rev. Lett.* **127**, 120502 (2021).
- [320] X. You and X. Wu, in *International Conference on Machine Learning*, edited by M. Meila and T. Zhang (PMLR, 2021), p. 12144.
- [321] J. Rivera-Dean, P. Huembeli, A. Acín, and J. Bowles, Avoiding local minima in variational quantum algorithms with neural networks, [ArXiv:2104.02955](#).
- [322] E. R. Anschuetz and B. T. Kiani, Beyond barren plateaus: Quantum variational algorithms are swamped with traps, *Nat. Commun.* **13**, 7760 (2022).
- [323] F. Rehm, S. Vallecorsa, M. Grossi, K. Borrás, and D. Krücker, A full quantum generative adversarial network model for high energy physics simulations, [ArXiv:2305.07284](#).
- [324] K. Borrás, S. Y. Chang, L. Funcke, M. Grossi, T. Hartung, K. Jansen, D. Kruecker, S. Kühn, F. Rehm, C. Tüysüz, *et al.*, IOP Publishing **438**, 012096 (2023).
- [325] S. Y. Chang, S. Herbert, S. Vallecorsa, E. F. Combarro, and R. Duncan, in *EPJ Web of Conferences*, Vol. 251 (EDP Sciences, 2021), p. 03050.
- [326] S. Y. Chang, B. Le Saux, S. Vallecorsa, and M. Grossi, in *IGARSS 2022-2022 IEEE International Geoscience and Remote Sensing Symposium* (IEEE, Kuala Lumpur, 2022), p. 4907.
- [327] P. Mernyei, K. Meichanetzidis, and I. I. Ceylan, in *Proceedings of the 39th International Conference on Machine Learning* (2022), <https://proceedings.mlr.press/v162/mernyei22a.html>.
- [328] M. C. Bañuls, K. Cichy, J. I. Cirac, K. Jansen, and S. Kühn, Efficient basis formulation for $(1+1)$ -dimensional SU(2) lattice gauge theory: Spectral calculations with matrix product states, *Phys. Rev. X* **7**, 041046 (2017).
- [329] T. Angelides, P. Naredi, A. Crippa, K. Jansen, S. Kühn, I. Tavernelli, and D. S. Wang, First-order phase transition of the Schwinger model with a quantum computer, [ArXiv:2312.12831](#).
- [330] Y. Chai, A. Crippa, K. Jansen, S. Kühn, V. R. Pascuzzi, F. Tacchino, and I. Tavernelli, Entanglement production from scattering of fermionic wave packets: A quantum computing approach, [ArXiv:2312.02272](#).
- [331] V. Belis, P. Odagiu, M. Grossi, F. Reiter, G. Dissertori, and S. Vallecorsa, Guided quantum compression for Higgs identification, [ArXiv:2402.09524](#).
- [332] J. Haah, A. W. Harrow, Z. Ji, X. Wu, and N. Yu, Sample-optimal tomography of quantum states, *IEEE Trans. Inf. Theory* **63**, 5628 (2017).
- [333] R. O'Donnell and J. Wright, in *Proceedings of the Forty-Eighth Annual ACM Symposium on Theory of Computing* (Association for Computing Machinery, New York, United States, 2016), p. 899.
- [334] A. Montanaro, Learning stabilizer states by Bell sampling, [ArXiv:1707.04012](#).
- [335] A. Anshu, S. Arunachalam, T. Kuwahara, and M. Soleimanifar, Sample-efficient learning of interacting quantum systems, *Nat. Phys.* **17**, 931 (2021).
- [336] M. Cramer, M. B. Plenio, S. T. Flammia, R. Somma, D. Gross, S. D. Bartlett, O. Landon-Cardinal, D. Poulin, and Y.-K. Liu, Efficient quantum state tomography, *Nat. Commun.* **1**, 149 (2010).
- [337] S. Aaronson, in *Proceedings of the 50th Annual ACM SIGACT Symposium on Theory of Computing, STOC* (ACM, New York, 2018), p. 325.
- [338] S. Chen, W. Yu, P. Zeng, and S. T. Flammia, Robust shadow estimation, *PRX Quantum* **2**, 030348 (2021).
- [339] S. Aaronson, X. Chen, E. Hazan, S. Kale, and A. Nayak, in *Advances in Neural Information Processing Systems* (NeurIPS, Montreal, Canada, 2018), p. 8962.
- [340] S. Aaronson, The learnability of quantum states, *Proc. R. Soc. A: Math. Phys. Eng. Sci.* **463**, 3089 (2007).

- [341] A. Anshu and S. Arunachalam, A survey on the complexity of learning quantum states, *Nat. Rev. Phys.* **6**, 59 (2024).
- [342] I. Cong, S. Choi, and M. D. Lukin, Quantum convolutional neural networks, *Nat. Phys.* **15**, 1273 (2019).
- [343] H.-Y. Huang, R. Kueng, G. Torlai, V. V. Albert, and J. Preskill, Provably efficient machine learning for quantum many-body problems, *Science* **377**, eabk3333 (2022).
- [344] A. V. Uvarov, A. S. Kardashin, and J. D. Biamonte, Machine learning phase transitions with a quantum processor, *Phys. Rev. A* **102**, 012415 (2020).
- [345] L. Banchi, J. Pereira, and S. Pirandola, Generalization in quantum machine learning: A quantum information standpoint, *PRX Quantum* **2**, 040321 (2021).
- [346] L. Schatzki, A. Arrasmith, P. J. Coles, and M. Cerezo, Entangled datasets for quantum machine learning, [ArXiv:2109.03400](https://arxiv.org/abs/2109.03400).
- [347] M. Bilkis, M. Cerezo, G. Verdon, P. J. Coles, and L. Cincio, A semi-agnostic ansatz with variable structure for quantum machine learning, *Quantum Mach. Intell.* **5**, 43 (2023).
- [348] S. Monaco, O. Kiss, A. Mandarino, S. Vallecorsa, and M. Grossi, Quantum phase detection generalization from marginal quantum neural network models, *Phys. Rev. B* **107**, L081105 (2023).
- [349] H.-Y. Huang, M. Broughton, J. Cotler, S. Chen, J. Li, M. Mohseni, H. Neven, R. Babbush, R. Kueng, J. Preskill, and J. R. McClean, Quantum advantage in learning from experiments, *Science* **376**, 1182 (2022).
- [350] K. Temme, S. Bravyi, and J. M. Gambetta, Error mitigation for short-depth quantum circuits, *Phys. Rev. Lett.* **119**, 180509 (2017).
- [351] E. van den Berg, Z. K. Mineev, A. Kandala, and K. Temme, Probabilistic error cancellation with sparse Pauli-Lindblad models on noisy quantum processors, *Nat. Phys.* **19**, 1116 (2023).
- [352] C. H. Bennett, G. Brassard, S. Popescu, B. Schumacher, J. A. Smolin, and W. K. Wootters, Purification of noisy entanglement and faithful teleportation via noisy channels, *Phys. Rev. Lett.* **76**, 722 (1996).
- [353] O. Kern, G. Alber, and D. L. Shepelyansky, Quantum error correction of coherent errors by randomization, *Eur. Phys. J. D—At., Mol., Opt. Plasma Phys.* **32**, 153 (2005).
- [354] M. R. Geller and Z. Zhou, Efficient error models for fault-tolerant architectures and the Pauli twirling approximation, *Phys. Rev. A* **88**, 012314 (2013).
- [355] A. Kandala, K. Temme, A. D. Córcoles, A. Mezzacapo, J. M. Chow, and J. M. Gambetta, Error mitigation extends the computational reach of a noisy quantum processor, *Nature* **567**, 491 (2019).
- [356] G. García-Pérez, M. A. Rossi, B. Sokolov, F. Tacchino, P. K. Barkoutsos, G. Mazzola, I. Tavernelli, and S. Maniscalco, Learning to measure: Adaptive informationally complete generalized measurements for quantum algorithms, *PRX Quantum* **2**, 040342 (2021).
- [357] H.-Y. Huang, R. Kueng, and J. Preskill, Predicting many properties of a quantum system from very few measurements, *Nat. Phys.* **16**, 1050 (2020).
- [358] I. Hellström, Quantum computer roadmaps, <https://ianhellstrom.org/quantum.html>.
- [359] A. Wack, H. Paik, A. Javadi-Abhari, P. Jurcevic, I. Faro, J. M. Gambetta, and B. R. Johnson, Quality, speed, and scale: Three key attributes to measure the performance of near-term quantum computers, [ArXiv:2110.14108](https://arxiv.org/abs/2110.14108).
- [360] J. Gambetta, IBM's roadmap for scaling quantum technology, <https://research.ibm.com/blog/ibm-quantum-roadmap>.
- [361] I. Newsroom, IBM unveils 400 qubit-plus quantum processor and next-generation IBM Quantum System Two, <https://newsroom.ibm.com/2022-11-09-IBM-Unveils-400-Qubit-Plus-Quantum-Processor-and-Next-Generation-IBM-Quantum-System-Two>.
- [362] I. Quantum, The IBM Quantum development roadmap (), <https://www.ibm.com/quantum/roadmap>.
- [363] W. G. Unruh, Maintaining coherence in quantum computers, *Phys. Rev. A* **51**, 992 (1995).
- [364] P. W. Shor, in *Proceedings 35th Annual Symposium on Foundations of Computer Science* (IEEE, Santa Fe, New Mexico, 1994), p. 124.
- [365] G. Brassard and P. Hoyer, in *Proceedings of the Fifth Israeli Symposium on Theory of Computing and Systems* (IEEE, Ramat-Gan, Israel, 1997), p. 12.
- [366] L. K. Grover, Quantum computers can search rapidly by using almost any transformation, *Phys. Rev. Lett.* **80**, 4329 (1998).
- [367] A. Y. Kitaev, Quantum measurements and the Abelian stabilizer problem, [ArXiv:quant-ph/9511026](https://arxiv.org/abs/quant-ph/9511026).
- [368] C. Gidney and M. Ekerå, How to factor 2048 bit RSA integers in 8 hours using 20 million noisy qubits, *Quantum* **5**, 433 (2021).
- [369] J. Lee, D. W. Berry, C. Gidney, W. J. Huggins, J. R. McClean, N. Wiebe, and R. Babbush, Even more efficient quantum computations of chemistry through tensor hypercontraction, *PRX Quantum* **2**, 030305 (2021).
- [370] N. P. Breuckmann and J. N. Eberhardt, Quantum low-density parity-check codes, *PRX Quantum* **2**, 040101 (2021).
- [371] C. Chamberland, G. Zhu, T. J. Yoder, J. B. Hertzberg, and A. W. Cross, Topological and subsystem codes on low-degree graphs with flag qubits, *Phys. Rev. X* **10**, 011022 (2020).
- [372] J. P. Bonilla Ataides, D. K. Tuckett, S. D. Bartlett, S. T. Flammia, and B. Brown, The XZZX surface code, *Nat. Commun.* **12**, 2172 (2021).
- [373] J. Roffe, L. Z. Cohen, A. O. Quintavalle, D. Chandra, and E. T. Campbell, Bias-tailored quantum LDPC codes, *Quantum* **7**, 1005 (2023).
- [374] M. McEwen, D. Bacon, and C. Gidney, Relaxing hardware requirements for surface code circuits using time-dynamics, *Quantum* **7**, 1172 (2023).
- [375] P. Faist, S. Nezami, V. V. Albert, G. Salton, F. Pastawski, P. Hayden, and J. Preskill, Continuous symmetries and approximate quantum error correction, *Phys. Rev. X* **10**, 041018 (2020).
- [376] L. Kong and Z.-W. Liu, Near-optimal covariant quantum error-correcting codes from random unitaries with symmetries, *PRX Quantum* **3**, 020314 (2022).
- [377] A. Rajput, A. Roggero, and N. Wiebe, Quantum error correction with gauge symmetries, *npj Quantum Inf.* **9**, 41 (2023).

- [378] Y.-A. Chen, A. V. Gorshkov, and Y. Xu, Error-correcting codes for fermionic quantum simulation, *SciPost Phys.* **16**, 033 (2024).
- [379] J. Stehlik, D. M. Zajac, D. L. Underwood, T. Phung, J. Blair, S. Carnevale, D. Klaus, G. A. Keefe, A. Carniol, M. Kumph, M. Steffen, and O. E. Dial, Tunable coupling architecture for fixed-frequency transmon superconducting qubits, *Phys. Rev. Lett.* **127**, 080505 (2021).
- [380] K. Temme, E. van den Berg, A. Kandala, and J. Gambetta, With fault tolerance the ultimate goal, error mitigation is the path that gets quantum computing to usefulness, <https://research.ibm.com/blog/gammabar-for-quantum-advantage>.
- [381] A. Kandala, A. Mezzacapo, K. Temme, M. Takita, M. Brink, J. M. Chow, and J. M. Gambetta, Hardware-efficient variational quantum eigensolver for small molecules and quantum magnets, *Nature* **549**, 242 (2017).
- [382] Y. Li and S. C. Benjamin, Efficient variational quantum simulator incorporating active error minimization, *Phys. Rev. X* **7**, 021050 (2017).
- [383] L. Viola and S. Lloyd, Dynamical suppression of decoherence in two-state quantum systems, *Phys. Rev. A* **58**, 2733 (1998).
- [384] L. Viola, E. Knill, and S. Lloyd, Dynamical decoupling of open quantum systems, *Phys. Rev. Lett.* **82**, 2417 (1999).
- [385] E. Knill, Fault-tolerant postselected quantum computation: Threshold analysis, [ArXiv:quant-ph/0404104](https://arxiv.org/abs/quant-ph/0404104).
- [386] K. Bharti, A. Cervera-Lierta, T. H. Kyaw, T. Haug, S. Alperin-Lea, A. Anand, M. Degroote, H. Heimonen, J. S. Kottmann, T. Menke, W.-K. Mok, S. Sim, L.-C. Kwek, and A. Aspuru-Guzik, Noisy intermediate-scale quantum algorithms, *Rev. Mod. Phys.* **94**, 015004 (2022).
- [387] J. Preskill, Quantum computing in the NISQ era and beyond, *Quantum* **2**, 79 (2018).
- [388] J. T. Seeley, M. J. Richard, and P. J. Love, The Bravyi-Kitaev transformation for quantum computation of electronic structure, *J. Chem. Phys.* **137**, 224109 (2012).
- [389] C. M. Dawson and M. A. Nielsen, The Solovay-Kitaev algorithm, *Quantum Inf. Comput.* **6**, 81 (2006).
- [390] M. Maronese, L. Moro, L. Rocutto, and E. Prati, in *Quantum Computing Environments*, edited by S. S. Iyengar, M. Matriani, and K. L. Kumar (Springer International Publishing, Cham, 2022), p. 39.
- [391] J. Koch, T. M. Yu, J. Gambetta, A. A. Houck, D. I. Schuster, J. Majer, A. Blais, M. H. Devoret, S. M. Girvin, and R. J. Schoelkopf, Charge-insensitive qubit design derived from the Cooper pair box, *Phys. Rev. A* **76**, 042319 (2007).
- [392] P. Krantz, M. Kjaergaard, F. Yan, T. P. Orlando, S. Gustavsson, and W. D. Oliver, A quantum engineer's guide to superconducting qubits, *Appl. Phys. Rev.* **6**, 021318 (2019).
- [393] F. Motzoi, J. M. Gambetta, P. Rebentrost, and F. K. Wilhelm, Simple pulses for elimination of leakage in weakly nonlinear qubits, *Phys. Rev. Lett.* **103**, 110501 (2009).
- [394] D. C. McKay, C. J. Wood, S. Sheldon, J. M. Chow, and J. M. Gambetta, Efficient Z gates for quantum computing, *Phys. Rev. A* **96**, 022330 (2017).
- [395] C. Rigetti and M. Devoret, Fully microwave-tunable universal gates in superconducting qubits with linear couplings and fixed transition frequencies, *Phys. Rev. B* **81**, 134507 (2010).
- [396] M. Ganzhorn, G. Salis, D. J. Egger, A. Fuhrer, M. Mergenthaler, C. Müller, P. Müller, S. Paredes, M. Pechal, *et al.*, Benchmarking the noise sensitivity of different parametric two-qubit gates in a single superconducting quantum computing platform, *Phys. Rev. Res.* **2**, 033447 (2020).
- [397] J. Schwinger, Gauge invariance and mass. II, *Phys. Rev.* **128**, 2425 (1962).
- [398] C. J. Hamer, Z. Weihong, and J. Oitmaa, Series expansions for the massive Schwinger model in Hamiltonian lattice theory, *Phys. Rev. D* **56**, 55 (1997).
- [399] L. Funcke, K. Jansen, and S. Kühn, Topological vacuum structure of the Schwinger model with matrix product states, *Phys. Rev. D* **101**, 054507 (2020).
- [400] J. C. Halimeh, H. Lang, J. Mildenerger, Z. Jiang, and P. Hauke, Gauge-symmetry protection using single-body terms, *PRX Quantum* **2**, 040311 (2021).
- [401] G. Wang, D. E. Koh, P. D. Johnson, and Y. Cao, Minimizing estimation runtime on noisy quantum computers, *PRX Quantum* **2**, 010346 (2021).
- [402] E. Farhi, J. Goldstone, and S. Gutmann, A quantum approximate optimization algorithm, [ArXiv:1411.4028](https://arxiv.org/abs/1411.4028).
- [403] E. Farhi and A. W. Harrow, Quantum supremacy through the quantum approximate optimization algorithm, [ArXiv:1602.07674](https://arxiv.org/abs/1602.07674).
- [404] B. Barak and K. Marwaha, in *13th Innovations in Theoretical Computer Science Conference (ITCS 2022)*, Leibniz International Proceedings in Informatics (LIPIcs), Vol. 215, edited by M. Braverman (Schloss Dagstuhl—Leibniz-Zentrum für Informatik, Dagstuhl, Germany, 2022), p. 14:1.
- [405] V. Akshay, H. Philathong, M. E. S. Morales, and J. D. Biamonte, Reachability deficits in quantum approximate optimization, *Phys. Rev. Lett.* **124**, 090504 (2020).
- [406] A. M. Dalzell, A. W. Harrow, D. E. Koh, and R. L. L. Placa, How many qubits are needed for quantum computational supremacy?, *Quantum* **4**, 264 (2020).
- [407] J. Weidenfeller, L. C. Valor, J. Gacon, C. Tornow, L. Bello, S. Woerner, and D. J. Egger, Scaling of the quantum approximate optimization algorithm on superconducting qubit based hardware, *Quantum* **6**, 870 (2022).
- [408] D. J. Egger, J. Mareček, and S. Woerner, Warm-starting quantum optimization, *Quantum* **5**, 479 (2021).
- [409] J. Wurtz and P. J. Love, Counterdiabaticity and the quantum approximate optimization algorithm, *Quantum* **6**, 635 (2022).
- [410] V. Vijendran, A. Das, D. E. Koh, S. M. Assad, and P. K. Lam, An expressive ansatz for low-depth quantum optimisation, *Quantum Sci. Technol.* **9**, 025010 (2024).
- [411] R. Herrman, P. C. Lotshaw, J. Ostrowski, T. S. Humble, and G. Siopsis, Multi-angle quantum approximate optimization algorithm, *Sci. Rep.* **12**, 6781 (2022).
- [412] S. Bravyi, A. Kliesch, R. Koenig, and E. Tang, Obstacles to variational quantum optimization from symmetry protection, *Phys. Rev. Lett.* **125**, 260505 (2020).
- [413] S. Lloyd, Least squares quantization in PCM, *IEEE Trans. Inf. Theory* **28**, 129 (1982).

- [414] S. Lloyd, M. Mohseni, and P. Rebentrost, Quantum algorithms for supervised and unsupervised machine learning, [ArXiv:1307.0411](#).
- [415] D. Kocczyk, Quantum machine learning for data scientists, [ArXiv:1804.10068](#).
- [416] E. Aïmeur, G. Brassard, and S. Gambs, in *Advances in Artificial Intelligence*, edited by L. Lamontagne and M. Marchand (Springer Berlin Heidelberg, Berlin, Heidelberg, 2006), p. 431.
- [417] C. Durr and P. Hoyer, A quantum algorithm for finding the minimum, [ArXiv:quant-ph/9607014](#).
- [418] J. Kübler, S. Buchholz, and B. Schölkopf, The inductive bias of quantum kernels, *Adv. Neural Inf. Process. Syst.* **34**, 12661 (2021).
- [419] Y. Liu, S. Arunachalam, and K. Temme, A rigorous and robust quantum speed-up in supervised machine learning, *Nat. Phys.* **17**, 1013 (2021).
- [420] M. Schuld, Supervised quantum machine learning models are kernel methods, [ArXiv:2101.11020](#).
- [421] A. Perdomo-Ortiz, M. Benedetti, J. Realpe-Gómez, and R. Biswas, Opportunities and challenges for quantum-assisted machine learning in near-term quantum computers, *Quantum Sci. Technol.* **3**, 030502 (2018).
- [422] B. Coyle, D. Mills, V. Danos, and E. Kashefi, The Born supremacy: Quantum advantage and training of an Ising Born machine, *npj Quantum Inf.* **6**, 60 (2020).
- [423] R. Sweke, J.-P. Seifert, D. Hangleiter, and J. Eisert, On the quantum versus classical learnability of discrete distributions, *Quantum* **5**, 417 (2021).
- [424] X. Gao, E. R. Anschuetz, S.-T. Wang, J. I. Cirac, and M. D. Lukin, Enhancing generative models via quantum correlations, *Phys. Rev. X* **12**, 021037 (2022).
- [425] M. Benedetti, D. Garcia-Pintos, O. Perdomo, V. Leyton-Ortega, Y. Nam, and A. Perdomo-Ortiz, A generative modeling approach for benchmarking and training shallow quantum circuits, *npj Quantum Inf.* **5**, 1 (2019).
- [426] M. H. Amin, E. Andriyash, J. Rolfe, B. Kulchytskyy, and R. Melko, Quantum Boltzmann machine, *Phys. Rev. X* **8**, 021050 (2018).
- [427] S. Lloyd and C. Weedbrook, Quantum generative adversarial learning, *Phys. Rev. Lett.* **121**, 040502 (2018).
- [428] S. Kullback and R. A. Leibler, On information and sufficiency, *Ann. Math. Stat.* **22**, 79 (1951).
- [429] J. Lin, Divergence measures based on the Shannon entropy, *IEEE Trans. Inf. Theory* **37**, 145 (1991).
- [430] A. Rényi, in *Proceedings of the Fourth Berkeley Symposium on Mathematical Statistics and Probability, Volume 1: Contributions to the Theory of Statistics* (University of California Press, Berkeley, 1961), p. 547.
- [431] M. Kieferova, O. M. Carlos, and N. Wiebe, Quantum generative training using Rényi divergences, [ArXiv:2106.09567](#).
- [432] A. Gretton, K. M. Borgwardt, M. J. Rasch, B. Schölkopf, and A. Smola, A kernel two-sample test, *J. Mach. Learn. Res.* **13**, 723 (2012).
- [433] S. Jerbi, C. Gyurik, S. Marshall, H. Briegel, and V. Dunjko, Parametrized quantum policies for reinforcement learning, *Adv. Neural Inf. Process. Syst.* **34**, 28362 (2021).
- [434] A. Skolik, S. Jerbi, and V. Dunjko, Quantum agents in the Gym: A variational quantum algorithm for deep Q-learning, *Quantum* **6**, 720 (2022).
- [435] S. Jerbi, L. M. Trenkwalder, H. Poulsen Nautrup, H. J. Briegel, and V. Dunjko, Quantum enhancements for deep reinforcement learning in large spaces, *PRX Quantum* **2**, 010328 (2021).
- [436] J.-Y. Hsiao, Y. Du, W.-Y. Chiang, M.-H. Hsieh, and H.-S. Goan, Unentangled quantum reinforcement learning agents in the OpenAL Gym, [ArXiv:2203.14348](#).
- [437] S. Y.-C. Chen, in *ICASSP 2023 – 2023 IEEE International Conference on Acoustics, Speech and Signal Processing (2023)*.
- [438] A. Skolik, M. Cattelan, S. Yarkoni, T. Bäck, and V. Dunjko, Equivariant quantum circuits for learning on weighted graphs, *npj Quantum Inf.* **9**, 47 (2023).
- [439] M. Schenk, E. F. Combarro, M. Grossi, V. Kain, K. S. B. Li, M.-M. Popa, and S. Vallecorsa, Hybrid actor-critic algorithm for quantum reinforcement learning at CERN beam lines, *Quantum Sci. Technol.* **9**, 025012 (2024).
- [440] A. Skolik, S. Mangini, T. Bäck, C. Macchiavello, and V. Dunjko, Robustness of quantum reinforcement learning under hardware errors, *EPJ Quantum Technol.* **10**, 8 (2023).
- [441] N. Sale, B. Lucini, and J. Giansiracusa, Probing center vortices and deconfinement in SU(2) lattice gauge theory with persistent homology, *Phys. Rev. D* **107**, 034501 (2023).
- [442] S. Lloyd, S. Garnerone, and P. Zanardi, Quantum algorithms for topological and geometric analysis of data, *Nat. Commun.* **7**, 10138 (2016).
- [443] C. Gyurik, C. Cade, and V. Dunjko, Towards quantum advantage via topological data analysis, *Quantum* **6**, 855 (2022).
- [444] R. Hayakawa, Quantum algorithm for persistent Betti numbers and topological data analysis, *Quantum* **6**, 873 (2022).
- [445] S. Ubaru, I. Y. Akhalwaya, M. S. Squillante, K. L. Clarkson, and L. Horesh, Quantum topological data analysis with linear depth and exponential speedup, [ArXiv:2108.02811](#).
- [446] S. McArdle, A. Gilyén, and M. Berta, A streamlined quantum algorithm for topological data analysis with exponentially fewer qubits, [ArXiv:2209.12887](#).
- [447] M. Crichigno and T. Kohler, Clique homology is QMA1-hard, [ArXiv:2209.11793](#).
- [448] E. Witten, Supersymmetry and Morse theory, *J. Differ. Geom.* **17**, 661 (1982).
- [449] A. Bocci, V. Innocente, M. Kortelainen, F. Pantaleo, and M. Rovere, Heterogeneous reconstruction of tracks and primary vertices with the CMS pixel tracker, *Front. Big Data* **3**, 49 (2020).